COVALENT IMMUNE PROXIMITY-INDUCTION STRATEGY USING SUFEX-ENGINEERED BIFUNCTIONAL VIRAL PEPTIDES

Harrison McCann, Anthony Rullo*

Department of Chemistry and Chemical Biology & Department of Medicine,

McMaster University

April 10th, 2023

A Thesis Submitted to the School of Graduate Studies in Partial Fulfilment of the Requirements for the Degree Master of Science

McMaster University MASTER OF SCIENCE (2023) Hamilton, Ontario (Science)

TITLE: Implementing SuFEx Chemistry into Covalent Antibody Recruiting Molecules AUTHOR: Harrison McCann, B.Sc. (McMaster University) SUPERVISOR: Professor Anthony F. Rullo NUMBER OF PAGES: 150.

Abstract

Harnessing the immune system is a powerful tool in chemical biology and is the focus of cancer immunotherapy. Often, this is accomplished through monoclonal antibodies which recognize and recruit immune effector cells to an over-expressed cancer antigen presented at the cancer cell surface. More recently, there has been great interest in developing small molecule therapeutics which replicate this, but with lower developmental costs, greater modularity, and improved tumor penetration. One such class of therapeutics are bifunctional molecules known as antibody recruiting molecules, which form molecular bridges between two targets, i.e., a cancer receptor and antibody. Limitations in ternary complex formation between bifunctional molecules and their two binding targets has presented the need for increasing residence time at key junctions. Demonstrated here is the development of a covalent proximity-induction approach which leverages molecular recognition to drive an electrophilic warhead near a nucleophile within a target antibody binding site. Subsequent irreversible labeling reprograms these antibodies with tumor binding handles in situ for enhanced tumor opsonization and immune clearance mechanisms. This was accomplished by equipping a viral peptide epitope with a sulfur (VI) fluoride exchange electrophile to irreversibly label anti-herpes simplex virus (HSV) antibodies. Using the aryl sulfonyl fluoride warhead, we demonstrate fast and selective labeling for both model monoclonal antibodies, as well as natural polyclonal anti-HSV antibodies. Covalently reprogrammed antibodies elicited superior potency at both lower concentrations and with cell lines having lower antigen presentation. This proof of concept has broad applicability in developing covalent bifunctional molecules for bridging one or more protein:protein interactions.

Acknowledgements

This thesis was made possible through the mentorship of Dr. Anthony Rullo, as well as the strong comradery demonstrated in the Rullo lab.

To start off, I would like to give the biggest thank you to Dr. Anthony Rullo for giving me the opportunity to explore my interests in chemical biology. Your mentorship and expertise were pivotal in my development as a researcher. I will always miss dropping by your office to talk science.

I would also like to thank my entire lab, with a special thank you to Ben Lake, Eden Kapcan, Rebecca Turner, Sissi Yang, Karolina Krygier, Arthur Srayeddin, Tomas Frankovich, and Maya da Luz. I appreciate the countless hours running problems by each of you, as well as the support you all gave along the way.

Lastly, a big thank you to my committee members Dr. Giuseppe Melacini and Dr. James McNulty. It was a pleasure to have your guidance and expertise throughout my graduate studies.

Table of Contents

List of Figures

List of tables

List of Equations

List of all Abbreviations and Symbols

17β-HSD1	17β-Hydroxysteroid dehydrogenase type 1
ABPP	Activity based protein profiling
ADC	Antibody drug conjugate
ADCC	Antibody dependent cellular cytotoxicity
ADCP	Antibody dependent cellular phagocytosis
ARM	Antibody recruiting molecule
ASF	Aryl sulfonyl fluoride
AURK	Aurora kinases
BLI	Bio-layer interferometry
BRD4	Bromodomain 4
BTK	Bruton's tyrosine kinase
cARM	Covalent antibody recruiting molecule
CDK	Cyclin dependent kinase
CoLDR	Covalent ligand directed release
CRL	Cullin RING ubiquitin ligase
DBCO	Dibenzylcyclooctyne
DNP	Dinitrophenyl
DUBTAC	Deubiquitinase targeting chimera
EGFR	epidermal growth factor receptor
Fab	Antibody fragment antigen-binding
FcR	Fragment crystallizable receptor
Fmoc	Fluorenylmethoxycarbonyl
FSY	Fluorosulfate tyrosine
gD	Glycoprotein D
GU	Glutamate urea
HMD2	Double minute 2 protein
Hsp90	Heat shock protein 90
HSV	Herpes simplex virus
IgG	Immunoglobulin G
ITAM	Immunoreceptor tyrosine-based activation motif
K_D	Dissociation equilibrium constant
KEAP1	Kelch-like ECH-associated protein 1
K_I	Inhibition equilibrium constant
k_{inact}	Inactivation rate constant
k_{off}	Dissociation rate constant
k_{on}	Association rate constant
KRAS	Kirsten Rat Sarcoma Viral Proto-Oncogene
LC-HRMS	Liquid chromatography-high resolution mass spectrometry
LC-MS	Liquid chromatography-mass spectrometry

LYTAC	Lysosomal targeting chimera
MAST3	Microtubule-associated serine/threonine-protein kinase 3
mTOR	Mammalian target of rapamycin
NASA	N-acyl N-alkyl sulfonamides
PBRM	3-(2-bromoethyl)-16β-(m-carbamoylbenzyl)-17β-hydroxy-1,3,5(10)-estratriene
PBS	Phosphate buffered saline
PHIC	Phosphorylating inducing chimera
PHORC	Dephosphorylation targeting chimera
PI3K	Phosphoinositide-3 kinase
Pin1	Peptidyl-prolyl cis-trans isomerase
PK	Pharmacokinetic
PLK-1	polo-like kinase 1
PROTAC	Proteolysis targeting chimera
PSMA	Prostate specific membrane antigen
SAR	Structure activity relationship
SDS-PAGE	Sodium dodecyl sulfate polyacrylamide gel electrophoresis
SGK3	Serum/glucocorticoid regulated kinase family member 3
SPAAC	Strain-promoted azide-alkyne cycloaddition
SPPS	Solid-phase peptide synthesis
SuFEx	Sulfur (VI) fluoride exchange
SuTEx	Sulfur (VI) triazole exchange
TFA	Trifluoroacetic acid
TPD	Targeted protein degradation
TPS	Targeted protein stabilization
VHL	Von Hippel–Lindau

Declaration of Academic Achievement

Towards the completion of this thesis, Harrison McCann was responsible for all synthesis and characterization of each final construct and intermediate. Additionally, Harrison was responsible for all kinetic labeling and selectivity studies, as well as planning and performing incubations for biological effector studies. Both the isolation of polyclonal anti-HSV and the selective covalent engagement of this IgG was performed by Harrison. Lastly, Harrison completed each illustration and assembled all results towards the completion of this report.

All flow cytometry experiments were performed by Benjamin P.M. Lake, a PhD student from the Rullo Lab.

All mouse work was performed by Maria E. Davola, a post-doctoral researcher from the Mossman lab.

All protein mass spectrometry characterization (using LP14 antibody) was performed by Kyle S. Hoffman from Bioinformatics Solutions Inc.

1. Introduction to Covalent Therapeutics

Cancer therapies have evolved dramatically over the last several decades.[1] A large focus of recent articles has been the development of targeted therapeutics, whose function is constrained to a particular target of choice.[2] Many advantages are realized from this approach, with the most significant being reduced off-target side effects. Thus, the angle taken for the design of these molecules has been to improve their affinity for a particular target, like a cancer antigen, to reduce dosing and ultimately limit non-specific or off-target binding to healthy cells.

One significant theme encompassing these compounds is the idea of proximity. Proximity, or increasing the effective concentration of two interacting molecules is a governing force in both chemistry and biology.[3] Biological process use proximity to achieve both catalysis and/or as an entropic driving force to achieve biological recognition/signalling and communication. Examples include enzyme substrate binding, avidity effects in transcription factor regulation of gene expression, and antibody dependent fragment crystallizable receptor (FcR) function. By leveraging proximity, chemical reactions typically limited by collision frequency and orbital alignment are dramatically accelerated through an apparent increase in concentration. Proximity also off-sets entropic penalties endowed by a combining of two groups by coupling the reaction to a favourable binding interaction.

1.1. The Emergence of Proximity-Inducing Therapies

Traditional *synthetic* therapeutics involve 1:1 binding between an agonist or antagonist ligand, and a receptor/target protein.[4] More recently, the utility of incorporating

such binding ligands into bifunctional/chimeric formats has been demonstrated for the purposes of leveraging additional protective/regulatory mechanisms of the host.[5] Here, a binding ligand for a target disease protein is linked to a “recruiting” ligand for an endogenous protein/receptor to couple target engagement to a biological host defence/regulatory response (e.g., targeted protein degradation (TPD) or immune elimination of diseased cells). Such bifunctional therapeutic modalities necessarily function through a minimal 3-component ternary complex, however several additional subsequent protein assembly processes are required for biological function.[6] These proximity-inducing “molecular bridges” are thus reminiscent of the many scaffolding molecules in nature (e.g., heparin enhancing the rate of antithrombin III catalytic inhibition of thrombin) via reduction in dimensionality.[7] The foundational bifunctional proximity-inducing therapeutic modalities encompass proteolysis targeted chimeras (PROTACs),[8–16] antibody recruiting molecules (ARMs),[17–19] lysosome-targeting chimeras (LYTACs),[20,21] phosphorylation inducing chimeras (PHICs),[22] phosphatase recruiting chimeras (PHORCs),[22] or deubiquitinase-targeting chimeras (DUBTACs).[23] A complementary class of proximity inducing molecules functioning through ternary complexes are called “molecular glues”.[24–26] Uniquely, these use a single molecule, traditionally a natural product selected by evolutionary pressure, to induce positive cooperative binding between two endogenous proteins. Examples include FK506, which induces ternary complex formation between FKBP12 and calcineurin,[27–29] or Rapamycin, which also binds FKBP12 but instead targets the mammalian target of rapamycin (mTOR) recognition interface.[29,30] These are powerful modalities given the high stability of resultant ternary complexes, with current efforts focused on the development of discovery

platforms to identify new molecules with molecular glue properties. Given the versatility of bifunctional approaches in their ability to leverage readily available binding ligands developed for several purposes, chemical strategies have been introduced to enhance their efficacy, ternary complex stability, and/or pharmacokinetic (PK) properties.

Bifunctional molecules address one main limitation of inhibitors, namely with respect to targets that have previously been considered undruggable.[31] Undruggable targets include disordered proteins or those with a lack of druggable binding grooves needed to guide medicinal chemistry structure activity relationships (SARs). Undruggable targets can also be diseased cells like various cancer types inert to the action of a single agonist or antagonist drug. By virtue of their recruitment capabilities, bifunctionals only need to bind the target protein or cell which “flags” it for host recognition and response. For example, ARMs only require binding to cancer cells to recruit serum antibodies.[17–19] The resultant high valency display of cancer cell bound antibodies (i.e., increased proximity) presents as foreign to the host immune response leading to tumor eradication. Thus, bifunctional therapeutic modalities represent a significant advancement in molecular medicine, which leverage the host response to combat disease.

1.2. **Complexities of Ternary (and Multi-) Complex Equilibrium and Pharmacokinetics**

In contrast to molecular glues, bifunctional modalities use separate binding ligands to bridge two proteins in close proximity. As such, it is difficult to predict the potential for favorable protein-protein interactions within the ternary complex leading to positive cooperativity.[32] It is possible that the two proteins can find the opportunity for favorable

protein:protein binding interfaces leading to enthalpic stabilization that would normally be opposed entropically (now that the bifunctional molecule has paid much or all of the entropic cost for protein:protein binding).[33,34] We propose in general, the more likely scenario is negative cooperativity due to steric clashes and/or charge repulsion depending on protein pI.[35,36] This would be especially true when bridging cell surface proteins in trans, as in the case of ARMs where negatively charged cell surfaces (i.e., tumor cells + immune cells) are necessarily brought in proximity.[37] A lack of positive cooperativity also renders the bifunctional susceptible to the pharmacological “hook” or “prozone” effect.[38] This means it is difficult to maximize ternary complex formation at any concentration of bifunctional molecule, especially as its binding affinities relative to the two endogenous protein concentrations decrease. Even if these affinities are high, excess concentrations of bifunctional will sharply autoinhibit the ternary complex. In the case of biological processes where catalytic turnover is required for efficacy as reported for PROTACs, the need for highly stable ternary complexes remains in question and could be detrimental if the bifunctional is trapped in the ternary complex.[39] In extracellular immune recruiting applications however, ternary complex stability appears critical for function, with the importance of molecular turnover currently not well defined.[40] In addition to the importance of ternary complex stability in bifunctional proximity inducing molecule therapeutic applications, the importance of target residence time remains largely undefined and unexplored. Indeed, studies investigating the stability of T cell:major histocompatibility complex and bi-specific T cell engager:cluster of differentiation 3 receptor (CD3) interactions, combined with data supporting the “kinetic proof-reading hypothesis” suggests a critical contact time is required for maximal immune cell

activation.[37,41–44] Such effects illuminate the complexities of receptor pharmacology beyond traditional target occupancy arguments. That is, 100% receptor occupancy may not confer maximal pharmacological response, if the microscopic ligand binding dissociation events occur too quickly.

Finally, independent of receptor pharmacology or mode of action, the low molecular weight of proximity inducing molecules promotes rapid in vivo clearance.[45–47] This complicates dosing profiles, the therapeutic window, and reduces control over the ability to enforce ternary complex formation in vivo. This may be especially true for indications where the bifunctional targets extracellular proteins and can only partition in the serum compartment.[20,21,48] The above considerations have inspired the development of new chemical "covalent" strategies to enhance bifunctional molecule efficacy and probe the variables discussed above.

1.3. **Covalency as a Tool to Enhance Simple "Binary" Ligand-Receptor Binding**

Proximity-induced covalent reactions circumvent time-consuming strategies used to enhance the affinity of binary interactions between inhibitors and their drug targets. New approaches have aimed to bypass these protocols and "infinitely" increase the binding affinity via irreversible proximity-induced covalent labeling (**Figure 1**). Well-known drugs like aspirin function through an irreversible labeling step which involves acetylation of Ser-530 upon binding to cyclooxygenase-2.[49] However, the nature of this mechanism was only recently discovered, and now serves as the conceptual foundation for many covalent drugs today.[50,51]

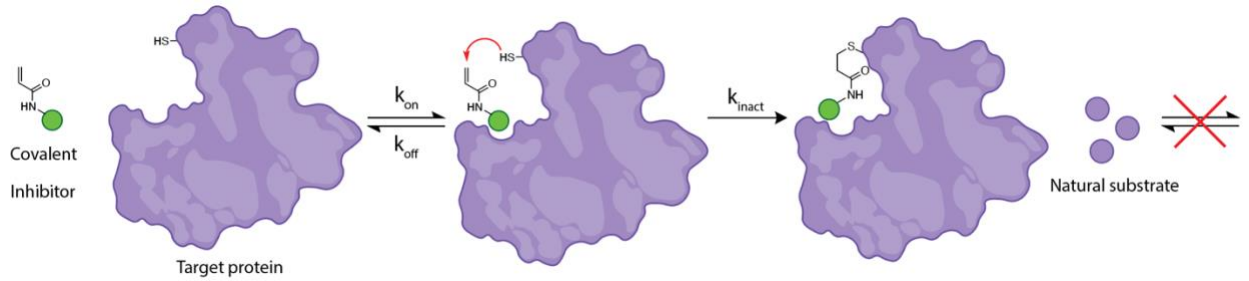

Figure 1. Introducing electrophilic modalities into small molecule ligands mediates a selective, proximity-induced covalent labeling reaction for permanent protein inhibition.

In the last decade, covalent drugs have been developed to target either active or allosteric sites on target proteins. By incorporating these moieties into a synthetic binding ligand, successful pre-orientation of the electrophile with a nucleophilic amino acid in the protein binding pocket facilitates a rapid, long-lived covalent linkage (**Figure 1**). This rate enhancement in the binding pocket also allows for less reactive electrophiles to be used. As such, selectivity is conferred by relying on successful pre-organization with nucleophilic amino acids like lysine, tyrosine, histidine, serine, or threonine. These proximity-induced covalent reactions are akin to a “click reaction” at physiological conditions. Examples include covalent kinase inhibitors, which function by irreversibly labeling the catalytic lysine, or cysteine in the kinase active site, preventing target protein phosphorylation.[52–54]

Covalent small molecules improve upon non-covalent binders by greatly enhancing the target residence time. In a binary binding system such as a small molecule or protein-based inhibitor, the binding equilibrium is governed by a dissociation equilibrium constant, K_D, a measure of affinity. The K_D value itself can then be broken down into an on rate (k_{on}) and off rate (k_{off}). At ligand concentrations near or greater than the K_D value, the k_{on} becomes large enough to enforce binding, i.e., as soon as the

complex dissociates, another one forms. At concentrations much lower than the K_D, the opposite occurs, and the fraction of bound complex decreases. Thus, when covalency is introduced to render this binding event irreversible, the respective k_{off} value is eliminated to stabilize the complex. In the context of covalent inhibitors, this effect has allowed researchers to permanently block enzyme active sites and receptor binding sites. Importantly, using the covalent inhibitor approach, even fractional binding of the target protein at sub-K_D concentrations will inevitably lead to irreversible binding of all available target protein, as a function of reaction time.

A key consideration in design of these inhibitors is the binding dependent rate enhancement of the covalent drug. This is critical for both selectivity and efficacy reasons. Covalent binders irreversibly label target proteins once bound. The rate of the covalent bond formation step is governed by the first order rate constant, k_{inact}. The concentration of ligand needed to provide a half-maximal k_{inact} is K_I. Often covalent inhibitor-like constructs are compared through a ratio of k_{inact}/K_I, a second order rate constant which describes the efficiency of the covalent reaction. In contrast, the rate of an intermolecular (bimolecular) reaction is governed by the second order rate constant k_{inter}, which is binding independent. As such, too weak a binding ligand (high K_I) will require high ligand concentrations to promote the covalent reaction. This represents a risk of fast bimolecular labeling of off target proteins. Ideally, the electrophile itself is relatively unreactive *until* it binds the target protein.[55] This might be accomplished using electrophiles that are optimally pre-organized upon binding the target, maximally benefitting from reaction effective molarity. We also hypothesize certain electrophiles may react through rate

limiting transition states that are differentially stabilized upon ligand binding to the target protein, relative to reactions with off target proteins that do not bind or bind weakly.[56,57]

1.4. **Electrophilic Moieties for Ligand-Directed Covalent Labeling Applications**

Covalency has been used extensively to enhance small molecule inhibitors for protein targets in applications including but not limited to cancer. Typical targets in cancer therapies include cyclin dependent kinases (CDKs), p53, polo-like kinase 1 (PLK-1), epidermal growth factor receptor (EGFR), Aurora kinases (AURKs), Kirsten Rat Sarcoma Viral Proto-Oncogene ($KRAS^{G12C}$), phosphoinositide-3 kinase (PI3K), and MYC.[58–60] Depending on the therapeutic target, the choice of electrophile requires careful consideration. Tuning of electrophiles with specific sterics or electronics may impart both a degree of chemoselectivity and/or reactivity. For example, some strategies may call for an electrophile which only reacts with a low pKa catalytic lysine. Other applications may call for a cysteine-reactive handle, or perhaps a much more promiscuous handle capable of cross-linking with a variety of amino acids for greater target engagement.

1.4.1. **Acrylamide Warheads**

Acrylamides represent one of the most widely used electrophilic handles in covalent drug applications.[61,62] This warhead reacts through a Michael addition mechanism with softer electrophilic properties. As such, these handles are typically used to label cysteine thiols due to their high lying HOMO, allowing for rapid labeling rates in close proximity. Even more, by modifying the substituents along the α,β-unsaturated carbonyl, reaction rates and selectivity can be carefully tuned through a combination of

electronics and sterics (**Table 1**, Group 1).[63,64] Implementation of highly electronegative fluorine atoms at the α carbon increases reactivity of the acrylamide by pulling electron density from the β carbon (**Table 1**, Electrophile 1H).[63] Similarly, a cyano group branching from the α-carbon functions in this way but has the added effect of *reversible* covalent bond formation (**Table 1**, Electrophile 1G).[65] Sterics may also be modified to impart selectivity by constraining the α,β-unsaturated carbonyl in a ring structure.[64]

Previously regarded undruggable proteins, like $KRAS^{G12C}$ and MYC,[66,67] are now being inhibited by leveraging proximity-induced covalent labeling to target uniquely reactive amino acids. For example, MYC driven tumors have recently been targeted with a functional covalent ligand via an intrinsically disordered cysteine at position C171.[68] By irreversibly labeling MYC, the Nomura group demonstrated reduced thermal stability of MYC, preventing DNA binding and tumorigenesis. In this study there was no mention of reaction rate, however high selectivity was demonstrated using an activity-based protein profiling (ABPP) assay where 8 of 1500 cysteine-containing compounds reacted with their acrylamide probe. In a similar example, the Cee group engrafted an acrylamide-based warhead into a quinazolinone scaffold to covalently label C12 of $KRAS^{G12C}$.[69] This compound demonstrated both a fast second order rate constant ~ 10^5 $M^{-1}s^{-1}$, while also exhibiting high selectivity by reacting only with $KRAS^{G12C}$ C12 peptide out of >6000 other cysteine-containing peptides.

1.4.2. **Aldehyde Warheads**

Aldehydes represent a group of more lysine-specific, “harder electrophile” covalent warheads. With rapid kinetics, aldehydes condense with amines to form hydrolytically

labile imine bonds. To stabilize these adducts, aldehydes are typically incorporated into aromatic rings with stabilizing ortho substituents like hydroxyl groups, which form hydrogen bonds with resulting imines (**Table 1**, Group 2).[70] Similarly, ortho boronic acids help stabilize imine adducts through the formation of iminoboronates, drastically increasing the half-life of the covalent bond (**Table 1**, Electrophiles 2C & 2D).[71–73]

Incorporation of neighboring reactive substituents not only has a stabilizing effect but can also aid in the reaction itself. Recent work by the Zhang, Gao, and Yao labs have produced a lysine-selective covalent aldehyde warhead by installing an alkyne ortho to an aromatic aldehyde (**Table 1**, Electrophile 2A).[74] After Schiff base formation with a proximal lysine in the binding pocket, an intramolecular cyclization reaction with the terminal alkyne carbon ortho to the imine creates an aromatic ring to stabilize the covalent adduct. With k_{inact} and K_I values of 5.54×10^{-3} s^{-1} and 3.2×10^{-6} M, respectively, this 2-ethynylbenzaldehyde demonstrates sufficiently high reaction rates. Selectivity was also observed through a mono-substituted target adduct via mass spectrometry analysis after a 2-hour reaction time.

Reversible covalent chemistries permit new opportunities for selective covalent labeling. The Taunton lab demonstrated this by using a salicylaldehyde probe to form a stable imine with kinases like AURKA (**Table 1**, Electrophile 2B).[75] Even more, they demonstrate that these salicylaldehyde probes selectively engage kinases in a residence-based manner; that is, the imine products with kinases like AURKA, AURKB, microtubule-associated serine/threonine-protein kinase 3 (MAST3), and serum/glucocorticoid regulated kinase family member 3 (SGK3) are kinetically stabilized through intramolecular hydrogen bonding and reduced solvent exposure. By obscuring the imine product in a

hydrophobic environment, the effective concentration of water was greatly diminished, and the rate of hydrolysis was reduced to create stable covalent adducts.

1.4.3. **Alkyl Halide and Haloacetamide Warheads**

Alkyl halides generally represent a more reactive, albeit less specific electrophilic warhead. These groups are typically incorporated through alkyl linkers with terminal C-Br or C-Cl bonds (**Table 1**, Group 2). A similar, yet more reactive class of halogenated electrophiles are haloacetamides. Several chloroacetamide inhibitors have been employed by the Gray and London labs to inhibit cancer targets like peptidyl-prolyl cis-trans isomerase (Pin1). In each of these examples, a chloroacetamide was used to irreversibly label cysteine 113 in a site-selective manner. Importantly, the α-carbonyl group serves to lower the C-Cl bond LUMO, a σ* antibonding orbital, thus enhancing the substitution reaction rate. Sulfopin exhibited sufficiently high reaction rates for complete Pin1 labeling within 4 hours.[76] Similarly, BJP-06-005-3 displayed a k_{inact}/K_I of 740 M^{-1} s^{-1}.[77] Using a competitive dose-response curve, BJP-06-005-3 also showed high selectivity for C113 of Pin1 which was the only modified cysteine in the 604 identifiable cysteine sites in the human embryonic kidney 293 (HEK293) proteome.

However, alkyl halides are not limited to cysteine nucleophiles. Using a bromoethyl electrophile, the Lin group demonstrated histidine labeling under proximity-inducing conditions with 17β-Hydroxysteroid dehydrogenase type 1 (17β-HSD1).[78] Using irreversible inhibitor 3-(2-bromoethyl)-16β-(m-carbamoylbenzyl)-17β-hydroxy-1,3,5(10)-estratriene (PBRM), co-crystal structure elucidation allowed for the Lin group to demonstrate sufficient proximity between His^{221} and the bromoethyl group. Interestingly,

the bromoethyl electrophile does not react with free excess histidine under physiological conditions, highlighting the importance of proximity and reaction effective molarity.

1.4.4. **Sulfonamide Warheads**

N-acyl N-alkyl sulfonamides (NASA) leverage an activated amide for proximity-induced lysine labeling (**Table 1**, Electrophile 4). Due to its novelty, the mechanism of NASA labeling is still relatively unknown. However, reactivity seems to be conferred through the electron withdrawing cyanomethyl group protruding from the tertiary nitrogen atom of the sulfonamide. It is plausible that reaction rates are accelerated when the methylene adjacent to the nitrogen leaving group is acidic enough to exchange protons with the nitrogen after leaving group expulsion. Supporting this is a correlation between stronger electron withdrawing groups, hydrolysis rates (indicative of intrinsic reactivity), and reaction rate with a target protein. To enhance reactivity, the negative charge accrued on the nitrogen leaving group must be reduced after reaction to stabilize the leaving group. Greater mechanistic insight should be given to investigate whether this is solely through a nearby EWG, or through an EWG-promoted acid/base reaction. Further contributing to target reactivity is steric hinderance of the EWG, i.e., 4-nitrobenzyl or 2,4-dinitrobenzyl rings have been found to impair labeling efficiencies.[79]

Importantly, the selectivity of NASA seems to be reliant on a specific binding interaction, i.e., when the electrophile was at low enough concentrations and confined to a binding interaction, high specificity was observed. NASA exhibits similar second-order reaction rates on the scale of 10^4 $M^{-1}s^{-1}$ when incorporated in a covalent inhibitor for heat

shock protein 90 (Hsp90).[79] However, when in the presence of excess competitor, several non-specific labeling reactions were seen in the cell lysate.

When NASA was incorporated into an inhibitor for double minute 2 protein (HMD2), slower reaction rates were observed on the order of 10^2 - 10^3 $M^{-1}s^{-1}$, likely due to the much larger K_D, despite a high k_{inact} of 4.8×10^{-4} s^{-1}.[80] Mass spectrometry digest/peptide mapping studies were performed, and it was found that the N-terminal α-amino group was being selectively modified (<12 Å away), as well as Tyr67 (~10 Å away). A proteome-wide selectivity study was also performed, revealing the NASA probe broadly reacted with ten total proteins.

1.4.5. **Sulfur Exchange Chemistry**

Sulfur (VI) fluoride exchange (SuFEx) chemistry has recently become a prominently used electrophile in proximity-induced covalent labeling applications. SuFEx itself represents a class of compounds with an R-SO_2F moiety (**Table 1**, group 5).[81] The chemoselectivity of SuFEx is much less constrained than other electrophiles, with reactions occurring between nucleophiles like lysine, tyrosine, and histidine. Despite having such a wide target scope, the low intrinsic reactivity of SuFEx leads to them being regarded as “latent electrophiles”. This is also observed through low hydrolysis rates under physiological conditions. Despite this apparent low reactivity, SuFEx forms covalent bonds in protein binding pockets at very fast rates, comparable with more reactive electrophiles.

One of the more prominent SuFEx chemistries is the aryl sulfonyl fluoride (ASF) (**Table 1**, Electrophiles 5A, 5C, & 5D), situated on the more electrophilic end of the SuFEx

spectrum. Several ASF derivatives (i.e., para vs meta substitution and phenyl vs benzoic acid derivatives) were explored by the Taunton group as broad kinase inhibitors.[82] They found the para ASF was generally more effective in targeting kinase catalytic lysines, likely due to the binding mode of the inhibitor and orbital overlap with the ε-NH_2. ASF has recently been used to covalently modify His353 of cereblon for covalent E3 ligase inhibition.[24] Other targets of ASF-equipped covalent inhibitors include human neutrophil elastase, via reaction with the catalytic Ser195 residue.[83] Between ASF and the less reactive fluorosulfate tyrosine (FSY) (**Table 1**, Electrophiles 5B & 5E), the latter exhibits higher selectivity and stability due to lower electrophilicity, yet much slower reaction rates in comparison, leading to reduced function under concentrations well below K_D values.

Another class of sulfur exchange chemistry is sulfonyl triazole exchange (SuTEx), which replaces the fluoride leaving group with a triazole derivative.[24,84] SuTEx has the advantage of enhanced chemoselectivity specifically for tyrosines and is often used to block catalytic tyrosines. This selectivity is reported to be imparted by the triazole leaving group, with a para-methoxyphenyl leaving group significantly improving the ratio of tyorinses/lysines labeled, without impairing tyrosine coverage (**Table 1**, Electrophile 6).[84] Several inhibitors have been made to contain SuTEx to target both catalytic and non-catalytic tyrosines, where reactivity in conferred through proximity.[85]

Sulfonimidoyl fluoride chemistry is another form of SuFEx that has yet to be incorporated into a proximity-induction format.[86] Sulfonimidoyl fluorides have been described as a less reactive, yet tunable sulfonyl fluoride, due to the potential substitution on the nitrogen atom participating as an imine (**Table 1**, Electrophile 7). As such, these

electrophiles have potential for highly tunable covalent binders for targeted covalent inhibition.

Table 1. Examples of electrophiles used in ligand-directed covalent labelers. Cancer protein targets are listed below each structure.

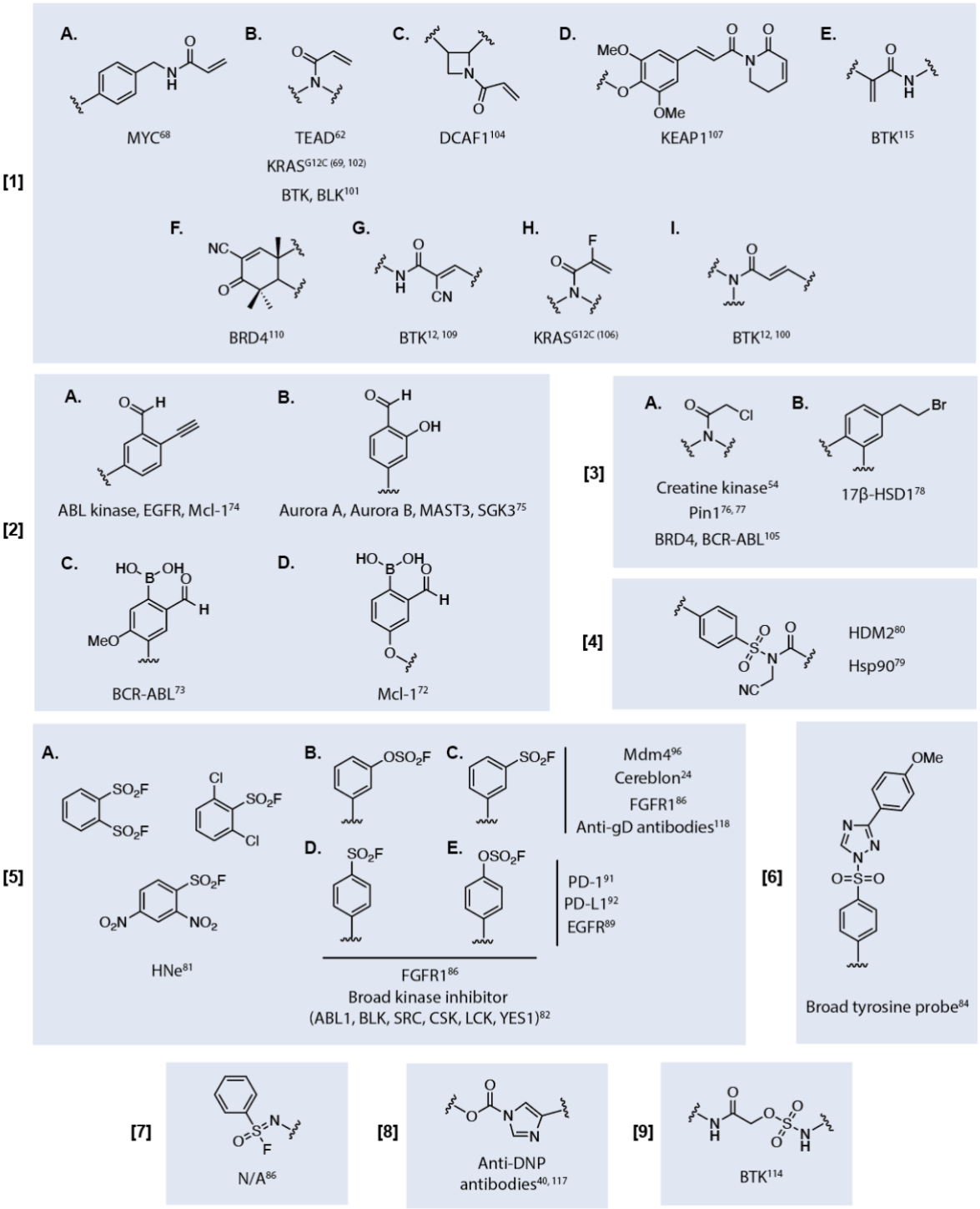

1.5. **Proximity-induced Covalent Protein Binders**

To extend the concept of covalent binders, covalent handles have been incorporated into the amino acid sequences of proteins and peptides to enhance the residence time of general protein:protein interactions. A key consideration in the development of covalent binding peptides and proteins is the stability of the construct prior to target protein engagement. Since the probe also contains reactive functionality, there may be a high propensity to “self-react” and quench the electrophile. These applications are also likely most useful when the protein ligand affinity is limiting, maximizing the effects of covalency.

One of the first examples of affinity driven protein:protein stapling used a Z_{SPA} affibody incorporated with a cysteine-reactive alkyl bromide electrophile to label the Z protein.[87] However the most prominent electrophile used in recent covalent protein applications has been SuFEx. The Wang group has pioneered the use of SuFEx chemistry in their strategies for genetically encoding latent bioreactive amino acids into protein binding interfaces.[88–90] They demonstrate this by genetically modifying the cell death protein 1 (PD-1) with SuFEx to irreversibly block the PD-1/PD-1 ligand (PD-L1) interaction on T cells to improve immune function.[91] Notably, they report a significant dose-response increase in the proportion of T cells with cytotoxic functions and enhanced IFN-γ production as a function of covalency. No self-reactivity was reported, i.e., labeling nearby nucleophilic amino acids due to intrinsic proximity through protein folding, supported by successful amino acid sequencing of the covalent protein binder.

Nanobodies represent a protein binder with high specificity and lack of immunogenicity, and are often used to block protein:protein interactions. Here, the Chen

group genetically incorporated SuFEx into a nanobody specific for PD-1 on T-cells.[92] In this example, a cell penetrating peptide and lysosomal sorting sequence attached to the covalent PD-1 was able to induce internalization and lysosomal degradation of PD-L1, restoring T cell function for eradication of non-small cell lung cancer cells. Numerous other examples have emerged including covalent protein labeling in vivo using Rab1b with the guanine nucleotide exchange factor of DrrA,[93] and recently a proximity-induced covalent labeling strategy to target both carbohydrates and RNA.[94,95]

Often times, protein:protein interactions are mimicked through the synthesis of a linear peptide epitope of one binding partner. Incorporation of covalent handles into these linear peptide epitopes has allowed for greater synthetic output of covalent protein binders. In these applications, SuFEx chemistry is most used, with the ASF electrophile dominating examples seen in literature. The first reported use of ASF in a covalent binding peptide was to target the p53-mdm4 interaction.[96] Both para-methyl and para-methoxy substituted ASF moieties have also been incorporated into covalent peptides to inhibit Mcl-1.[97]

1.6. Translating the Advantages of Covalency to Bifunctional Proximity-Inducers

The benefits of covalency in a monovalent binding interaction are also realized when incorporated into a bifunctional format. With intrinsic limitations in bifunctionals arising from inherently low affinity ligands, ternary complex instability, and potential for negative cooperativity, inducing irreversible interactions is very advantageous. Several

strategies have already began employing covalency as a strategy for therapeutic design, including PROTACs, DUBTACs, PHICs, and covalent ARMs (cARMs).

1.6.1. **Covalent PROTACs**

1.6.1.1. Irreversible covalent PROTACs

Several covalent PROTACs have been generated to target cytosolic proteins for degradation (**Figure 2**). Covalency has allowed for the chemical modification of binding interactions to enhance ternary complex formation between ubiquitin ligases, PROTACs, and target proteins. In the design of such molecules, covalency has either been incorporated into the target binding side or ubiquitin ligase binding side, each of which has its own respective consequences.[98] For example, the catalytic function of PROTACs is lost once irreversibly engaged protein targets are degraded. In this scenario, covalency is a tool to enhance target occupancy at concentrations well below the governing K_D, as is the case for many intracellular applications. On the ubiquitin ligase targeting side, covalency does not interfere with the catalytic effect. However, comparing the large substrate scope for target proteins with those for ubiquitin ligases, it is much more likely to find binders that have much more to gain from covalency on the target binding side.

The earliest example of a covalent PROTAC was the HaloPROTAC from the Crews lab, which used a chloroalkane tag to irreversibly label HaloTag7 for Von Hippel–Lindau (VHL) recruitment.[99] Other examples soon followed including a covalent PROTAC for Bruton's tyrosine kinase (BTK) in 2019,[100] and 2020.[101] Soon after, the Gray lab followed up with a covalent PROTAC which used an acrylamide to bridge $KRAS^{G12C}$ with E3 ligase cereblon for ubiquitination and subsequent protein degradation.[102] To

demonstrate the effects of irreversible E3 ligase recruitment, the Nomura group utilized a chloroacetamide warhead to irreversibly tag FEM1B with ligands for target proteins BRD4 and BCR-ABL/c-ABL.[103] Although no comparison was made with a non-covalent analogue, TPD was found to occur regardless of linker length. Linker constitution is an essential parameter to optimize in these studies, and this finding suggests a role for covalency in stabilizing ternary complexes with negative cooperativity.

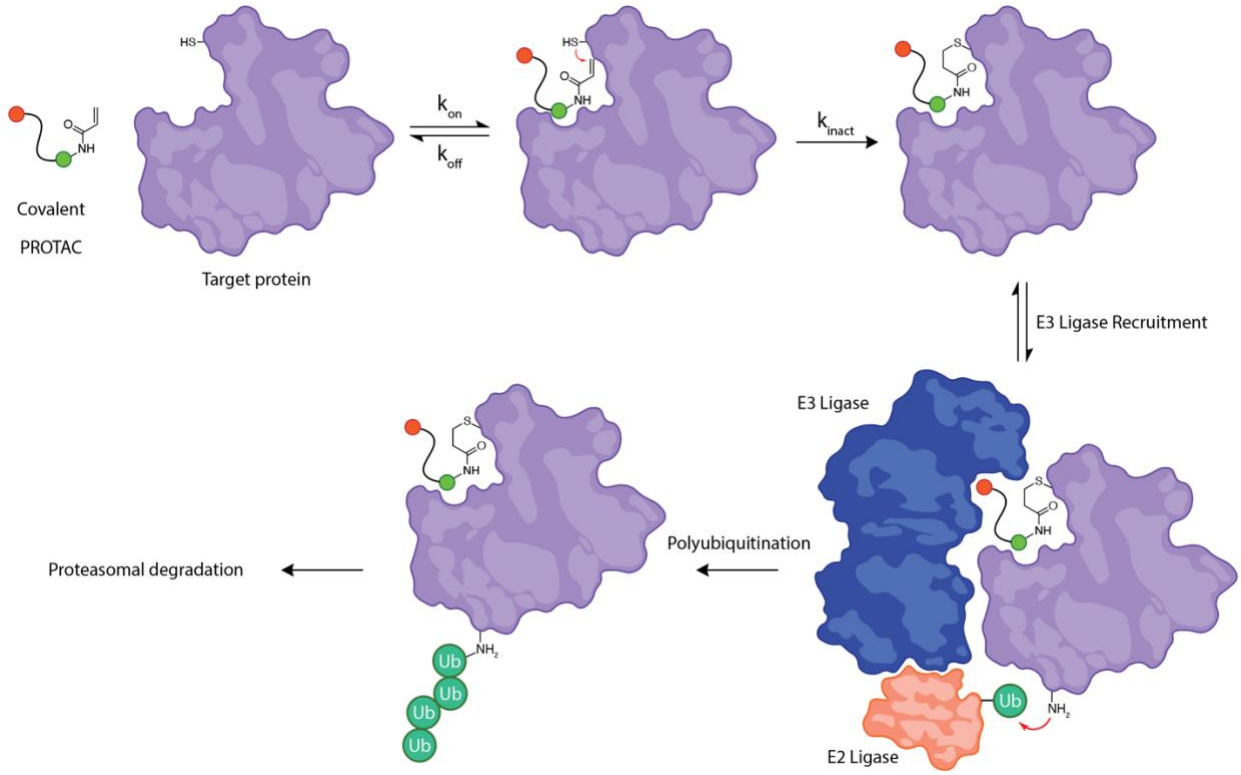

Figure 2. Bifunctional proximity engagers equipped with electrophilic modalities irreversibly label a target protein for enhanced ternary complex formation.

A common problem with covalent labeling is off-target engagement through non-specific cross-linking. By increasing the reactivity of the covalent handle, off-target labeling is likely to be increased as well. A recent study by the Cravatt group has

demonstrated that by replacing the α-chloroacetamide on covalent PROTACs with an N-acyl acrylamide on an azetidine core, a greater degree of selectivity is gained (**Table 1**, Electrophile 1C). The chirality of the azetidine core also conferred stereoselectivity between mutant protein targets.[104] They demonstrate that preferential binding of one stereoisomer allows for a "preferred interaction". Successful binding and thus pre-orientation of the electrophile next to Cys1113 enables a cross-linking reaction that otherwise occurs at negligible rates.

The effects of covalently stabilized ternary complexes on PROTAC function are complex and non-trivial to predict. Enhancing the binding interaction with the E3 ligase or target protein through an irreversible linkage can stabilize the ternary complex but can also inhibit biological function.[100] Many early studies with irreversible covalent PROTACs focus solely on covalent analogues, as opposed to non-covalent.[99,102,105,106] Since the majority of studies do not perform a head to head comparison between covalent and non-covalent PROTACs, it is inherently unclear whether "irreversible" covalency is beneficial or detrimental. Recently, a covalent PROTAC was developed which uses a dual acrylamide warhead for cullin RING ubiquitin ligase (CRL) recruitment and performed a rigorous head-to-head comparison of covalent vs non-covalent analogues.[107] Here, they reduced both alkenes and saw covalency was required for TPD in their case (**Table 1**, Electrophile 1D). To challenge this claim, we suggest that by altering the binding ligand itself, the lack of TPD may also be a result in lost affinity with the CRL substrate. By reducing the long, conjugated system, the planarity of the molecule was eliminated, potentially hurting the binding interaction. Despite this, they claim covalency is necessary, while it may just be that the non-covalent binder is not a binder after all.

1.6.1.2. Reversible covalent PROTACs

Recently, there has been great interest in utilizing reversible covalent linkages for proximity induction. Covalent binders equipped with reversible electrophiles can also kinetically stabilize ternary complex formation, however, there exists an equilibrium that can favor the reverse reaction under specific conditions and release of the bifunctional molecule. Akin to traditional irreversible covalent warheads, this emerging class of covalent drug can increase target residence time with corresponding decreased rates of in vivo clearance. Reversible covalency allows the bifunctional drug to retain the catalytic turnover properties of their non-covalent counterparts and provides a self-correction mechanism for off-target labeling (**Figure 3**). These factors are especially important in the intracellular environment when PROTACs are stapled to their target protein/E3 ligase. A reversible covalent bond in this scenario would undoubtedly enhance TPD by allowing successive ternary complexes to form after initial protein degradation.

Most, if not all reversible covalent PROTACs make use of the cyanoacrylamide warhead (**Figure 3**). What grants this electrophile reversibility in contrast to traditional acrylamide moieties is the electron withdrawing and conjugated cyanomethyl group that increases the acidity of the α-proton after Michael addition. Cyanoacrylamide warheads have been incorporated into PROTACs to target BTK.[108] Incorporation of a reversible covalent bond aided in selectivity, especially in a modified cyanoacrylamide warhead with a geminal dimethyl group. They demonstrate that reducing the affinity for the target while maintaining a reversible covalent bond reduces several additional non-covalent off-target interactions.

Intracellular accumulation is another essential parameter for designing therapeutics which target intracellular proteins. It was found that the cyanoacrylamide warhead improved PROTAC intracellular accumulation to improve target occupancy of BTK.[109] In this scenario, the reversible chemistry outperformed the irreversible and non-covalent chemistries by 3- and 30-fold, respectively. A thorough comparison was then performed between analogous non-covalent controls to determine if the reversible covalent bond was responsible for enhanced potency solely through enhanced intracellular accumulation. Despite having similar levels of intracellular accumulation, the reversible covalent bond conferred an order of magnitude lower IC_{50} for BTK degradation when compared to non-covalent controls.

Reversible recruitment of E3 ligases also presents a promising strategy for enhancing TPD.[110] Here, only when the cyanoacrylamide warhead was installed into a Kelch-like ECH-associated protein 1 (KEAP1) ligand, bardoxolone, did bromodomain 4 (BRD4) degradation occur. Notably with either the alkene or nitrile groups removed, no TPD occurred, highlighting the importance of the reversible covalent linkage.

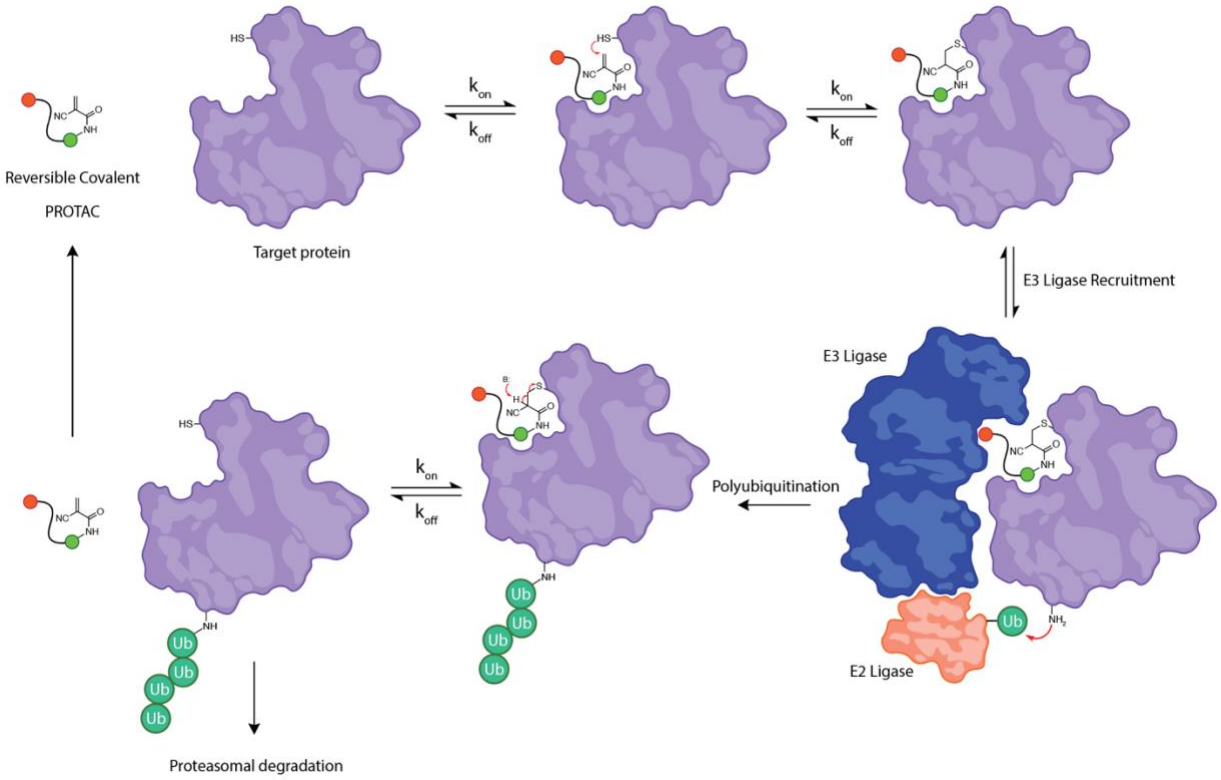

Figure 3. Reversible covalent engagement of target proteins by PROTACs facilitates high target occupancy while preserving the PROTAC catalytic cycle.

1.6.2. **Additional Platforms Which Leverage Covalency for Proximity-Induction**

1.6.2.1. Reversible Covalent DUBTACs

With TPD being a prominent topic in many recent studies, a similar platform has been gaining traction for the reciprocal function, i.e., targeted protein stabilization (TPS). TPS serves to address either a loss of function mutation, or upregulate an enzyme involved in mediating a dysregulated pathway in cancer. TPS is conceptually related to TPD, but instead recruits deubiquitinases to reduce basal TPD in a cell. DUBTACs, introduced by the Nomura group, demonstrate this by using an acrylamide warhead to covalently target ΔF508-CFTR and enhance trafficking to the membrane in cystic fibrosis.[111] The need to stabilize ternary complexes for trafficking to distal sub-cellular

locations represents another potentially useful aspect of covalent recruitment. Additionally, recent work by the Buhrlage group has discovered novel DUB-targeting covalent handles for the discovery of future DUBTACs using a large library of covalent fragments screened in an activity-based protein profiling protocol.[112]

1.6.2.2. Covalent Phosphorylating Inducing Chimeras (PHICs)

Branching away from TPD/TPS, controlling post-translational modifications of proteins remains a relatively unexplored subset of bifunctional proximity inducing molecules. One existing example induced tyrosine phosphorylation through bifunctional PHICs to perturb intracellular protein function.[113] The Choudhary lab recently advanced this platform by incorporating an α-methyl acrylamide to covalently engage BRD4 and induce phosphorylation. They note that resistance to classical BTK-inhibitor resistant cells can be overcome using this strategy.

1.6.2.3. Covalency to Enact Targeted Release of Cancer Therapeutics

Often in ligand-directed covalent labeling applications which historically focused on the development of chemical probes and biosensors, the binding motif itself is eliminated from the covalent ligand after nucleophilic attack. Taking advantage of this, the London lab strategically flipped the electrophile to provide targeted release of a desired therapeutic. This was accomplishes using both a substituted methacrylamide and sulfamate acetamide warhead for covalent ligand directed release (CoLDR) chemistry (**Table 1**, Electrophiles 1E & 9).[114,115] These constructs function like previous examples mentioned above, but instead of ejecting an irrelevant binding ligand leaving group after

a substitution reaction, a prodrug is released inside a target cell, i.e., tumors expressing BTK. Thus, this is a targeted approach for delivering potent inhibitors or cytotoxic agents directly to targets via ligand-directed covalent labeling. We envision related chemistry could have strategic use serving as a masking agent for bifunctional molecules like PROTACs to control function spatially and temporally. Conceptually, covalent engagement of an aberrant protein by a masked PROTAC could be coupled to linker cleavage, generating an accessible E3 ligase-binding domain.

1.7. **Leveraging Covalency in Immune Recruitment**

The immune system is a powerful tool that can be leveraged to target pathogens like cancer with therapeutic interventions. In a healthy individual, the immune system performs immune surveillance of cells to scan for cancer markers. Upon recognition, various clearance mechanisms are initiated to remove the cells before establishment of a tumor. However, through various mechanisms, tumors adapt to evade immune recognition, allowing for unregulated tumor growth. Monoclonal antibodies have been generated to target receptors overexpressed on tumors, allowing for immune recognition. Chemical biologists have taken steps to mimic these interactions with small molecule therapies to reduce drug development times and increase modularity of therapies.

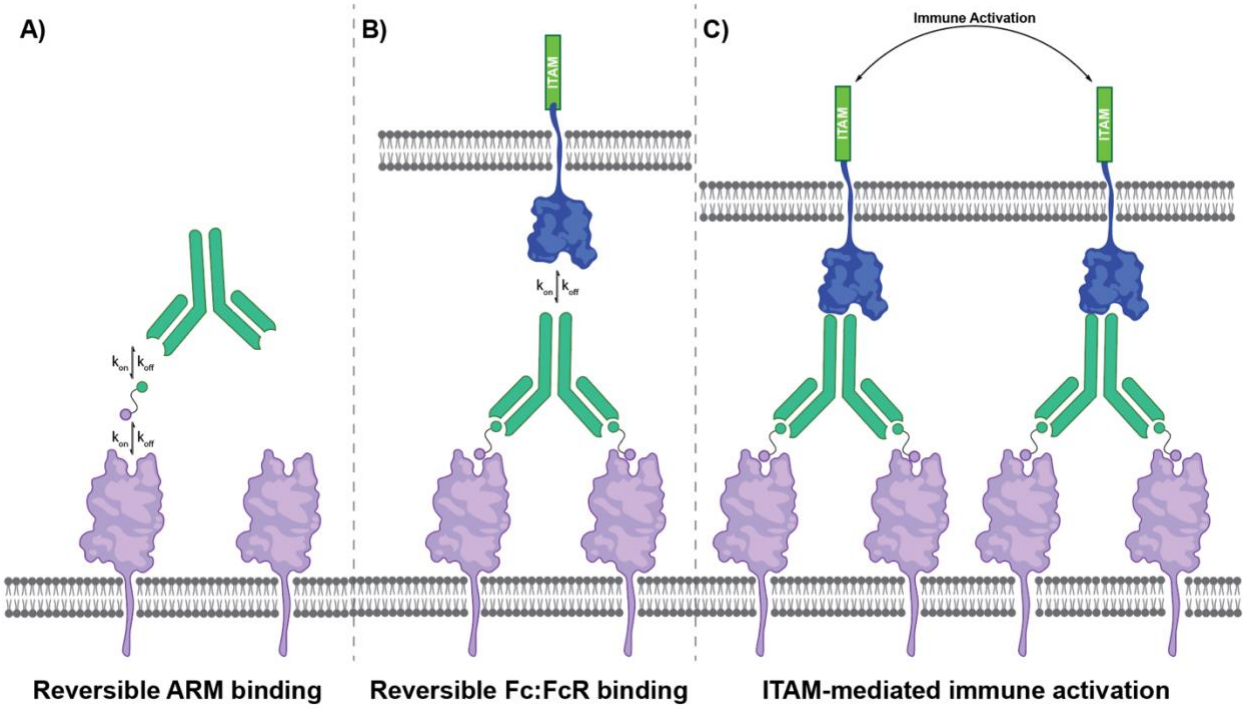

Figure 4. Bifunctional compounds facilitate quaternary complexes at cell/cell interfaces. **A)** ARMs mediate ternary complex formation between antibodies and cancer cell receptors. **B)** Opsonized cancer cells present antibody Fc domains for immune cell FcR recognition. **C)** Clustering of FcRs across the immune cell membrane activates immune effector functions via ITAMs.

As mentioned earlier, ARMs represent another key example of proximity inducing bifunctional molecules, and from a chemical biology perspective analogous to those discussed above.[17–19,116] For example, while PROTACs contain a handle for E3 ligase recruitment and another for target protein binding, ARMs contain a handle for antibody recognition and another for a specific cell surface marker on cancer. ARM function is also conferred through a “ternary complex” akin to PROTACs, however in the case of the former, this comprises a cancer receptor and antibody bridged by the ARM. Resultant “antibody recruitment” or “tumor opsonization” (**Figure 4**), flags previously invisible tumors for FcR-mediated immune recognition and clearance. Theoretically, ARMs can be made to target any antibody which exists in circulation, allowing for broad recruitment of

pre-existing antibodies in vivo against a variety of targets. However, the same limitations for other non-covalent bifunctionals discussed above also apply to ARMs. As such, a covalent immune recruiting (CIR) technology was developed which included covalent ARMs (cARMs). cARMs are designed to irreversibly label antibody fragment antigen-binding (Fab) domains, essentially creating antibody drug conjugates (ADCs) in situ (**Figure 5**).[40,117,118]

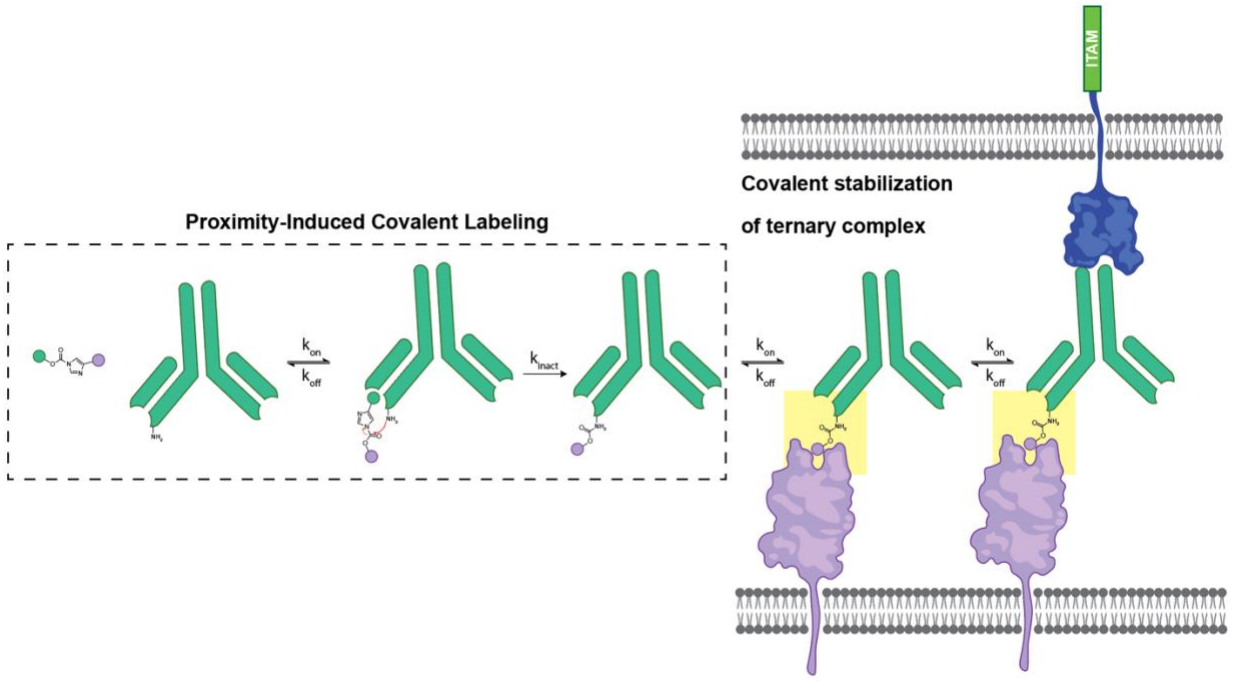

Figure 5. Antibodies are irreversibly reprogrammed in situ with tumor binding ligands. cARMs are among the earliest literature examples of covalent proximity inducing molecules and strategically covalently link to the antibody and not the tumor antigen for the following reasons: 1. The antibody:ARM complex must remain intact for extend periods of time to enable localization from the blood to the tumor site, in the face of fast ARM clearance in vivo. 2. Endogenous ligands are recognized by serim antibodies which compete for ARM binding 3. The limiting interaction in the ARM ternary complex is antibody binding due to an intrinsically weaker K_D e.g., rhamnose for anti-rhamnose IgG Upon localization of antibodies to the cancer cell, the resultant immune complex comprising FcRs bound to tumor opsonized antibody has increased kinetic stability by reducing one reversible binding component (i.e., between ARM and antibody).

Prior to this work, only one general construct existed for the cARM platform. This used a dinitrophenyl (DNP) analogue to target relatively low affinity anti-DNP antibodies

present naturally at low nM concentrations.[40,117] By incorporating a reactive acyl imidazole (**Table 1**, Electrophile 8), anti-DNP antibodies were irreversibly labeled with a prostate specific membrane antigen (PSMA)-targeting, glutamate urea (GU) motif. When compared to non-covalent antibody recruitment, covalency was found to significantly enhance tumoricidal immune function in both antibody dependent cellular phagocytosis (ADCP) and cytotoxicity (ADCC) assays.[40]

In the context of antibody recruitment, reversible covalent bond formation has not yet been explored and the importance of “catalytic turnover” is not well understood. However, we hypothesize current cARMs linked to the antibody would enable such turnover if the antibodies are not degraded during the tumor killing mechanisms of ADCP/ADCC. The ability of cARMs to both reversibly and covalently engage the tumor antigen however may represent a strategic way to further stabilize ternary complexes and enhance immunotherapeutic efficacy while enabling cARM recycling/turnover.

Interestingly, even when target occupancy/ternary complex formation is equivalent between ARMs and cARMs, significant differences have been observed in the magnitude of immune activation. These findings suggest an additional mode of covalent enhancements that arise from differences in target residence time. Here microscopic residence times of individual binding interactions may play a critical role in stabilizing immune complexes and activating effector functions.

1.7.1. Understanding the Limitations of cARMs: A Temporal and Strain Hypothesis

To date, there is still very little known about the mechanism of cARM-induced immune activation. It is insufficient to extrapolate concepts derived from a simple ternary complex in solution to a quaternary immune complex on a cell surface. Based on our findings above, we hypothesize the effect of covalently engaging the antibody leads to enhanced immune activation for reasons beyond forming a higher equilibrium concentration of “quaternary complexes”.

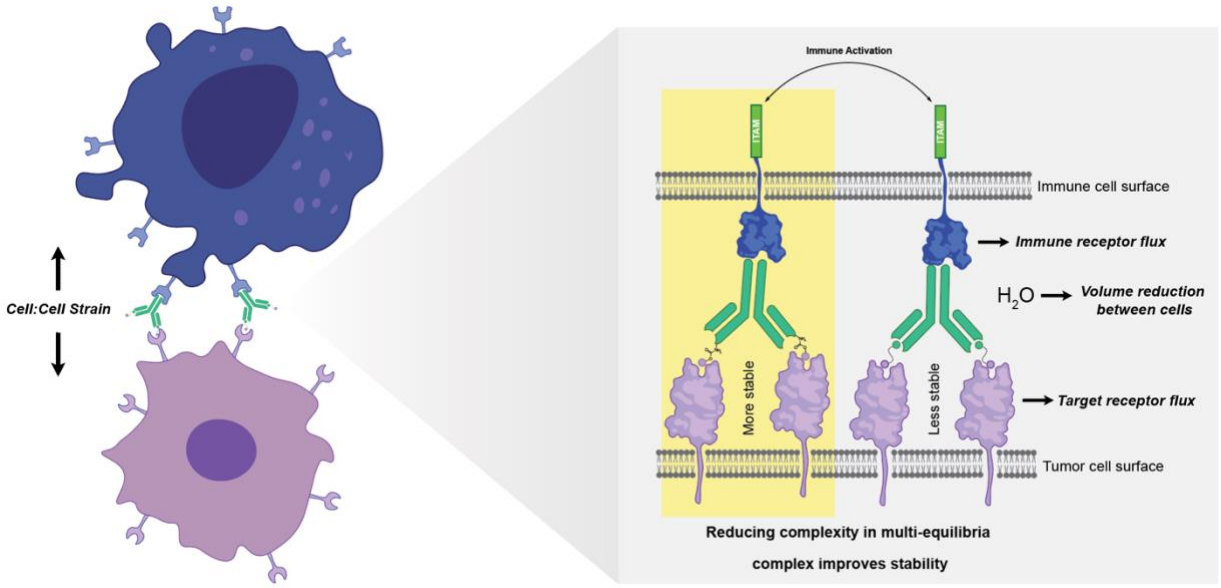

Figure 6. Immune activation may be limited by various opposing forces and governed by factors beyond the “concentration/number of ternary complexes formed. Improving complex stability through covalency is now hypothesized to increase immune receptor residence time and the efficiency of signal propagation towards tumoricidal immune effector functions.

In typical immune synapses, there are several potential opposing interactions/forces that can disfavor receptor binding and subsequent immune activation. Namely, micro clusters of interacting receptors must come together into super clusters

for a sufficient period.[37] Intuitively, this presents both important spatial and temporal considerations that can be modulated via covalent recruitment.

Clustering of receptors in a tight space is required for immunoreceptor tyrosine-based activation motif (ITAM) clusters and exclusion of dephosphorylating phosphatase enzymes.[37] However, this is also a very entropically demanding process, with various forces acting to oppose it including: cell diffusion, receptor diffusion, membrane tension, and the movement of extracellular water/protein solutes (**Figure 6**).

Following a binding event, time is needed for the formation of each cluster and for secondary messengers to be transmitted. Thus, these physically demanding receptor clusters must be held together for enough time for activation. As such the dissociation rate of the bifunctional is a critical parameter that can be essentially eliminated via covalent engagement.

In the context of “quaternary complexes” templated by ARMs (i.e., FcR:antibody:ARM:tumor antigen (**Figure 6**), the two terminal proteins in the complex are membrane bound. To initiate intracellular signalling needed for immune activation, the binding complex must be stabilized through sufficiently small off rates to prevent dissociation of the complex and subsequent receptor diffusion (on the time scale of ITAM signalling), which further decreases the effective concentration of FcR. The overall result can also translate to a loss in apparent affinity due to competing receptor diffusion. Covalent engagement may serve to increase the immune residence time beyond the necessary threshold for ITAM signalling and activation.

Additionally, with respect to the mechanics of this interaction, we need to consider that bringing two cells together is likely much more difficult than bringing two proteins

together. In a typical interaction between a T cell receptor and its target, the interacting proteins are *membrane bound*. This consideration is important, as the strain of each cell and repulsion of negative charge is focused directly on the single binding interaction. Translating this to a quaternary complex introduces strain on three equilibria now, each with transient unbinding and rebinding. The tension between two interacting cells thus has a preventative role in rebinding, limiting immune function. This can also be thought to reduce the apparent affinity of each interaction by accelerating the off rate and deaccelerating the on rate, through sheer force. From this perspective, covalent engagement of proteins within the quaternary complex, e.g., cARMs, can resist these repulsive forces, to enforce activation signalling.

Examining how covalency imparts stability at each component in this quaternary complex is essential in shedding light into how we can improve covalent bifunctionals like cARMs as immunotherapeutics. For example, is function limited by bifunctional affinity towards the antibody, or the target? Is the limiting factor the antibody Fc:FcR interaction itself? If the latter is the case, then covalently targeting the immune receptor directly would be hypothesized to translate to enhanced tumor immunotherapeutic function. By understanding what constraints are limiting in these interactions, we can design better therapeutics as well as better understand the biology of these interactions.

1.8. **Thesis Objectives**

In the last decade, emergence of covalency in cancer therapeutics has revolutionized the field. Covalent drugs exhibit improved target occupancy, selectivity, pharmacokinetics, and function when compared to their non-covalent counterparts.

Examples like cARMs have helped shed light into this. However, both the range of antibody targets and electrophiles used in current cARM platforms remains narrow.

We suggest that protein:protein interactions remain an unexplored platform for cARM therapeutics, despite being so prevalent throughout biological processes. One such interaction occurs through viral opsonization. Herpes simplex virus (HSV) is one such example which uses a range of glycoproteins to target host receptors for entry and subsequent replication. From an immunity perspective, these glycoproteins then present themselves as key targets for an adaptive immune response which physically *block* these viral entry mechanisms through antibody neutralization.

To strategically target these neutralizing antibodies, choice of immunogenic peptide is imperative for success. Notably, the peptide must be i) short enough to synthesize by solid phase peptide synthesis, ii) soluble in physiological conditions, iii) a linear peptide epitope, and iv) not possess its own nucleophilic amino acids capable of inducing intra- or intermolecular cross-linking. We chose to target glycoprotein D (gD) due to the prevalence of antibodies targeting its linear N-terminal peptide epitope (residues 9-22) (**Figure 7**).[119]

By incorporating one of these immunogenic peptide ligands as the antibody binding domain, we also hoped to explore an emerging electrophilic modality; SuFEx. SuFEx presents many advantages over other electrophiles, namely enhanced hydrolytic stability, high reactivity in binding pockets, as well as poising as a latent electrophile when free in solution. Incorporation of SuFEx into a peptide backbone is also easily obtainable under SPPS conditions, making it a prime candidate for this application.

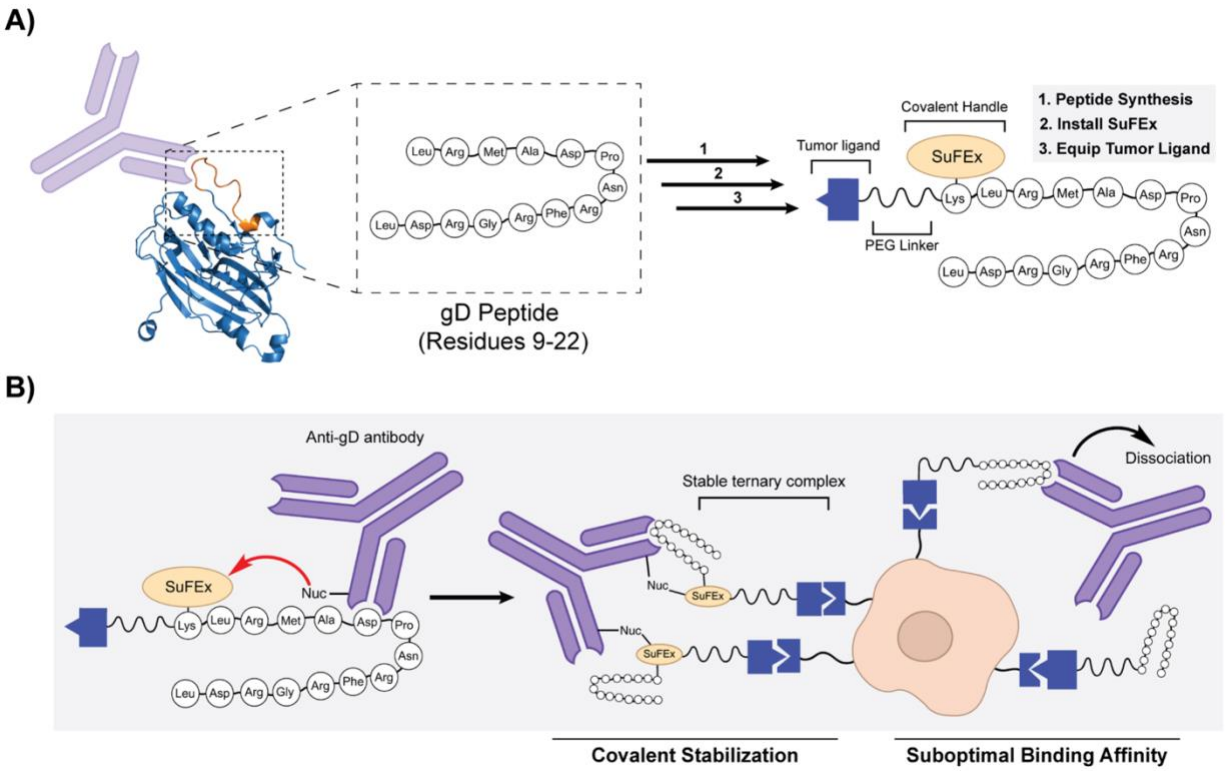

Figure 7. Covalent ligand-directed labeling of anti-gD antibodies enhances immune recognition of target cancer cells. The gD peptide epitope (residues 9-22) from the N-terminal domain of gD was incorporated into a bifunctional cARM. B) After binding, a nucleophilic amino acid in the antibody Fab reacts with the nearby SuFEx electrophile installed on the gD peptide. Covalently reprogrammed anti-gD antibodies can then more effectively template ternary complexes on the surface of cancer cells.

2. Synthesis and Stability of Covalent Peptides

2.1. Objectives

To advance the cARM platform to target protein:protein interactions, a peptide-based approach was chosen. For this proof of concept, the choice of peptide was imperative for targeting a significant antibody population naturally present in human serum. As such, we decided a viral peptide epitope would be sufficiently immunogenic and be targeted by antibodies enriched with the correct isotypes, i.e., immunoglobulin 1/3 (IgG1/3).[120]

We chose to synthesize the N-terminal peptide epitope of gD on HSV-1/2. This short amino acid sequence (residues 9-22) represents one of the most immunogenic peptide epitopes on HSV-1/2 that may be synthesized, i.e., a linear epitope as opposed to a conformational epitope.[119] Thus, this gD peptide (LKMADPNRFRGKDL; "gD") was synthesized by solid phase peptide synthesis (SPPS) with an azide click handle for facile incorporation of affinity handles, fluorogenic handles, or bonafide tumor binding handles.

2.2. **Assembly of cARM Constructs**

Modular assembly of cARM compounds was performed by strain promoted azide alkyne cycloaddition (SPAAC) click chemistry. Peptides were synthesized by SPPS on rink amide resin using fluorenylmethoxycarbonyl (Fmoc) protecting groups. Peptides were made to contain a reactive azide group via azido-lysine incorporation at the N-terminus. SuFEx was incorporated at either the N-terminus (FSY-gD or ASF-gD), an internal phenylalanine residue (gD(F10FSY)), or the C-terminus (gD-FSY) (**Figure 8**). To do this, an O-allyl-tyrosine was installed at the desired location during SPPS, followed by de-allylation using a homogenous palladium Pd(0) catalyst. Subsequent fluorosulfonylation using an 4-(Acetylamino)phenyl]imidodisulfuryl difluoride salt delivered the final electrophilic peptide.

A series of small molecule handles were then synthesized with dibenzylcyclooctyne (DBCO) click handles to participate in the designated SPAAC reactions for final cARM syntheses. These handles include fluorescein-DBCO for fluorescent readouts, biotin-DBCO for binding studies and pull-down assays, as well as GU-DBCO for effector cell assays, i.e., ADCP. Final cARM compounds were synthesized

using 200 µM azido peptide and 200 µM handle-DBCO in 1x phosphate buffered saline (PBS). Reaction completion was verified by liquid chromatography-mass spectrometry (LC-MS) to confirm sufficient purity of final compounds.

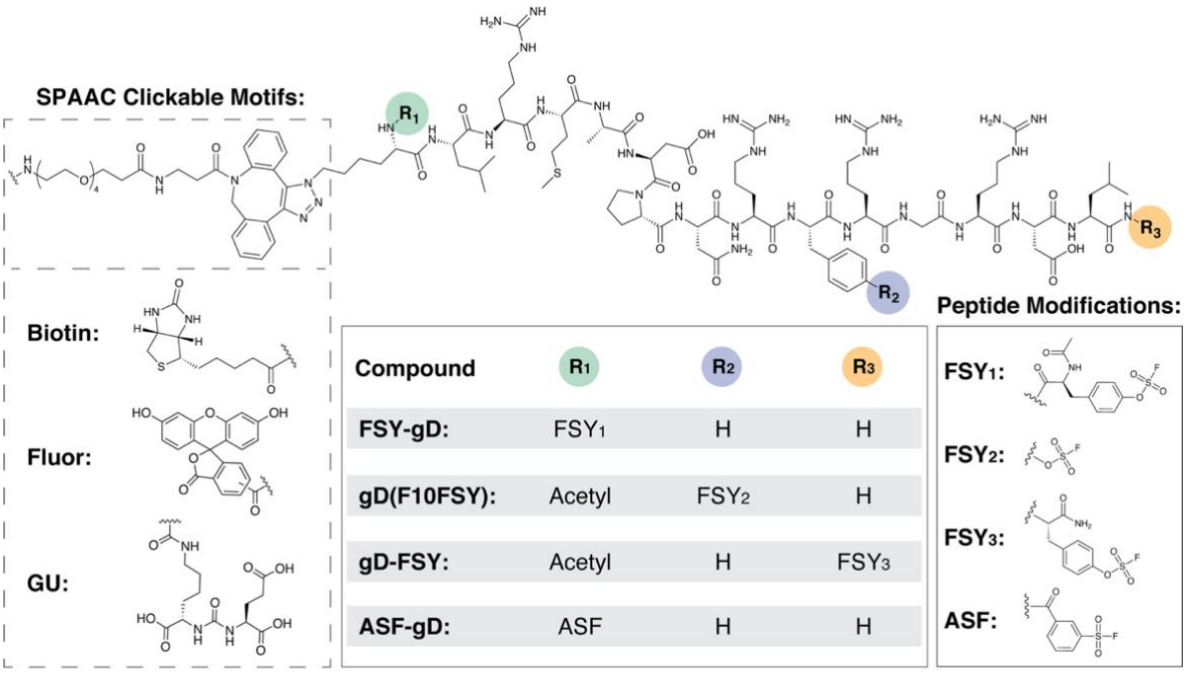

Figure 8. A blueprint of SuFEx-equipped peptide cARMs constructed for this study. SPAAC chemistry was used to modularly attach biotin, fluorescein (fluor), or glutamate-urea (GU) motifs. FSY or ASF electrophiles were incorporated by SPPS into positions R1-R3.

2.3. **Evaluation of SuFEx stability by LC-HRMS**

Stability of the electrophilic handles used in these covalent binders is imperative for function. If the SuFEx group is hydrolyzed at a rate significantly faster than binding and subsequent covalent labeling of target proteins, then the advantages conferred through covalency are not realized. As such, the stability of SuFEx was monitored at near-physiological conditions (i.e., pH 7.4 1x PBS) by high resolution LC-MS (LC-HRMS). The presence of specific m/z -20 amu (loss of H^+ & F^-) and m/z -2 amu (F/OH exchange)

masses were monitored to probe off-pathway cyclization and hydrolysis reactions, respectively. Additionally, the presence of larger masses indicative of intermolecular crosslinking was investigated.

The stability of FSY was found to be negligible over a four-day timespan (**Figure 9**). In comparison, ASF was found to have an estimated half-life of 24 hours (**Figure 10**). ASF degradation was found to be primarily through hydrolysis, seen through a m/z -2 amu loss. No m/z -20 amu loss was observed for these constructs (GU-FSY-gD or GU-ASF-gD), although this was seen for fluor-ASF-gD (data not shown).

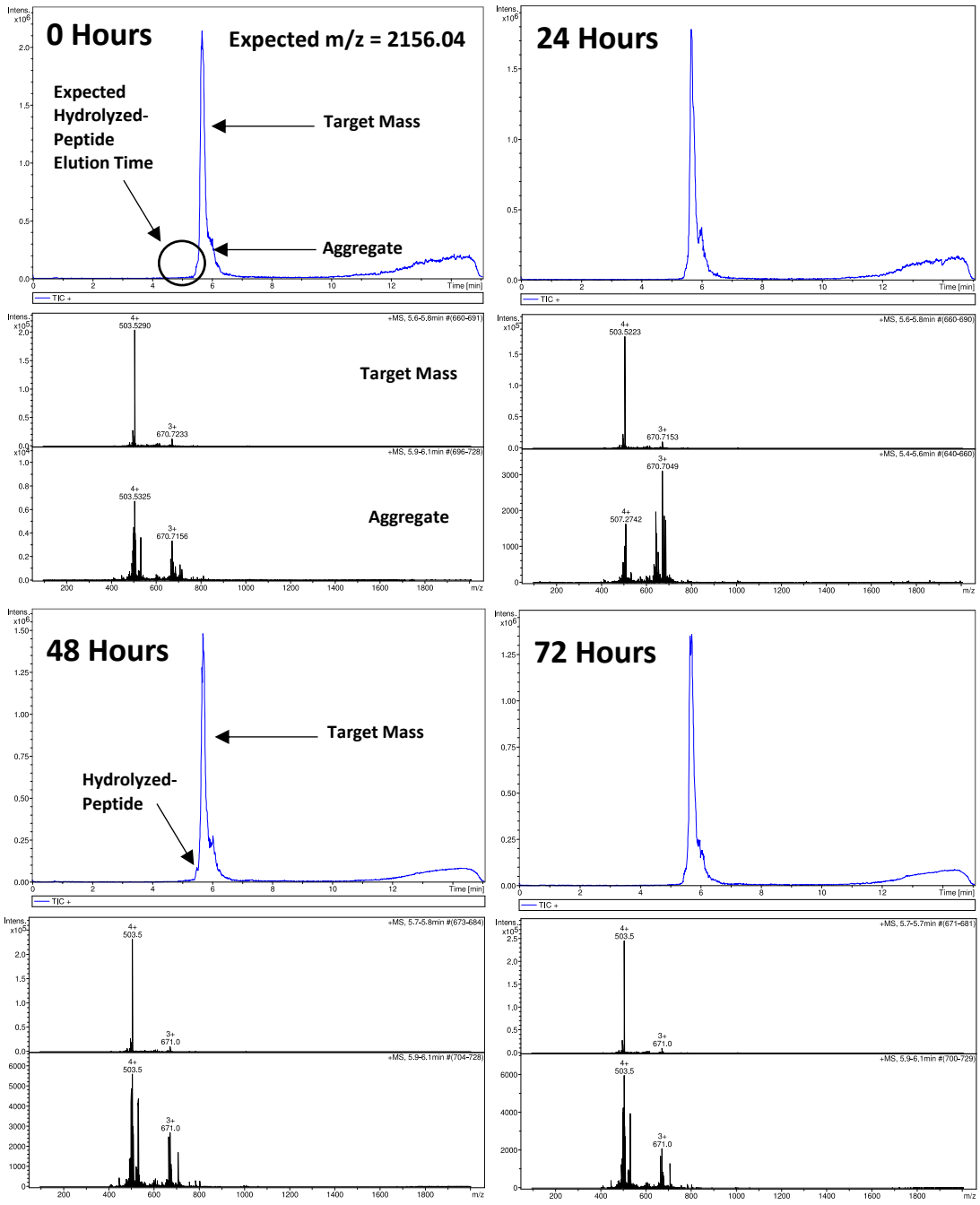

Figure 9. LC-HRMS was used to monitor FSY stability over time. Azido-gD(F10FSY) (500 µM, 1x PBS, room temperature) was analyzed at each indicated timepoint.

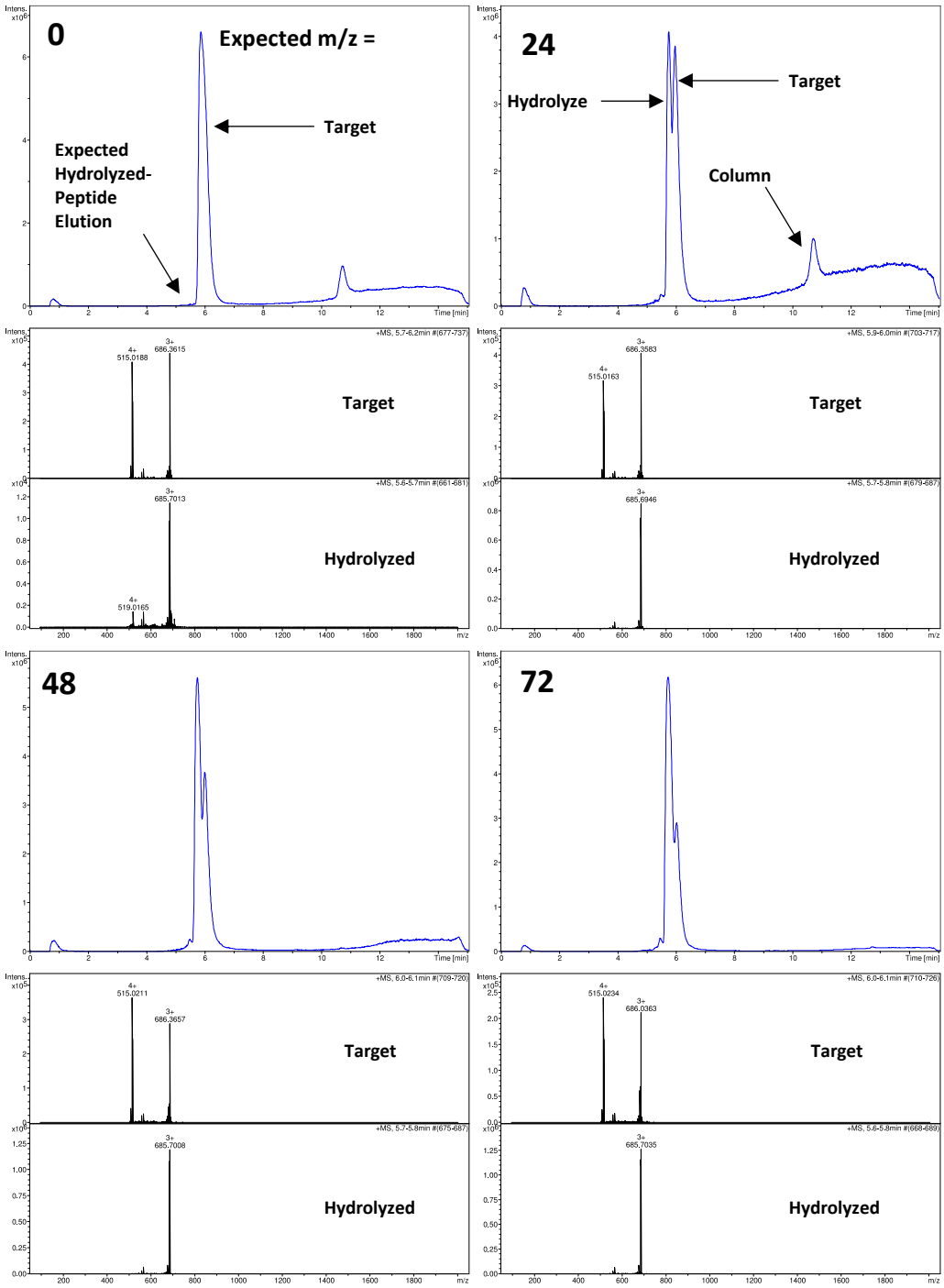

Figure 10. LC-HRMS was used to monitor the stability of ASF. Azido-ASF-gD (500 µM, 1x PBS, room temperature) was incubated and analyzed at each indicated timepoint. After 24 hours, ASF hydrolysis approached 50%, appearing as an $[(M-2)+3H]^{3+}$ peak (F/OH substitution).

2.4. **Discussion**

Demonstrated here is the synthesis of a viral peptide epitope capable of facile SuFEx incorporation. The diversity of reaction conditions needed to synthesize a peptide makes it difficult to incorporate a range of reactive electrophilic handles. For example, amine-reactive groups may not survive the basic conditions required for Fmoc deprotection, which typically uses a reagent like piperidine. Final peptide cleavage conditions also present an issue if electrophile decomposition is acid catalyzed, as these conditions typically range from 90-95% trifluoroacetic acid (TFA). Thus, this modified strategy, representing a conglomerate approach from several literature examples, allows us to incorporate SuFEx chemistry into these sequences with relative ease.[121,122]

Adding to the modularity of this approach is the incorporation of SPAAC click chemistry. By installing azide motifs in a strategic location along the peptide backbone, DBCO-modified handles were appended to peptides with ease. This allowed for the convergent synthesis of complex cARM constructs containing fluorophores, affinity handles, or tumor binding ligands.

Equally as important as being able to attach an electrophile to a ligand is to ensure the electrophile survives physiological conditions until a specific cross-linking reaction can occur. If the half-life of the electrophile is too quick, the advantages conferred through covalency are lost. We demonstrated that SuFEx represents an extremely promising reactive handle in this regard. The less reactive FSY demonstrated no observable hydrolysis under pH 7.4 in 1x PBS buffer. Even the much more reactive ASF exhibited promising hydrolysis rates with a half-life of only ~24 hours. Assuming favorable binding kinetics with sufficiently high antibody titers, these rates are sufficient for covalent labeling

applications. Even in comparison with typical small molecule in vivo clearance rates, the cARM will be eliminated from the body even before it has a chance to become entirely hydrolyzed.[45]

3. Evaluation of Antibody-Mediated Peptide Recognition

3.1. Objectives

Proximity induction between a protein and its ligand is governed by its K_D, composed of k_{on} and k_{off} values. Discerning these values is often the goal of binding studies and allows for accurate predictions of fraction bound protein:ligand complex at a given concentration. To accomplish this, bio-layer interferometry (BLI) was used to monitor antibody association and dissociation from peptide-coated streptavidin biosensors. By fitting these curves to their respective non-linear regression equations, the k_{on} (**Equation 1**), k_{off} (**Equation 2**), and K_D (k_{off}/k_{on}) of the cARM/Fab binding interaction was calculated.

Equation 1. Two Phase Association

$$A)\ \ SpanFast\ =\ (Plateau - Y_0)PercentFast \times 0.01$$

$$B)\ \ SpanSlow\ =\ (Plateau - Y_0)(100 - PercentFast) \times 0.01$$

$$C)\ \ Y\ =\ Y_0\ +\ SpanFast(1 - exp(-K_{Fast}X))\ +\ SpanSlow(1 - exp(-K_{Slow}X))$$

Y_0 = Y value when (X = 0)

Plateau = Y value after infinite X values

K_{Fast} = Fast rate constant, calculated as a reciprocal of the rate constant

K_{Slow} = Slow rate constant, calculated as a reciprocal of the rate constant

PercentFast = Fraction from Y_0 to plateau accounted for by K_{Fast}

Equation 2. One phase exponential decay

$$Y = (Y_0 - NS)(exp(-KX)) + NS$$

X: Time

Y: nm Shift

Y_0: Y at time 0

NS: Binding at very long time points

K: Rate constant (s^{-1})

3.2. **BLI Sensograms for cARM:Antibody Binding**

Association and dissociation rates were compared between each biotin-peptide construct and a model anti-gD antibody, LP14. The rising part of each curve represents LP14 binding to a probe coated with immobilized peptide. Due to the bivalent nature of antibody binding, dissociation was performed in excess competitor gD peptide (200 µM) to prevent Fab rebinding to probe, otherwise known as “avidity” effects.

Results from BLI indicated K_D values centered around 100 nM for each peptide (**Table 2**). Prior to FSY/ASF cARM synthesis, an initial peptide control was created with all lysine to arginine mutations, to ensure no intra- or intermolecular crosslinking. This peptide (biotin-gD-R) was found to possess an improved binding interaction with LP14, most notably through a smaller k_{off}. As such, each cARM was also synthesized to contain these arginine mutations. When FSY was installed at the N-terminal or C-terminal position of the gD peptide (biotin-FSY-gD or biotin-gD-FSY, respectively), there was an additional decrease in k_{off}. However, biotin-gD(F10FSY) saw a significant increase in k_{off}. No observable binding occurred between biotin-gD and isotype IgG, indicating selectivity in the binding interaction.

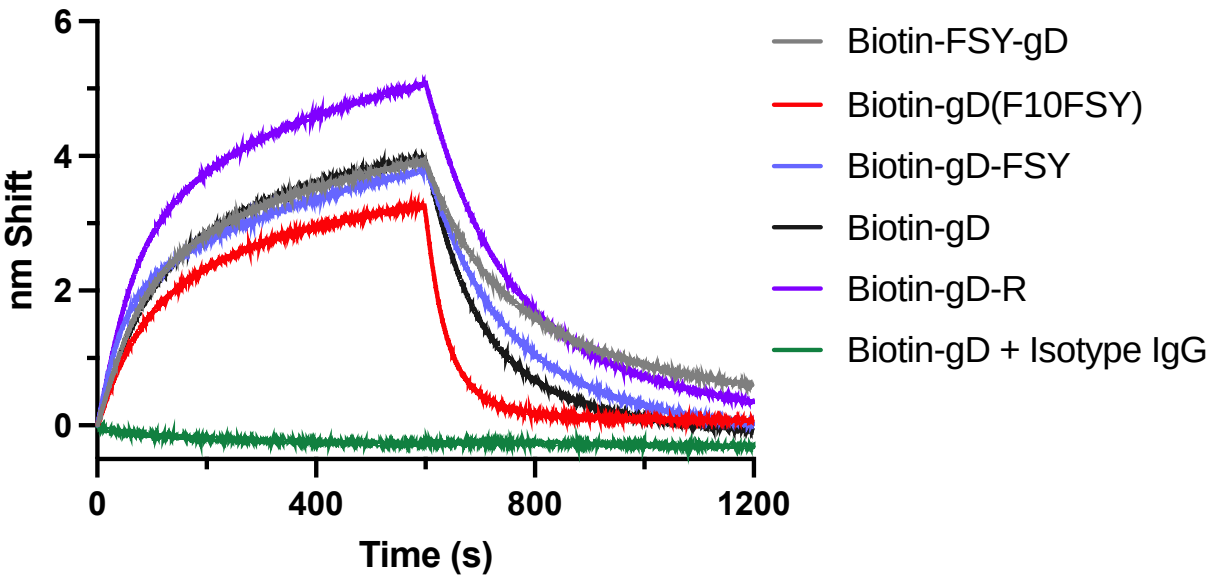

Figure 11. The binding affinity of monoclonal LP14 antibody for each SuFEx cARM was monitored by BLI. Unmodified biotin-gD was used as a reference for baseline specific binding to LP14 antibody. To evaluate the effects of K→R mutations, LP14/biotin-gD-R binding was monitored. Selectivity was monitored through an isotype IgG control. Association was performed with 100 nM LP14/isotype IgG over 600 seconds. Dissociation was performed with 200 µM competitor gD peptide over 600 seconds.

Table 2. Calculated binding constants between LP14 antibody and immobilized gD peptide variants using BLI.

Peptide	k_{on} ($M^{-1}s^{-1}$)	k_{off} (s^{-1})	K_D (nM)
Biotin-FSY-gD	67200 ± 800	$5.688 \times 10^{-3} \pm 4.2 \times 10^{-5}$	84.7 ± 0.8
Biotin-gD(F10FSY)	68800 ± 600	$2.211 \times 10^{-2} \pm 1.7 \times 10^{-4}$	321 ± 3
Biotin-gD-FSY	119000 ± 1000	$6.374 \times 10^{-3} \pm 1.4 \times 10^{-5}$	53.6 ± 0.3
Biotin-ASF-gD	70600 ± 400	$4.784 \times 10^{-3} \pm 2.3 \times 10^{-5}$	67.8 ± 0.7
Biotin-gD	60300 ± 400	$1.130 \times 10^{-2} \pm 3 \times 10^{-5}$	187 ± 2
Biotin-gD-R	77400 ± 500	$6.015 \times 10^{-3} \pm 1.4 \times 10^{-5}$	77.7 ± 0.6

Each cARM also demonstrated tight binding to another monoclonal anti-gD antibody clone, H170 (**Table 3**). Here, very similar binding rates were observed for biotin-FSY-gD, biotin-gD-FSY, and biotin-ASF-gD. Like the results seen from LP14 binding

curves, the internal phenylalanine substitution to FSY resulted in markedly reduced binding parameters (**Figure 12**). In addition to a large increase in k_{off}, the biotin-gD(F10FSY) cARM now exhibited little to no k_{on} value.

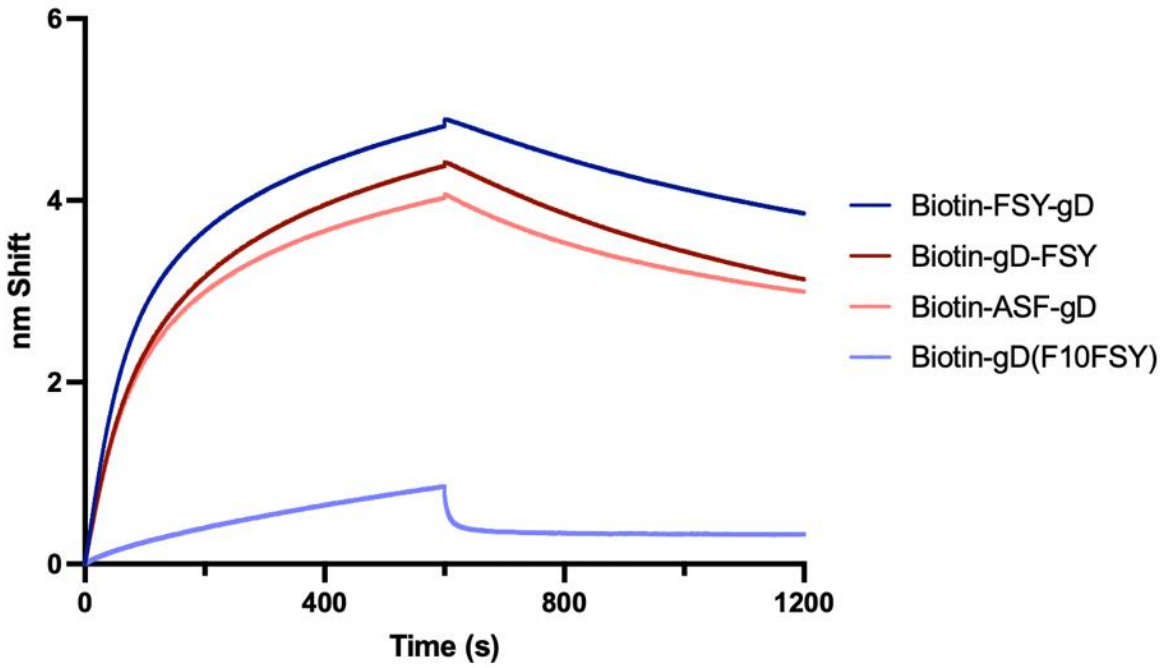

Figure 12. The binding affinity of monoclonal H170 antibody for each SuFEx cARM was monitored by BLI. Association of 100 nM H170 onto cARM-coated biosensors was monitored to calculate k_{on} values. Dissociation was performed in 200 µM competitor gD peptide to extract a k_{off} value. Minimal binding was observed after an F10FSY substitution.

Table 3. Calculated binding constants between H170 antibody and immobilized gD peptide variants using BLI.

Peptide	k_{on} ($M^{-1}s^{-1}$)	k_{off} (s^{-1})	K_D (nM)
Biotin-FSY-gD	89600 ± 400	$1.272 \times 10^{-3} \pm 4 \times 10^{-6}$	14.2 ± 0.1
Biotin-gD(F10FSY)	4800 ± 100	$4.9 \times 10^{-2} \pm 1 \times 10^{-3}$	$1.02 \times 10^{5} \pm 5 \times 10^{3}$
Biotin-gD-FSY	85300 ± 300	$1.595 \times 10^{-3} \pm 4 \times 10^{-6}$	18.7 ± 0.1
Biotin-ASF-gD	84000 ± 300	$2.331 \times 10^{-3} \pm 8 \times 10^{-6}$	27.8 ± 0.2

3.3. **Discussion**

One obvious yet critical aspect of proximity-induced covalent labeling is the actual binding interaction with the target protein. For a targeted covalent therapeutic to succeed, there are several barriers that need to be overcome. Namely, initial binding must occur quickly, observed by a large k_{on} value. If the association of the ligand:protein complex is not very favourable, then the likelihood of binding in vivo is low, represented by low target engagement. However, under saturating conditions, even a small k_{on} value can be overcome, due to the second-order nature of the term.

A more intrinsically limiting constant is how quickly the complex dissociates, governed by a k_{off} value. This first-order constant cannot be overcome by increasing ligand concentrations. If target occupancy is the objective, then still saturating the system is enough, as new binders replace old binders after dissociation. However, if the complex formed requires a specific *residence time*, then the stability, or k_{off} of the interaction becomes more important.

Specifically impacting the success of covalent therapeutics is a combination of residence time, proximity of electrophile to nucleophile, reactivity of the electrophile, and any catalytic contributions provided in the binding pocket. Balancing residence time and electrophilicity is complicated and often comes with trade-offs. For example, by increasing residence time to increase the likelihood of a covalent reaction, the affinity is also increased, and at what point does covalency become irrelevant? Additionally, increasing electrophilicity also increases off-target reactions.

Of importance in this section is the residence time. Here, we observed that these peptides are associated with low to mid nanomolar binding affinities (**Table 2**). The best

binders exhibit k_{off} values on the order of 10^{-3} s^{-1}, while the worst are on the order of 10^{-2} s^{-1}. Interestingly, installation of SuFEx generally reduced the k_{off} term, thus increasing the overall affinity of the ligand. One exception to this observation was when an internal phenylalanine implicated to be important in binding was mutated to a FSY moiety.[119] This mutation resulted in an order of magnitude loss in binding affinity and enhancement in k_{off}. With this observation, we predicted that despite the loss in expected complex residence time, that a possible decrease in distance to a residue like tyrosine would confer quicker covalent labeling, i.e., increased effective molarity.

When binding studies were translated from the model LP14 antibody to another, H170, similar results were seen (**Table 3**). In this system, peptide binding was an order of magnitude tighter, now closer to low nanomolar affinities. The biotin-gD(F10FSY) cARM demonstrated an even greater drop in affinity for H170 relative to other cARM variants. Here, almost no binding was observed, now with a much smaller k_{on} and k_{off}. These results highlight the importance of this phenylalanine, a result previously reported in literature.[119]

4. **Reaction Kinetics and Selectivity of cARMs**

4.1. **Objectives**

The rate of covalent bond formation between a covalent binder and its target protein is an important parameter to optimize. Equally important is to minimize the rate of covalent bond formation between the covalent binder and *non-specific* proteins. To assess these parameters for these peptide cARMs, sodium dodecyl sulfate polyacrylamide gel electrophoresis (SDS-PAGE) was performed to monitor covalent

labeling via a fluorescent readout. By quantifying fluorescent band intensity over time, or compared to control conditions, the reaction kinetics and degree of selectivity was found, respectively (**Figure 13**).

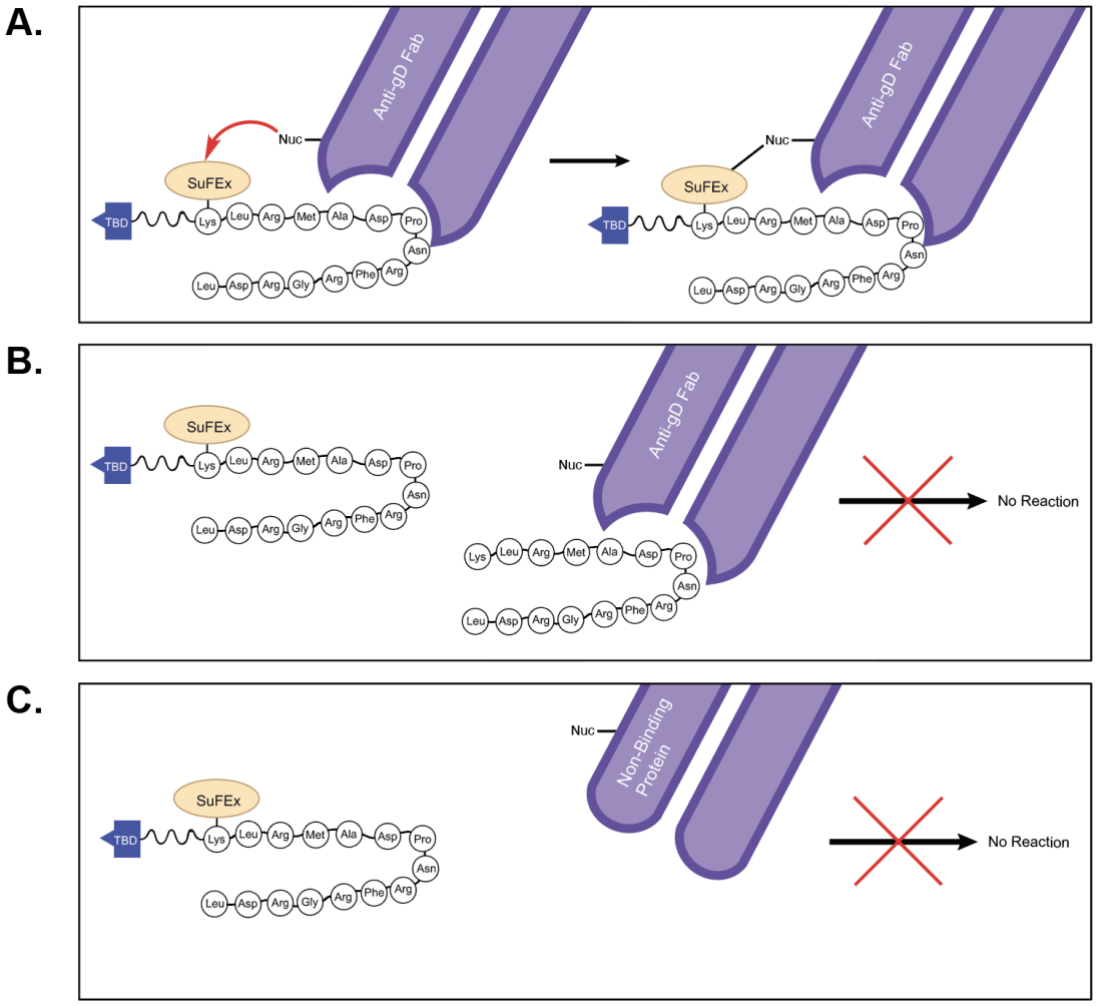

Figure 13. Selectivity in a ligand-direct covalent labeling reaction is granted by a specific binding interaction. **A)** Recognition of the gD peptide epitope by anti-gD Fab domains brings a nucleophilic amino acid in proximity with SuFEx to facilitate a covalent linkage. **B)** Excess competitor peptides prevents peptide:Fab binding and subsequent covalent labeling. **C)** No reaction occurs when the gD peptide remains free in solution.

4.2. Selectivity Controls for Ligand-Directed cARM Labeling of Anti-gD Antibodies

The selectivity of the binding-induced reaction was compared to the bimolecular reaction between cARM and non-binding antibody. To accomplish this, isotype IgG with a similar amino acid composition was used, differing only in the complementary determining regions of the Fab. Additionally, competition experiments were performed by incubating LP14 anti-gD antibody with 100x excess competitor gD peptide to prevent cARM binding.

All selectivity controls indicated a highly selective binding-induced reaction between peptide cARMs and LP14 (**Figure 15**). When FSY was incorporated into the N-terminal, internal, and C-terminal position of the gD peptide, comparable levels of selectivity were observed with non-binding controls. Additionally, labeling predominately occurred at the antibody light chain. When a non-covalent fluorescent peptide control was incubated with LP14, no labeling was seen, suggesting covalency is required to form fluorescent bands. Despite the higher reported reactivity of the ASF electrophile, comparable selectivity for LP14 was found under the same conditions. Interestingly, it was found that preference for light chain labeling switched to heavy chain for ASF.

To demonstrate the versatility of these covalent peptides, selectivity experiments were performed with an additional monoclonal anti-gD antibody, H170. Here, only N-terminal incorporation of SuFEx mediated a covalent linkage, either for FSY or ASF electrophiles. Both the internal and C-terminal FSY variants demonstrated no reactivity. In this new antibody format, covalent labeling between the fluor-ASF-gD and H170 was observed only at the light chain now, as opposed to heavy chain labeling seen with LP14.

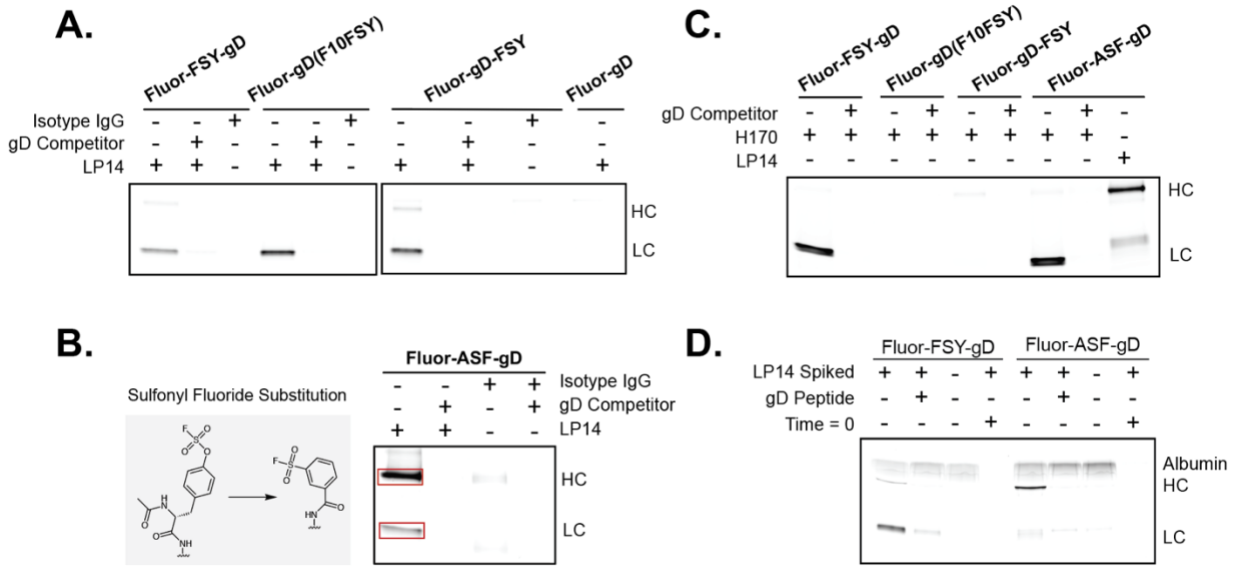

Figure 14. The selectivity of ligand-directed covalent labeling was assessed by fluorescence SDS-PAGE. **A)** FSY cARMs (2 µM) form a fluorescent band with LP14 (1 µM) light chains by SDS-PAGE. This band was prevented when in the presence of excess gD peptide competitor (200 µM), or when LP14 was substituted for isotype IgG (1 µM). Coomassie stained image is provided in the SI (**Figure 48**). **B)** Substituting ASF for FSY at the gD N-terminus results in HC labeling. Excess gD peptide competitor prevents labeling, and no reaction occurs with isotype IgG. Coomassie stained image is provided in the SI (**Figure 49**). **C)** Covalent H170 labeling was prevented with excess gD peptide competitor. Only the N-terminal functionalized cARMs led to a successful covalent adduct. Coomassie stained image is provided in the SI (**Figure 50**). **D)** LP14 (1 µM) antibody was spiked into 60% human serum to assess selectivity in serum, in the presence and absence of competitor gD peptide (**Figure 51**).

4.3. **Reaction kinetics of peptide cARMs**

Analysis of proximity-induced covalent labeling reaction kinetics were observed under pseudo first-order conditions. To do this, concentrations of each binding species were brought to 10x that of the observed binding affinity. As well, the concentration of cARM was made to be 10x that of the antibody Fab to ensure maximum binding at later reaction timepoints. By ensuring pseudo first-order conditions, the reaction kinetics

followed a first order curve and was only dependent on the concentration of antibody Fab and the rate constant of the reaction. Using GraphPad Prism software for non-linear regression and **Equation 2**, the rate constant, k_{inact}, and half-life of the reaction was found.

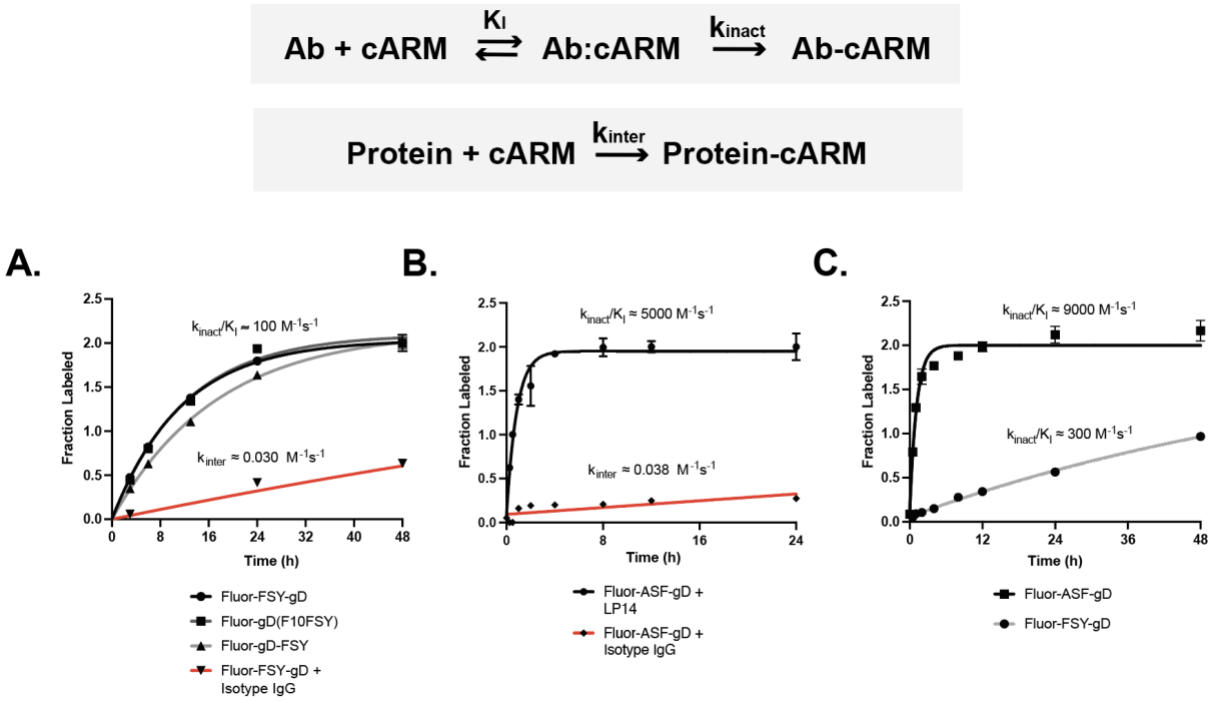

Figure 15. Ligand-direct covalent labeling kinetics between cARMs was investigated by fluorescence SDS-PAGE. Labeling rates between FSY-substituted cARMs and LP14 was performed under pseudo-first order conditions (10x excess cARM, 10x K_D). The non-specific bimolecular rate constant, k_{inter}, was found between fluor-FSY-gD and isotype IgG (red). Gel images provided in supplementary information (see Supporting Information **Figure 52**). B) Labeling rates between the ASF-substituted cARM and LP14 was performed as above. A bimolecular rate constant was calculated similarly with isotype IgG (red). Gel images provided in supplementary information (see Supporting Information **Figure 53**). C) The rate of labeling was compared between H170 and fluor-FSY-gD or fluor-ASF-gD and was performed as above. Gel images provided in supplementary information (see Supporting Information **Figure 54** & **Figure 55**).

Labeling studies between LP14 and each FSY cARM were conducted to monitor how FSY location impacts k_{inact}. By setting up bulk incubations, timepoints were generated by

aliquoting and freezing indicated timepoints for analysis by SDS-PAGE. This was done to maintain consistent concentrations of antibody and cARM between each timepoint. Technical replicate values were created (n=2) by loading each sample twice to control for differences in band diffusion between gels.

Despite significant changes in FSY location along the gD peptide backbone, calculated k_{inact} values remained consistent, i.e., on the order of magnitude of 10^{-5} s^{-1} between each cARM (**Figure 15** & **Table 4**). In comparison, ASF incorporated at the N-terminus of the gD peptide (fluor-ASF-gD) reacted ~10x faster with a $k_{inact} > 10^{-4}$ s^{-1} (**Figure 15** & **Table 4**).

The ratio of the pseudo first-order rate constant k_{inact} to the second order bimolecular rate constant k_{inter} provides information about reaction effective molarity (EM). To determine k_{inter} values of fluor-FSY-gD and fluor-ASF-gD, bimolecular reaction rates between isotype IgG and each cARM were determined. Despite their differences in intrinsic reactivity reported in literature, both FSY and ASF had k_{inter} values ~ 0.03-0.04 $M^{-1}s^{-1}$ (**Table 5**). As such, the rate enhancement or EM of ASF is ~10x greater than FSY.

Covalent labeling rates were then determined between fluor-FSY-gD or fluor-ASF-gD and H170 antibody. Here, the k_{inact} value of FSY was reduced ~10-fold, whereas ASF maintained a k_{inact} value ~10^{-4} s^{-1} (**Table 6**). Despite these results, stronger binding observed in BLI assays feed into greater second-order rate constants for each cARM (**Table 6**).

Table 4. Rate constants calculated for covalent peptides and LP14 mAb.

Peptide	k_{inact}	k_{inact}/K_I	Half Life (h)
Fluor-FSY-gD	$2.41 \times 10^{-5} \pm 3.3 \times 10^{-6}$	280 ± 40	8 ± 1
Fluor-gD(F10FSY)	$2.51 \times 10^{-5} \pm 6.8 \times 10^{-6}$	78 ± 22	8 ± 2
Fluor-gD-FSY	$1.62 \times 10^{-5} \pm 3.6 \times 10^{-6}$	300 ± 100	12 ± 2
Fluor-ASF-gD	$3.31 \times 10^{-4} \pm 8.5 \times 10^{-5}$	4900 ± 1300	0.6 ± 0.1

Table 5. EM enhancements between N-terminal covalent peptides and LP14 mAb.

Peptide	k_{inter} ($M^{-1}s^{-1}$)	Rate Enhancement	*EM* (mM)
Fluor-FSY-gD	0.030 ± 0.004	9000 ± 2000	0.8 ± 0.2
Fluor-ASF-gD	0.038 ± 0.01	130000 ± 40000	8.6 ± 4.7

Table 6. Rate constants calculated for N-terminal covalent peptides and H170 mAb.

Peptide	k_{inact}	k_{inact}/K_I	Half Life (h)
Fluor-FSY-gD	$4 \times 10^{-6} \pm 2 \times 10^{-6}$	300 ± 10	50 ± 20
Fluor-ASF-gD	$2.5 \times 10^{-4} \pm 6 \times 10^{-5}$	9000 ± 2000	0.8 ± 0.1

4.4. **Discussion**

With the development of covalent proximity-inducing molecules, it is important to understand the reaction kinetics and selectivity of the binding-induced cross-linking reaction. What separates a good from a bad covalent binder is the ability to form a fast covalent linkage with a specific protein. A fast covalent labeler has the added benefit of improved target occupancy at low concentrations, allowing for i) lower dosing protocols, and ii) improved potency in extracellular environments where local concentrations may be lower. This advantage is conferred through either a tight binding affinity (i.e., low K_D)

and/or a fast inactivation constant (i.e., k_{inact}) that leads to a higher second order rate constant, k_{inact}/K_I.

We were able to assume pseudo-first order conditions based **Equation 3**, which describes the formation of a reversible Fab:peptide complex. Here, we estimate $K_I = K_D$, a value which describes the concentration of inhibitor for half-maximal ligand-directed covalent adduct formation.[123] We also assume that total Fab (Fab_T) domains are available for binding. After binding, a pseudo-intramolecular irreversible covalent labeling step occurs between the electrophile and a nucleophile in the Fab, whose rate is represented by k_{inact}. By ensuring saturating conditions, i.e., [peptide] >> K_D, the model may be simplified as a pseudo first-order reaction, where $k_{obs} = k_{inact}$ (

Equation 4).[123] Following this rationale, the concentration of bound complex remains sufficiently high until [Fab] << K_D. We assume that after this point, the fluorescent changes become negligible, and thus the bulk of the reaction used to calculate k_{obs} holds saturating conditions, allowing for this equation to be used.

Equation 3. Equation for reversible binding between covalent peptides and total Fab domains.[124]

$$Compound + Fab \underset{\rightleftarrows}{K_I} Fab{:}\,Peptide$$

$$A)\ K_I = \frac{[Fab][Peptide]}{[Fab{:}\,Peptide]}$$

$$B)\ [Fab{:}\,Compound] = \frac{[Peptide][Fab_T]}{[Peptide] + K_I}$$

Equation 4. Equation for irreversible covalent labeling of Fab domains by our peptides.[123]

$$k_{obs} = \frac{k_{inact}[Peptide]}{K_I + [Peptide]}$$

Another property of a good covalent binder is negligible reactivity with non-binding proteins. By using a less reactive electrophile, or a latent electrophile, the reaction can be controlled solely through proximity with a highly nucleophilic amino acid like cysteine, lysine, or tyrosine.[55] As such, selectivity of covalent binders is predominantly controlled through both specific binding and covalent handle electrophilicity.

Unexpectedly, it was found that FSY location along the peptide sequence played a minimal role in determining the reaction rate when in the Fab binding site. This suggests that there is a degree of flexibility in the required effective molarity of these constructs. It is likely that flexibility in the binding interaction confers sufficient proximity to each respective nucleophile regardless of FSY location, so long as FSY does not impair binding.

In comparison, ASF reaction rate vastly exceeded that of FSY, a result in agreement with general reactivity/electrophilicity trends between the two chemistries.[125] A more reactive electrophilic centre is more prone to nucleophilic attack, suggesting this is a rate limiting step in the reaction mechanism. In comparison, if fluoride departure were a rate limiting step, we would see comparable reaction rates due to similar effects imparted by neighbouring amino acids in the binding pocket.

However, once outside the binding pocket, reaction rates between ASF and FSY deviate from their known reactivities. Here, both chemistries demonstrate no significant difference in the bimolecular reaction rate with a non-binding IgG. This contrasts with previous results in literature which suggest FSY behaves as a *latent electrophile*, or one which only reacts once activated in the binding pocket.[55] We suggest that neighboring arginine residues along the peptide backbone "activate" FSY to facilitate a bi-molecular reaction. It is even suggested in literature that arginine has this effect, which represents a significant portion of this peptide's amino acid profile.[81] This hypothesis also agrees with nucleophilic attack being the rate limiting step within the binding pocket, due to the catalytic nature of nearby amino acids promoting fluoride departure, i.e., through hydrogen bonding, acid catalysis, or general electric fields.[56]

These results suggest that SuFEx can be effectively used on a peptide backbone for proximity-induced covalent labeling. With relative ease, incorporation of SuFEx into desired sites along the sequence allows for rate or binding optimization. Additionally, by modifying the SuFEx chemistry itself, reactivity may be tuned to optimize both reaction rates and selectivity under physiological conditions.

5. **Mass Spectrometry Analysis of Covalently Modified LP14**

5.1. **Objectives**

Mass spectrometry presents another method to validate covalent protein modifications. As opposed to fluorescent visualization of protein bands in SDS-PAGE, mass spectrometry enables visualization of a specific mass difference between unmodified and modified antibody. Additionally, mass spectrometry serves as one of the

only ways for determining the site of modification between the antibody and cARM. By modifying LP14 antibody with both fluor-FSY-gD and fluor-ASF-gD, MS will allow for confirmation of labeling as well as the degree of labeling, i.e., number of cARMs per antibody. By then enzymatically digesting these antibody-cARM conjugates and analyzing the peptide fragments by LC-MS/MS for de novo sequencing, the site of labeling was determined.

5.2. **Results**

Through a collaboration with Bioinformatics Solutions Inc. based in Waterloo, covalently modified LP14 was analyzed by intact LC-MS to confirm a specific mass change corresponding to the respective cARM. To do this, fluor-FSY-gD and fluor-ASF-gD were incubated with LP14 for 48 hours to promote complete reaction conversion. The FSY cARM was found to have 100% covalent labeling through this method (**Figure 16C**). In comparison, the ASF cARM was observed to have almost no covalent adduct with the LP14 antibody (**Figure 16B**).

To determine the site of labeling, modified LP14 underwent a trypsin digest with subsequent LC-MS/MS. It was expected that because the cARM probe itself was a peptide, that the appended molecule would be cleaved at this closest arginine, leaving fluorescein-PEG7-KLR. Sequencing data supports a covalent linkage at the N-terminal amine of the light chain (**Figure 16D**). No significant linkage was observed for the ASF cARM.

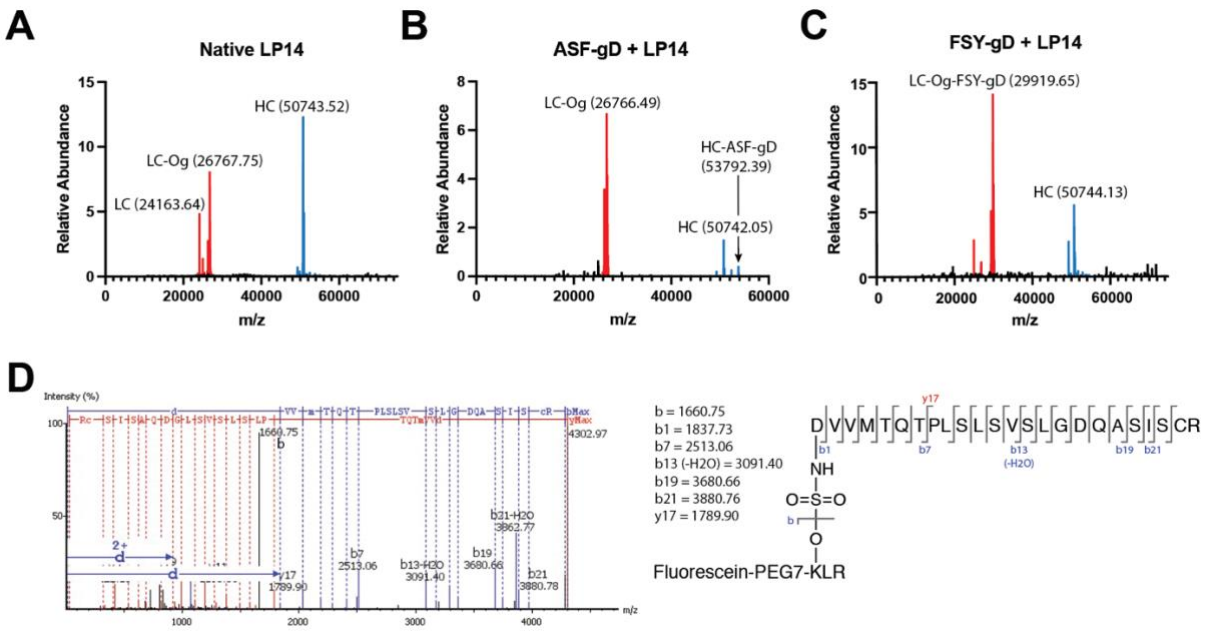

Figure 16. Analysis of covalently modified LP14 using mass spectrometry. Intact mass chromatograms were obtained for **A)** native LP14 antibody (unmodified), B) fluor-ASF-gD labeled LP14 antibody, and C) fluor-FSY-gD labeled LP14 antibody. The site of labeling between fluor-FSY-gD and LP14 was found to be the N-terminal amine of the light chain (aspartic acid residue).

5.3. **Discussion**

Mass spectrometry analysis of covalently modified LP14 confirmed a successful and site-specific modification using the FSY cARM. In contrast, the ASF cARM appeared to have been unsuccessful in forming a covalent linkage. These results directly contradict all labeling experiments thus far and serves as indirect evidence for a less stable covalent adduct with an amino acid other than lysine. We suggest that the more reactive ASF electrophile allows this cARM to switch modification sites from the light to heavy chain with either a tyrosine or histidine. The resulting aryl sulfonate ester or aryl sulfonamide linkage is then stable in solution conditions, however results in almost complete fragmentation in the gas phase during MS.

By using next generation de novo sequencing of digested LP14-cARM conjugates, we determined the Fluor-FSY-gD site of modification. Modification sites were determined based on differences between unmodified and modified amino acid side chains, typically designated as post-translational modifications. However, by observing a specific mass shift corresponding to our probe along a peptide until the amino acid conjugation site, but not after, the site of conjugation was found.

Interestingly, the nucleophile which reacted with the FSY electrophile was the N-terminus of the entire light chain. These a α-amino groups have a lower pKa than ε- NH_2 groups on lysine. As such, they tend to act as better nucleophiles and are often the target of bioconjugation strategies because of this. Altogether, this result further supports the claim for a difference in chemoselectivity between FSY and ASF. It would be unsurprising if a closer, less nucleophilic amino acid were in closer proximity than this α-NH_2 group, which ASF can react with, but FSY cannot.

6. **Evaluation of Biological Ternary Complexes using ADCP Assays**

6.1. **Objectives**

Forming a successful ternary complex between two target proteins is essential to elicit a productive biological response. Even two optimized binary binding systems are often hindered when connected by a linker. Known as negative cooperativity, this occurs when unfavourable interactions between each protein reduce the apparent affinity of either binding ligand. As such, it is important to demonstrate adequate ternary complex formation to ensure a successful binding interaction between A:B:C. Further complicating this is the requirement for a productive interaction, such that the residence time of each

binding interaction is sufficient for the desired biological response. The aims of this section are to therefore investigate whether a) a ternary complex can form between antibody:cARM:receptor, and b) this interaction leads to a biological response like antibody dependent cellular phagocytosis (ADCP).

6.2. **Ternary Complex Formation Using BLI**

BLI was used to directly monitor ternary complex formation between LP14:cARM:PSMA (**Figure 17**). It was first assumed that in a natural setting, the LP14:cARM interaction would occur prior to cARM:PSMA, and so the former was pre-incubated for the indicated periods of time. By loading probes with antibody-cARM, followed by a competitor condition to remove non-covalently bound cARM, the direct impact of covalency was monitored. Covalently labeled LP14 was then placed into wells with PSMA to monitor association, where the binding rate and amplitude are indicative of LP14-cARM labeling.

It was found that there was a time-dependent reaction between GU-FSY-gD and LP14, whose rate matched values found through SDS-PAGE experiments. Without antibody, there was no increase in signal, and without GU-FSY-gD there was minimal non-specific binding to the BLI probes.

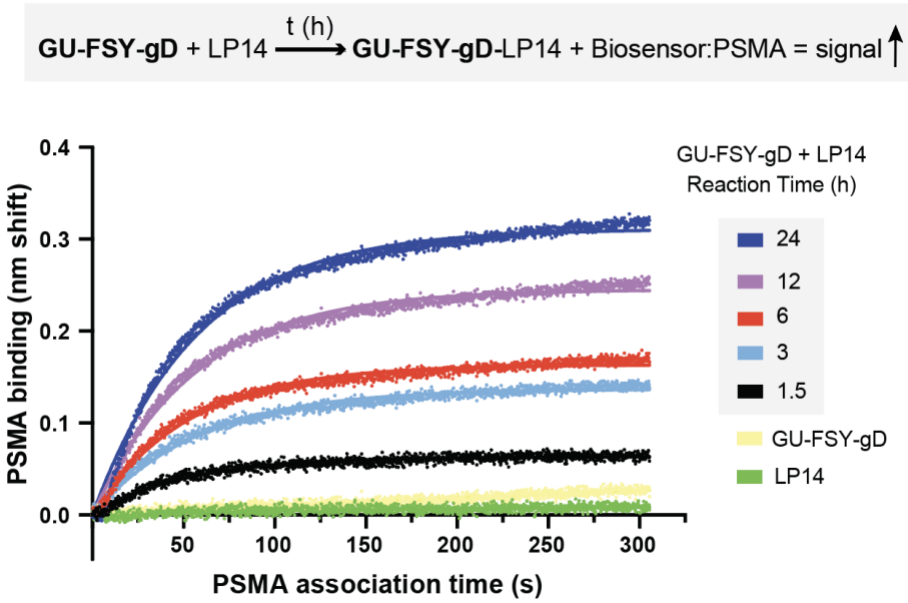

Figure 17. Ternary complex formation was monitored between covalently modified LP14-GU and PSMA in BLI. Covalent labeling was performed by pre-incubating GU-FSY-gD (15 µM) with antibody (750 nM) at different timepoints before performing a 10x dilution. Before association with PSMA (500 nM), probes were dipped in excess competitor to disrupt non-covalent interactions.

6.3. **Evaluation of ADCP as a Measure of Biological Ternary Complexes**

The capacity for target opsonization and subsequent immune activation was evaluated using two-colour flow cytometry ADCP assays. By staining activated monocytes and PSMA-expressing tumor cell lines with different dyes, the co-localization of each colour in one cell was visualized by flow cytometry. The extent of ADCP, or phagocytosis, can be measured by comparing the movement of the target cell population from a baseline control to a population containing both dyes. Both GU-gD (non-covalent) and GU-FSY-gD (covalent) were pre-incubated with LP14 overnight before introduction to activated monocytes and target cells. To determine how dosage influences ADCP, a dilution series of antibody-cARM or antibody:ARM was prepared.

6.3.1. **ADCP of HEK-PSMA Cells**

An initial assessment of ADCP was conducted by using HEK293 cells engineered to express PSMA (HEK-PSMA). This engineered cell line typically has high PSMA expression and so provides an “ideal” readout for low affinity binders.

The cARM construct was found to significantly outperform the ARM at concentrations below 6.25 nM antibody (**Figure 18**). However, at higher concentrations, both cARM and ARM displayed equal potencies for inducing ADCP of HEK-PSMA cells. To demonstrate covalency, excess competitor gD peptide was spiked into both the ARM and cARM incubations prior to initiation of ADCP. As expected, no phagocytosis was observed for the ARM “quench” control, however, the quenched cARM maintained function. Selectivity was demonstrated by adding excess gD competitior *prior* to the cARM/antibody incubation. Here, no ADCP was observed for either ARM or cARM, suggesting no non-specific covalent cross-linking occurred away from the Fab binding site. Similarly, LP14 alone, ARM/cARM alone, or ARM/cARM with isotype IgG were not found to induce ADCP.

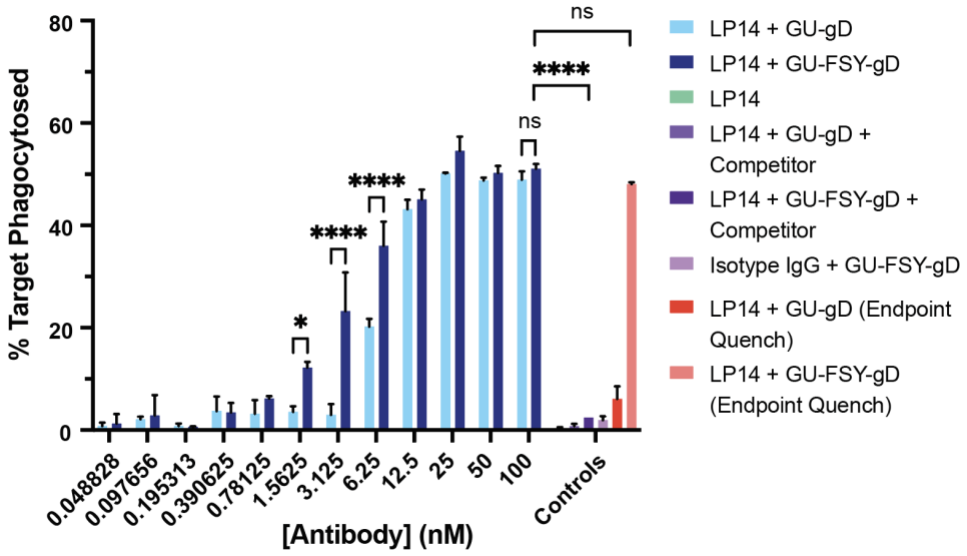

Figure 18. ADCP analysis of HEK-PSMA cells using two-color flow cytometry. GU-gD or GU-FSY-gD (2 eq) were incubated with LP14 (1 eq) for 24 hours before diluting 4x to the indicated concentrations. Phagocytosis was monitored by comparing FL-1 (DIO) dye stained HEK293 (PSMA+) cell population and the FL-4 (DID) dye stained u937 human monocyte population by flow cytometry. Selectivity was demonstrated by pre-equilibrating LP14 with gD peptide (100 µM) prior to cARM addition. Covalency was demonstrated by adding gD peptide (100 µM) after the 24-hour incubation with ARM/cARM. Data was quantified from two replicate measurements and summarized as the mean and standard error of the mean.

6.3.2. **Isogenic HEK Control Cell Line**

To ensure the PSMA binding interaction at the cancer cell surface was responsible for observed phagocytosis, a PSMA negative HEK cell line was used. Covalent GU-FSY-gD was compared to GU-gD for their ability to bridge LP14 to the PSMA negative cell line (**Figure 19**). No phagocytosis was observed in any condition, highlighting the importance of PSMA in this interaction.

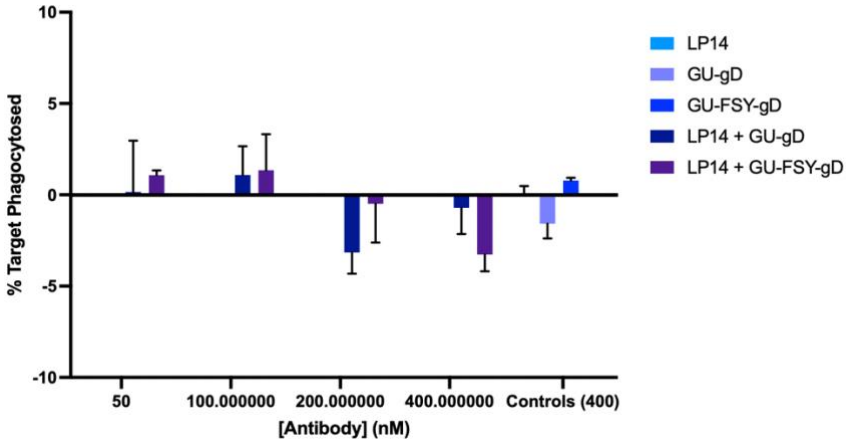

Figure 19. Isogenic control HEK cells with no PSMA expression were used to assess selectivity at the tumor targeting end in two-color flow cytometry ADCP assays. GU-gD or GU-FSY-gD (2 eq) were incubated with LP14 (1 eq) for 24 hours before diluting 4x to the indicated concentrations. Phagocytosis was monitored by comparing FL-1 (DIO) dye stained HEK293 (PSMA+) cell population and the FL-4 (DID) dye stained u937 human monocyte population by flow cytometry. Data was quantified from two replicate measurements and summarized as the mean and standard error of the mean.

6.3.3. **ADCP of LnCAP and C4-2 Cells**

To expand the target scope, lower antigen expressing tumor cell lines were used in similar ADCP experiments. Specifically, prostate cancer cell lines lymph node carcinoma of the prostate (LnCAP) (**Figure 20A)** and C4-2 (**Figure 20B**) were used. Here, covalency improved function at all concentration ranges where phagocytosis was observed. Like HEK-PSMA cells, all controls indicated a highly specific covalent labeling reaction occurred between cARM (GU-FSY-gD) and LP14. Additionally, controls confirm the need for a combination of target cells, ARM/cARM, specific antibody, and monocytes for the induction of phagocytosis.

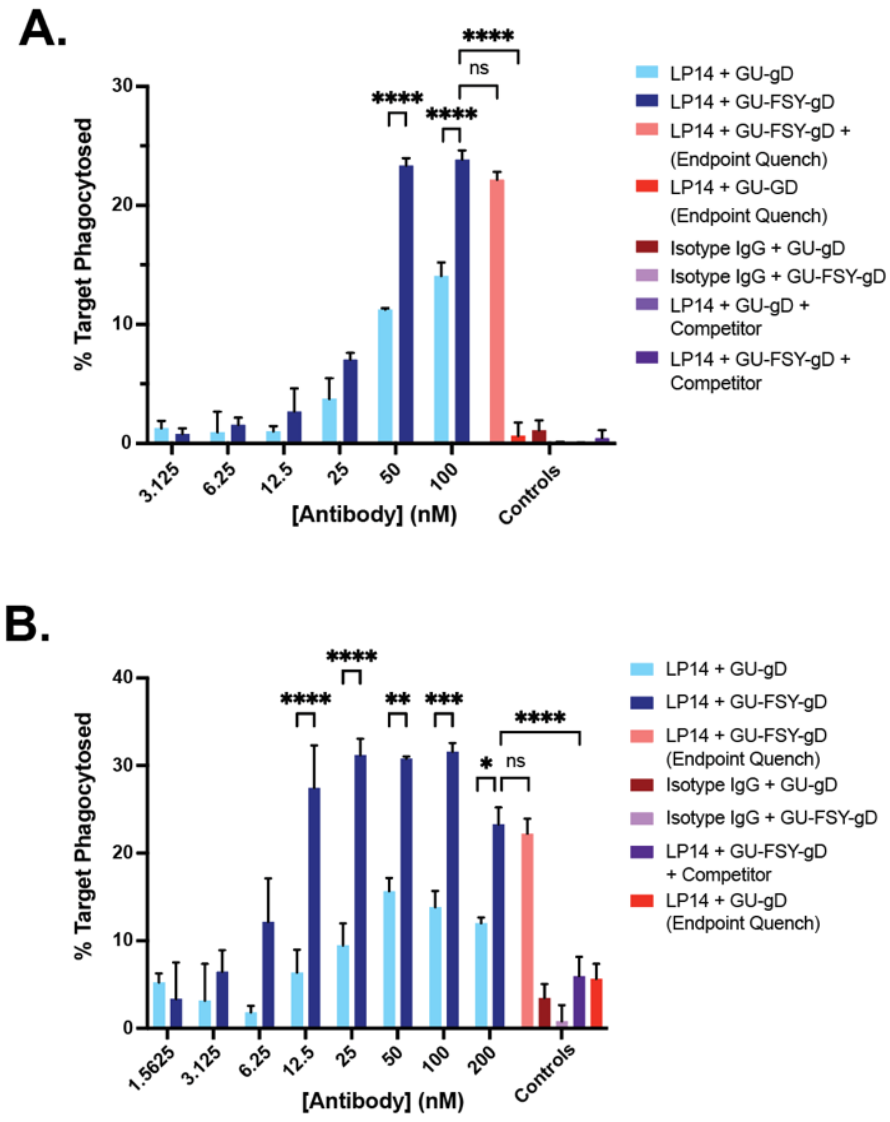

Figure 20. ADCP analysis of tumor targeting with lower antigen density tumor cell lines.Two-color flow cytometry was used to anayze ADCP of A) LncAP and B) C4-2 cells. Each experiment was performed as above, with exception of the target cell lines used.

6.3.4. **Antibody Recruiting Experiment Using HEK-PSMA Cells**

Total antibody recruitment to PSMA expressing HEK cells was monitored using flow cytometry with fluorescent secondary antibodies as a readout. When comparing GU-gD and GU-FSY-gD, no significant difference in antibody recruitment was observed from a dilution series ranging over 1.56 nM - 100 nM (**Figure 21**). Covalent engagement of

LP14 antibodies was confirmed by adding excess competitor after a 24-hour LP14/GU-FSY-gD incubation. Here, maximal antibody recruitment was observed for the covalent bifunctional, whereas the non-covalent counterpart saw no antibody recruitment.

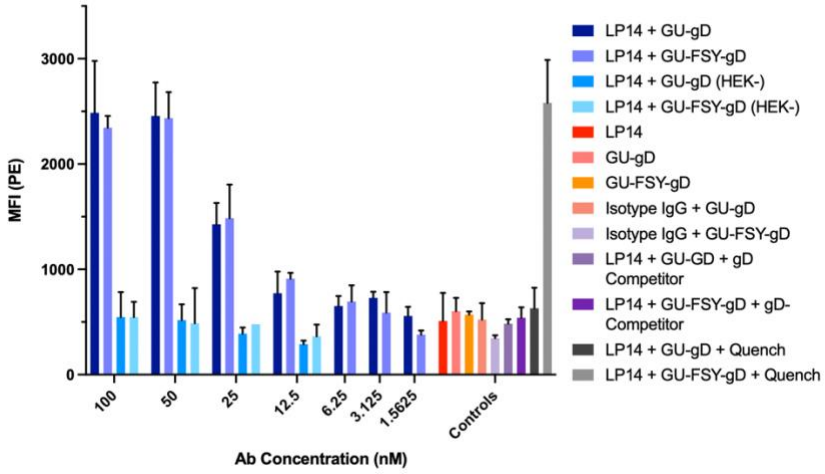

Figure 21. Antibody recruitment to HEK-PSMA cells was monitored by flow cytometry to measure total ternary complex formation at the cell surface. Recruitment of LP14 was observed after incubation with GU-FSY-gD or the non-covalent GU-gD over a range of concentrations. Detection of antibody recruitment was performed using a PE-conjugated secondary anti-mouse (H+L chain) antibody. Antibody recruitment was measured by the mean fluorescence intensity (MFI) associated with each cell population. Covalency was distinguished from non-covalency by performing an end-point quench with 25x gD competitor peptide. Above 50 nM antibody, all available PSMA binding sites are saturated. Multivalent binding of antibody Fabs at the cell surface promotes high avidity binding and thus no potency advantage between cARMs and ARMs in antibody recruitment.

6.4. **Discussion**

Highlighted in these results is the significance of how forming stable immune complexes impacts immune function. Using BLI assays, greater amounts of LP14-cARM adduct facilitated more PSMA recruitment to probes (**Figure 17**). This experiment removed any non-covalently bound cARM and serves as a simulation for how diffusion might remove ARM in a system that is not in equilibrium, i.e., in vivo.

Using two-colour flow cytometry ADCP assays, we demonstrate the utility of cARMs in forming stable biological ternary complexes. In the simplest context, i.e., cells engineered to express high levels of PSMA, cARMs outperformed ARMs at lower concentrations (**Figure 18**). In these ternary complexes there are two binding interactions, each with their own binding constants. The highest affinity binder will have a higher fraction bound at lower concentrations, whereas the lower affinity binder will need higher concentrations to stay bound. Thus, when the cARM outperforms the ARM at lower concentrations, we are likely seeing the overlap of these binding affinities. In this scenario, the final loss of function is likely shared between each construct, either arising from the GU:PSMA or Fc:FcR interactions. The lower affinity interaction between the peptide:Fab thus has its own “region” in these ADCP dose-response curves, where covalency improves function of cARMs over ARMs. If these peptides were low micromolar binders, the cARM would outperform ARMs at much higher concentrations than seen in these experiments.

At high concentrations of Ab-cARM/:ARM, similar levels of ADCP were observed for HEK-PSMA cells. When this system was moved to lower PSMA-expressing LnCAP or C4-2 cell lines, this observation no longer held, and cARM significantly outperformed ARM (**Figure 20**). We suggest this effect arises from differences in avidity between cell surfaces. With high levels of PSMA expression, bivalent antibody binding dominates, increasing the apparent affinity of the complex (**Figure 22**). This increase in apparent affinity is due to dissociation/rebinding, where excess available receptor in proximity promotes rebinding. If this rebinding step occurs before dissociation of the second Fab, the entire antibody remains bound to the cell surface, i.e., the antibody “walks”. In

scenarios where cell surfaces do not contain high levels of PSMA, this rebinding step does not occur in time, and the antibody:ARM:PSMA complex dissociates. This interaction is more akin to a traditional ternary complex, where each binding interaction plays a much larger role in the stability of the complex. Thus, covalency imparted by cARMs eliminates one source of instability, allowing for greater bound complex at lower concentrations.

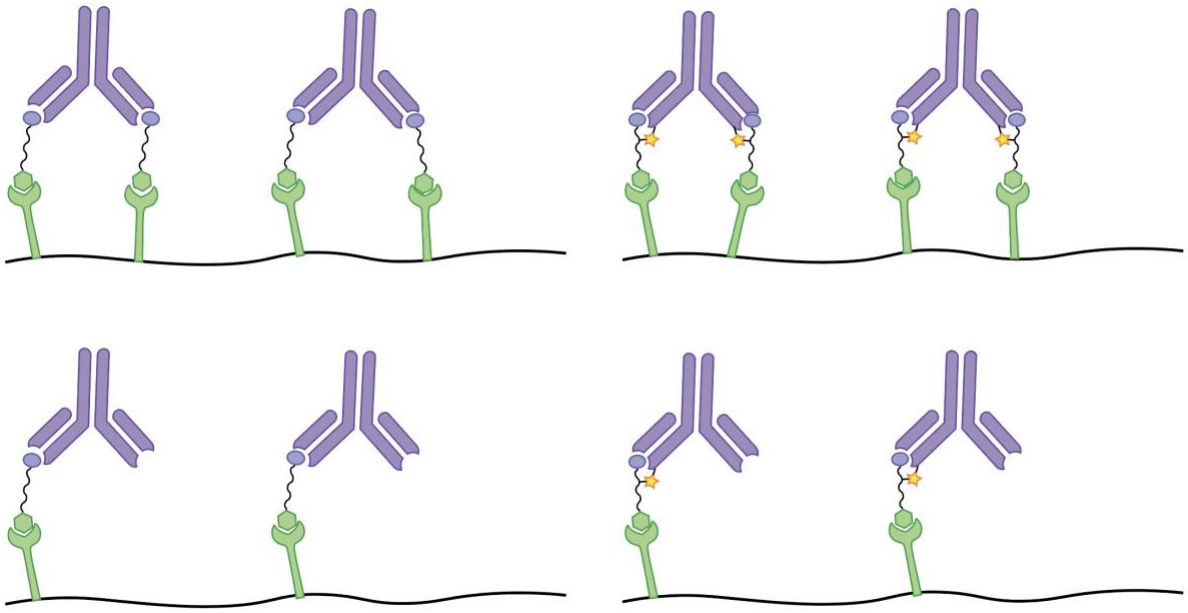

Figure 22. Multivalent antigen presentation on a cell surface promotes avidity with antibodies. Lower antigen presentation produces more monovalent binding interactions, leading to reduced ternary complex stability. Covalency improves monovalent binding by eliminating one equilibrium constant.

Intuitively, greater coverage of a cell surface with antibody Fc receptors leads to greater engagement of immune FcRs and subsequent immune activation. Comparing between cancer cell lines used in this study, this hypothesis follows this line of thought. However, a measure of antibody recruitment to the HEK-PSMA cell surface does not

indicate this is the case (**Figure 21**). Here, both the cARM and ARM mediate the same level of antibody recruitment throughout the dose-response curve, suggesting some other mechanism is responsible for greater cARM efficacy at lower concentrations. We suggest that it is the residence time of the binding interaction responsible for greater immune activation.

7. Covalency Improves Polyclonal Antibody Engagement

7.1. Objectives

To establish this proof of concept as a general approach for targeting endogenous antibodies, we next set out to target polyclonal anti-HSV antibodies. Both serum from mice inoculated with oncolytic HSV and pan human IgG were used as anti-HSV sources for these experiments. It was hypothesized that anti-HSV antibodies would be present in both sources and would represent a specific binding interaction capable of in situ covalent reprogramming.

7.2. Isolation of Anti-HSV IgG from Mouse and Human IgG

In collaboration with the Mossman lab at McMaster University, a source of mice infected with oncolytic HSV was generated. To do this, oncolytic HSV-1d810 was used to initiate an immune response in C57Bl/6 mice for the generation of natural oncolytic HSV immunity. Five mice were injected intraperitoneally with oncolytic HSV, and blood was collected on day 24 after mice were euthanized by cardiac puncture. Serum was separated by centrifugation with an RCF of 33,000g and stored at −80 °C until further use.

Sera from mice inoculated with oncolytic HSV-1d810 was probed for antibodies generated against the N-terminal gD peptide (**Figure 23**). To accomplish this, the serum of five mice "boosted" with HSV OV was pooled and compared against the pooled serum of three control mice. To optimize signal, a three-point dilution series was constructed for serum incubations, ranging from 0.2%-20% serum. Significant absorbance was only observed when immobilized gD peptide was introduced to boosted mouse serum, confirming the existence of specific antibodies (**Figure 23**).

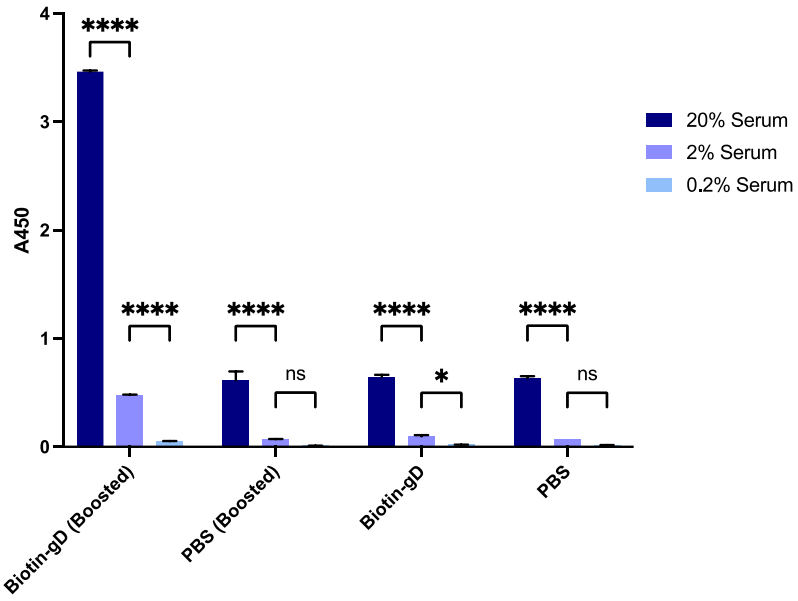

Figure 23. Detection of anti-HSV antibodies in OV-infected mouse serum using ELISA. Biotin-gD was loaded onto streptavidin-coated wells and incubated with 0.2-20% mouse serum before detection by an anti-mouse-HRP IgG conjugate. Data was quantified from two replicate measurements and summarized as the mean and standard error of the mean (*p = 0.0332, ****p < 0.0001, one-way analysis of variance, ANOVA).

To enhance the signal of anti-gD antibodies in the mouse polyclonal IgG, two successive pull-down assays were performed. The first was done by isolating all IgG from the mouse serum using a Protein G resin with an acidic elution step. Enrichment of anti-gD antibodies was then accomplished by immobilizing biotin-gD onto streptavidin coated

beads. Isolated mouse IgG was then passed over these beads several times to isolate sufficiently high affinity anti-gD antibodies. To further generalize this experiment, anti-gD antibodies were also pulled down from pan human IgG the same way.

7.3. **SDS-PAGE Selectivity Experiments Using Enriched Anti-HSV IgG**

Using the same fluorescent SDS-PAGE assays as before, enriched anti-gD antibodies were compared to whole mouse IgG and the resultant “depleted” IgG after enrichment. A similar set of conditions were also carried out using pan human IgG. It was found that fluor-ASF-gD was required for selective covalent engagement of polyclonal anti-gD antibodies (**Figure 24**). The less reactive FSY group was unable to form sufficient covalent adducts. Selectivity was demonstrated by pre-incubating either a non-covalent or covalent competition control prior to addition of cARM (**Figure 24**).

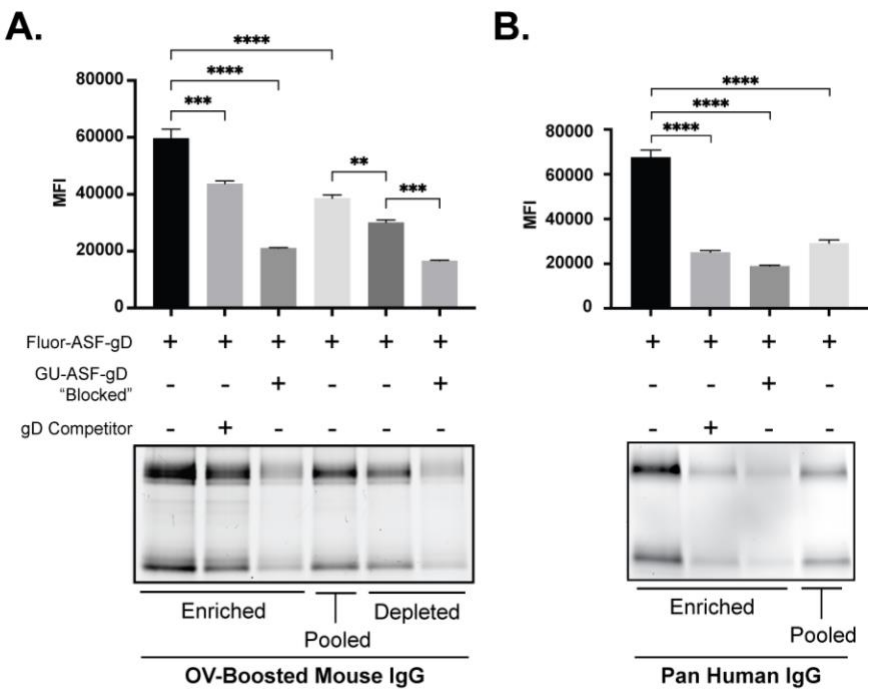

Figure 24. Selective covalent engagement of polyclonal anti-gD antibodies using fluor-ASF-gD. Anti-gD antibodies were enriched from A) OV-boosted mouse IgG, or B) pan human IgG. Fluorescent SDS-PAGE assays were used to analyze the selectivity of enriched, depleted, or whole IgG (pooled). Selectivity itself was measured through an absence of labeling in the presence of non-covalent gD peptide competitor or covalent GU-ASF-gD competitor. Data was quantified from two replicate measurements and summarized as the mean and standard error of the mean.

7.4. Human Polyclonal Anti-HSV IgG can be Selectively Covalently Repurposed for ADCP Assays

Due to the accessibility of pan human IgG, enriched anti-gD antibodies generated from this source were then used in effector ADCP assays. Using the same two-colour flow cytometry method as before, covalently modified polyclonal anti-gD antibodies were assessed for their ability to induce ADCP of HEK-PSMA cells using activated monocytes (**Figure 25**). It was found that when using these low affinity antibodies, covalency is necessary for inducing ADCP. When a non-covalent analogue was used, no ADCP

occurred. Similarly, by preventing labeling with a competitor pre-equilibration step, no ADCP was observed.

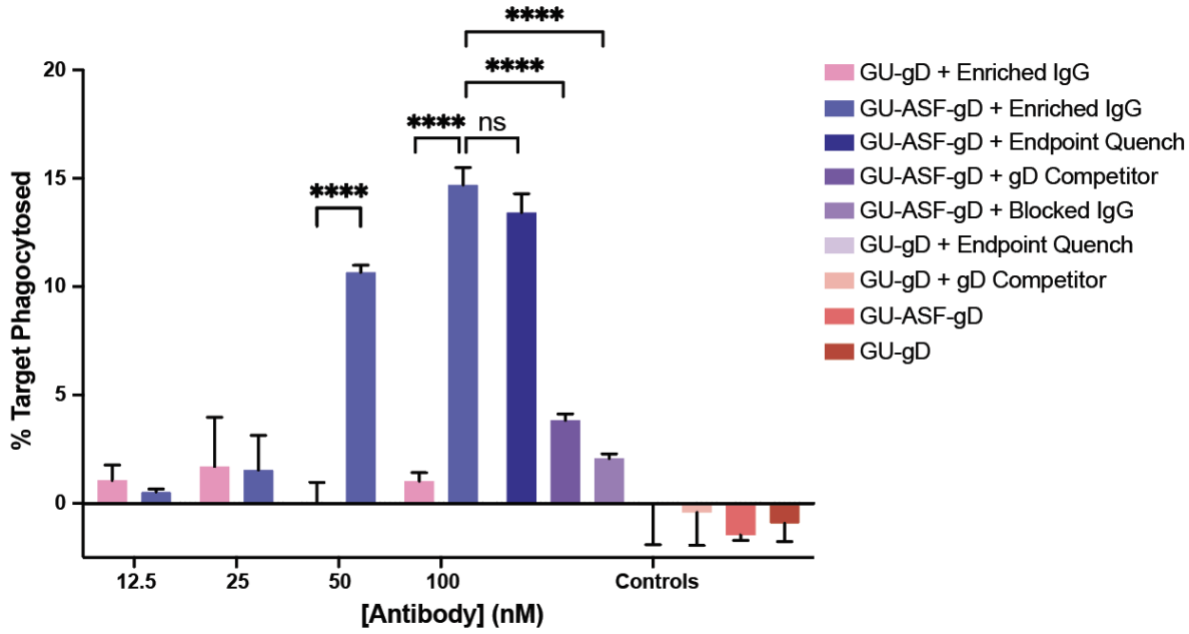

Figure 25. ADCP analysis of HEK-PSMA cells using two-color flow cytometry. GU-gD or GU-ASF-gD (2 eq) were incubated with enriched polyclonal anti-gD antibodies from pan human IgG (1 eq) for 24 hours before diluting 4x to the indicated concentrations. Phagocytosis was monitored by comparing FL-1 (DIO) dye stained HEK293 (PSMA+) cell population and the FL-4 (DID) dye stained u937 human monocyte population by flow cytometry. Selectivity was demonstrated by pre-equilibrating LP14 with gD peptide (100 µM) prior to cARM addition. Covalency was demonstrated by adding gD peptide (100 µM) after the 24-hour incubation with ARM/cARM. Data was quantified from two replicate measurements and summarized as the mean and standard error of the mean.

7.5. **Discussion**

In situ engagement of naturally derived polyclonal anti-HSV is essential for this proof of concept to have any therapeutic potential. We chose two antibody sources to validate this aspect of our peptide cARMs, namely from pan human IgG and mice inoculated with oncolytic HSV.

Pan human anti-HSV antibodies were targeted due to the prevalence of HSV infection in the human population. It has been reported that ~70-90% of people have been infected with either HSV-1 or HSV-2 in the United States.[126,127] Thus, this source serves as a general starting point for developing a peptide based cARM. The mouse IgG source that was chosen for this study was selected based on the usage of oncolytic HSV as a current immunotherapy. Many sources report oncolytic HSV administration is followed by an adaptive immune response which generates neutralizing antibodies for the therapy.[128,129] Thus, this approach serves as a means of relieving the inhibitory effects of neutralizing antibodies on oncolytic HSV, while also allowing for additional immune recruitment to the specific cancer target.

By enriching anti-gD antibodies from these sources, we demonstrate selective covalent labeling with fluor-ASF-gD (**Figure 24**). Notably, very little labeling was observed when fluor-FSY-gD was incubated with either antibody source (data not shown). These results highlight the importance of a rapid covalent labeling chemistry in a low affinity binder. With low residence time in a binding interaction with a large k_{off}, a less reactive electrophile like FSY does not have time to complete a cross-linking reaction. In contrast, the probability of ASF nucleophilic attack is much greater due to its reactivity, allowing for greater total conversion at the concentrations used.

Using a low affinity polyclonal IgG source allows for greater visualization of the advantages granted by covalent binding in an ADCP assay (**Figure 25**). As opposed to seeing either greater potency at lower concentrations, or with low antigen density targets, covalency is now necessary for function altogether. With concentrations < 10 x K_D, the fraction of bound complex is next to zero. Thus, so long as the K_D of these polyclonal

antibodies and this gD peptide ligand is > 1 μM, very little binding will occur, as the maximum concentration of antibody used was 100 nM in a 1:2 ratio with cARM. The rapid covalent labeling performed by the ASF electrophile is thus a necessary component in inducing not only a successful ternary complex, but also a successful binary complex with antibody Fab.

Altogether, the selectivity and reaction kinetics of the ASF electrophile poses it as a promising tool for proximity-induced covalent labeling. In this more biologically relevant experiment, ASF was essential in both forming irreversible linkages with polyclonal anti-HSV antibodies, as well as inducing subsequent immune complexes and phagocytosis.

8. **Conclusion**

Proximity induction is a powerful tool in chemical biology that allows specific biological processes to be hijacked towards an intended purpose. Demonstrated here was a covalent approach to enhance proximity induction by stably templating ternary complexes. Covalency was achieved itself through proximity, by leveraging a specific binding interaction between a gD peptide epitope expressed on the surface of HSV, and anti-gD antibodies. By rationally equipping this peptide with SuFEx electrophiles, a pseudo-intramolecular crosslinking reaction irreversibly labeled these antibodies in situ with tumor-targeting ligands. To develop this proof of concept, two SuFEx chemistries, FSY and ASF, were assessed for their ability to quickly and selectively modify two model monoclonal anti-gD antibodies, LP14 and H170. ASF was found to react with either model antibody ~10x faster than FSY, while demonstrating similar levels of selectivity. In ADCP flow cytometry assays it was found that covalently modified antibodies significantly

outperformed their non-covalent counterparts in inducing biological ternary complexes. The benefit of covalency specifically arose at low antibody/cARM concentrations or when tumor receptor density was lower. In the context of natural polyclonal anti-gD antibodies, the ASF electrophile was essential for both covalent labeling and successful biological proximity induction, visualized using SDS-PAGE and ADCP assays, respectively. Overall, ASF represents a promising candidate for incorporation into peptide ligands as a ligand-directed affinity labeling chemistry for use in bifunctional proximity-induction applications.

9. **References**

(1) Falzone, L.; Salomone, S.; Libra, M. Evolution of Cancer Pharmacological Treatments at the Turn of the Third Millennium. *Frontiers in Pharmacology*. Frontiers Media S.A. November 13, 2018. https://doi.org/10.3389/fphar.2018.01300.

(2) Rosenblum, D.; Joshi, N.; Tao, W.; Karp, J. M.; Peer, D. Progress and Challenges towards Targeted Delivery of Cancer Therapeutics. *Nature Communications*. Nature Publishing Group December 1, 2018. https://doi.org/10.1038/s41467-018-03705-y.

(3) Gerry, C. J.; Schreiber, S. L. Unifying Principles of Bifunctional, Proximity-Inducing Small Molecules. *Nature Chemical Biology*. Nature Research April 1, 2020, pp 369–378. https://doi.org/10.1038/s41589-020-0469-1.

(4) Zhong, L.; Li, Y.; Xiong, L.; Wang, W.; Wu, M.; Yuan, T.; Yang, W.; Tian, C.; Miao, Z.; Wang, T.; Yang, S. Small Molecules in Targeted Cancer Therapy: Advances, Challenges, and Future Perspectives. *Signal Transduction and Targeted Therapy*. Springer Nature December 1, 2021. https://doi.org/10.1038/s41392-021-00572-w.

(5) Zhao, L.; Zhao, J.; Zhong, K.; Tong, A.; Jia, D. Targeted Protein Degradation: Mechanisms, Strategies and Application. *Signal Transduction and Targeted Therapy*. Springer Nature December 1, 2022. https://doi.org/10.1038/s41392-022-00966-4.

(6) Rosenberg, S. C.; Shanahan, F.; Yamazoe, S.; Kschonsak, M.; Zeng, Y. J.; Lee, J.; Plise, E.; Yen, I.; Rose, C. M.; Quinn, J. G.; Gazzard, L. J.; Walters, B. T.; Kirkpatrick, D. S.; Staben, S. T.; Foster, S. A.; Malek, S. Ternary Complex Dissociation Kinetics Contribute to Mutant-Selective EGFR Degradation. *Cell Chem Biol* **2023**, *30* (2), 175-187.e15. https://doi.org/10.1016/j.chembiol.2023.01.007.

(7) Goodwin, C. A.; Deadman, J. J.; Le Bonniec, B. F.; Elgendy, S.; Kakkar, V. V; Scully, M. F. *Heparin Enhances the Catalytic Activity of Des-ETW-Thrombin*; 1996; Vol. 315.

(8) Bond, M. J.; Chu, L.; Nalawansha, D. A.; Li, K.; Crews, C. M. Targeted Degradation of Oncogenic KRASG12Cby VHL-Recruiting PROTACs. *ACS Cent Sci* **2020**, *6* (8), 1367–1375. https://doi.org/10.1021/acscentsci.0c00411.

(9) Gabizon, R.; Shraga, A.; Gehrtz, P.; Livnah, E.; Shorer, Y.; Gurwicz, N.; Avram, L.; Unger, T.; Aharoni, H.; Albeck, S.; Brandis, A.; Shulman, Z.; Katz, B. Z.; Herishanu, Y.; London, N. Efficient Targeted Degradation via Reversible and Irreversible Covalent PROTACs. *J Am Chem Soc* **2020**, *142* (27), 11734–11742. https://doi.org/10.1021/jacs.9b13907.

(10) Bond, M. J.; Chu, L.; Nalawansha, D. A.; Li, K.; Crews, C. M. Targeted Degradation of Oncogenic KRASG12Cby VHL-Recruiting PROTACs. *ACS Cent Sci* **2020**, *6* (8), 1367–1375. https://doi.org/10.1021/acscentsci.0c00411.

(11) Alabi, S.; Jaime-Figueroa, S.; Yao, Z.; Gao, Y.; Hines, J.; Samarasinghe, K. T. G.; Vogt, L.; Rosen, N.; Crews, C. M. Mutant-Selective Degradation by BRAF-Targeting PROTACs. *Nat Commun* **2021**, *12* (1). https://doi.org/10.1038/s41467-021-21159-7.

(12) Gabizon, R.; Shraga, A.; Gehrtz, P.; Livnah, E.; Shorer, Y.; Gurwicz, N.; Avram, L.; Unger, T.; Aharoni, H.; Albeck, S.; Brandis, A.; Shulman, Z.; Katz, B. Z.; Herishanu, Y.; London, N. Efficient Targeted Degradation via Reversible and Irreversible Covalent PROTACs. *J Am Chem Soc* **2020**, *142* (27), 11734–11742. https://doi.org/10.1021/jacs.9b13907.

(13) Bond, M. J.; Chu, L.; Nalawansha, D. A.; Li, K.; Crews, C. M. Targeted Degradation of Oncogenic KRASG12Cby VHL-Recruiting PROTACs. *ACS Cent Sci* **2020**, *6* (8), 1367–1375. https://doi.org/10.1021/acscentsci.0c00411.

(14) Gasic, I.; Groendyke, B. J.; Nowak, R. P.; Yuan, J. C.; Kalabathula, J.; Fischer, E. S.; Gray, N. S.; Mitchison, T. J. Tubulin Resists Degradation by Cereblon-Recruiting PROTACs. *Cells* **2020**, *9* (5). https://doi.org/10.3390/cells9051083.

(15) Nalawansha, D. A.; Li, K.; Hines, J.; Crews, C. M. Hijacking Methyl Reader Proteins for Nuclear-Specific Protein Degradation. *J Am Chem Soc* **2022**, *144* (12), 5594–5605. https://doi.org/10.1021/jacs.2c00874.

(16) Forte, N.; Dovala, D.; Hesse, M. J.; McKenna, J. M.; Tallarico, J. A.; Schirle, M.; Nomura, D. K. Targeted Protein Degradation through E2 Recruitment. *ACS Chem Biol* **2023**. https://doi.org/10.1021/acschembio.3c00040.

(17) Rullo, A. F.; Fitzgerald, K. J.; Muthusamy, V.; Liu, M.; Yuan, C.; Huang, M.; Kim, M.; Cho, A. E.; Spiegel, D. A. Re-Engineering the Immune Response to Metastatic Cancer: Antibody-Recruiting Small Molecules Targeting the Urokinase Receptor. *Angewandte Chemie* **2016**, *128* (11), 3706–3710. https://doi.org/10.1002/ange.201510866.

(18) Murelli, R. P.; Zhang, A. X.; Michel, J.; Jorgensen, W. L.; Spiegel, D. A. Chemical Control over Immune Recognition: A Class of Antibody-Recruiting Small Molecules That Target Prostate Cancer. *J Am Chem Soc* **2009**, *131* (47), 17090–17092. https://doi.org/10.1021/ja906844e.

(19) Owen, R. M.; Carlson, C. B.; Xu, J.; Mowery, P.; Fasella, E.; Kiessling, L. L. Bifunctional Ligands That Target Cells Displaying the α Vβ3 Integrin. *ChemBioChem* **2007**, *8* (1), 68–82. https://doi.org/10.1002/cbic.200600339.

(20) Ahn, G.; Banik, S. M.; Miller, C. L.; Riley, N. M.; Cochran, J. R.; Bertozzi, C. R. LYTACs That Engage the Asialoglycoprotein Receptor for Targeted Protein Degradation. *Nat Chem Biol* **2021**, *17* (9), 937–946. https://doi.org/10.1038/s41589-021-00770-1.

(21) Banik, S. M.; Pedram, K.; Wisnovsky, S.; Ahn, G.; Riley, N. M.; Bertozzi, C. R. Lysosome-Targeting Chimaeras for Degradation of Extracellular Proteins. *Nature* **2020**, *584* (7820), 291–297. https://doi.org/10.1038/s41586-020-2545-9.

(22) Yamazoe, S.; Tom, J.; Fu, Y.; Wu, W.; Zeng, L.; Sun, C.; Liu, Q.; Lin, J.; Lin, K.; Fairbrother, W. J.; Staben, S. T. Heterobifunctional Molecules Induce Dephosphorylation of Kinases-A Proof of Concept Study. *J Med Chem* **2020**, *63* (6), 2807–2813. https://doi.org/10.1021/acs.jmedchem.9b01167.

(23) Henning, N. J.; Boike, L.; Spradlin, J. N.; Ward, C. C.; Liu, G.; Zhang, E.; Belcher, B. P.; Brittain, S. M.; Hesse, M. J.; Dovala, D.; McGregor, L. M.; Valdez Misiolek, R.; Plasschaert, L. W.; Rowlands, D. J.; Wang, F.; Frank, A. O.; Fuller, D.; Estes, A. R.; Randal, K. L.; Panidapu, A.; McKenna, J. M.; Tallarico, J. A.; Schirle, M.; Nomura, D. K. Deubiquitinase-Targeting Chimeras for Targeted Protein

Stabilization. *Nat Chem Biol* **2022**, *18* (4), 412–421. https://doi.org/10.1038/s41589-022-00971-2.

(24) Cruite, J. T.; Dann, G. P.; Che, J.; Donovan, K. A.; Ferrao, S.; Ficarro, S. B.; Fischer, E. S.; Gray, N. S.; Huerta, F.; Kong, N. R.; Liu, H.; Marto, J. A.; Metivier, R. J.; Nowak, R. P.; Zerfas, B. L.; Jones, L. H. Cereblon Covalent Modulation through Structure-Based Design of Histidine Targeting Chemical Probes. *RSC Chem Biol* **2022**, *3* (9), 1105–1110. https://doi.org/10.1039/d2cb00078d.

(25) Dong, G.; Ding, Y.; He, S.; Sheng, C. Molecular Glues for Targeted Protein Degradation: From Serendipity to Rational Discovery. *Journal of Medicinal Chemistry*. American Chemical Society August 12, 2021, pp 10606–10620. https://doi.org/10.1021/acs.jmedchem.1c00895.

(26) King, E. A.; Cho, Y.; Hsu, N. S.; Dovala, D.; McKenna, J. M.; Tallarico, J. A.; Schirle, M.; Nomura, D. K. Chemoproteomics-Enabled Discovery of a Covalent Molecular Glue Degrader Targeting NF-KB. *Cell Chem Biol* **2023**. https://doi.org/10.1016/j.chembiol.2023.02.008.

(27) Kino, T.; Hatanaka, H.; Miyata, S.; Inamura, N.; Nlshiyama, Toshimi Yajima, Toshio Goto, M.; Okuhara, M.; Kohsaka, M.; Aoki, H.; Ochiai, T. *THE JOURNAL OF ANTIBIOTICS FK-506, A NOVEL IMMUNOSUPPRESSANT ISOLATED FROM A STREPTOMYCES II. IMMUNOSUPPRESSIVE EFFECT OF FK-506 IN VITRO*.

(28) Kissinger, C. R.; Parge, H. E.; Knighton, D. R.; Lewis, C. T.; Pelletier, L. A.; Tempczyk, A.; Kalish, V. J.; Tucker, K. D.; Showalter, R. E.; Moomaw, E. W.; Gastinel, L. N.; Habuka, N.; Chen, X.; Maldonado, F.; Barker, J. E.; Bacquet, R.; Villafranca, J. E. *Crystal Structures of Human Calcineurin and the Human FKBP12-FK506-Calcineurin Complex*; 1995.

(29) Vellanki, S.; Garcia, A. E.; Lee, S. C. Interactions of FK506 and Rapamycin With FK506 Binding Protein 12 in Opportunistic Human Fungal Pathogens. *Frontiers in Molecular Biosciences*. Frontiers Media S.A. October 16, 2020. https://doi.org/10.3389/fmolb.2020.588913.

(30) Choi, J.; Chen, J.; Schreiber, S. L.; Clardy, J. *Structure of the FKBP12-Rapamycin Complex Interacting with the Binding Domain of Human FRAP*; 1996; Vol. 273.

(31) Dang, C. V.; Reddy, E. P.; Shokat, K. M.; Soucek, L. Drugging the “undruggable” Cancer Targets. *Nature Reviews Cancer*. Nature Publishing Group July 25, 2017, pp 502–508. https://doi.org/10.1038/nrc.2017.36.

(32) Park, D.; Izaguirre, J.; Coffey, R.; Xu, H. Modeling the Effect of Cooperativity in Ternary Complex Formation and Targeted Protein Degradation Mediated by Heterobifunctional Degraders. *ACS Bio and Med Chem Au* **2023**, *3* (1), 74–86. https://doi.org/10.1021/acsbiomedchemau.2c00037.

(33) Farnaby, W.; Koegl, M.; Roy, M. J.; Whitworth, C.; Diers, E.; Trainor, N.; Zollman, D.; Steurer, S.; Karolyi-Oezguer, J.; Riedmueller, C.; Gmaschitz, T.; Wachter, J.; Dank, C.; Galant, M.; Sharps, B.; Rumpel, K.; Traxler, E.; Gerstberger, T.; Schnitzer, R.; Petermann, O.; Greb, P.; Weinstabl, H.; Bader, G.; Zoephel, A.; Weiss-Puxbaum, A.; Ehrenhöfer-Wölfer, K.; Wöhrle, S.; Boehmelt, G.; Rinnenthal, J.; Arnhof, H.; Wiechens, N.; Wu, M. Y.; Owen-Hughes, T.; Ettmayer, P.; Pearson, M.; McConnell, D. B.; Ciulli, A. BAF Complex Vulnerabilities in Cancer Demonstrated via Structure-Based PROTAC Design. *Nat Chem Biol* **2019**, *15* (7), 672–680. https://doi.org/10.1038/s41589-019-0294-6.

(34) Gadd, M. S.; Testa, A.; Lucas, X.; Chan, K. H.; Chen, W.; Lamont, D. J.; Zengerle, M.; Ciulli, A. Structural Basis of PROTAC Cooperative Recognition for Selective Protein Degradation. *Nat Chem Biol* **2017**, *13* (5), 514–521. https://doi.org/10.1038/nchembio.2329.

(35) Zorba, A.; Nguyen, C.; Xu, Y.; Starr, J.; Borzilleri, K.; Smith, J.; Zhu, H.; Farley, K. A.; Ding, W. D.; Schiemer, J.; Feng, X.; Chang, J. S.; Uccello, D. P.; Young, J. A.; Garcia-Irrizary, C. N.; Czabaniuk, L.; Schuff, B.; Oliver, R.; Montgomery, J.; Hayward, M. M.; Coe, J.; Chen, J.; Niosi, M.; Luthra, S.; Shah, J. C.; El-Kattan, A.; Qiu, X.; West, G. M.; Noe, M. C.; Shanmugasundaram, V.; Gilbert, A. M.; Brown, M. F.; Calabrese, M. F. Delineating the Role of Cooperativity in the Design of Potent PROTACs for BTK. *Proc Natl Acad Sci U S A* **2018**, *115* (31), E7285–E7292. https://doi.org/10.1073/pnas.1803662115.

(36) Roy, M. J.; Winkler, S.; Hughes, S. J.; Whitworth, C.; Galant, M.; Farnaby, W.; Rumpel, K.; Ciulli, A. SPR-Measured Dissociation Kinetics of PROTAC Ternary Complexes Influence Target Degradation Rate. *ACS Chem Biol* **2019**, *14* (3), 361–368. https://doi.org/10.1021/acschembio.9b00092.

(37) Carlson, A.; Mahadevan, L. Elastohydrodynamics and Kinetics of Protein Patterning in the Immunological Synapse. *PLoS Comput Biol* **2015**, *11* (12). https://doi.org/10.1371/journal.pcbi.1004481.

(38) Roy, R. D.; Rosenmund, C.; Stefan, M. I. Cooperative Binding Mitigates the High-Dose Hook Effect. *BMC Syst Biol* **2017**, *11* (1). https://doi.org/10.1186/s12918-017-0447-8.

(39) Bondeson, D. P.; Mares, A.; D Smith, I. E.; Ko, E.; Campos, S.; Miah, A. H.; Mulholland, K. E.; Routly, N.; Buckley, D. L.; Gustafson, J. L.; Zinn, N.; Grandi, P.; Shimamura, S.; Bergamini, G.; Faelth-Savitski, M.; Bantscheff, M.; Cox, C.; Gordon, D. A.; Willard, R. R.; Flanagan, J. J.; Casillas, L. N.; Votta, B. J.; den Besten, W.; Famm, K.; Kruidenier, L.; Carter, P. S.; Harling, J. D.; Churcher, I.; Crews, C. M. Catalytic in Vivo Protein Knockdown by Small-Molecule PROTACs AOP. **2015**. https://doi.org/10.1038/ncheMbio.XXX.

(40) Kapcan, E.; Lake, B.; Yang, Z.; Zhang, A.; Miller, M. S.; Rullo, A. F. Covalent Stabilization of Antibody Recruitment Enhances Immune Recognition of Cancer Targets. **2021**. https://doi.org/10.1021/acs.biochem.1c00127.

(41) Stone, J. D.; Kranz, D. M. Role of T Cell Receptor Affinity in the Efficacy and Specificity of Adoptive T Cell Therapies. *Front Immunol* **2013**, *4*. https://doi.org/10.3389/fimmu.2013.00244.

(42) Garcia, K. C.; Scott, C. A.; Brunmark, A.; Carbone, F. R.; Peterson, P. A.; Wilson, I. A.; Teyton, L. CD8 Enhances Formation of Stable T-Cell Receptor/MHC Class I Molecule Complexes. *Nature* **1996**, *384* (6609), 577–581. https://doi.org/10.1038/384577a0.

(43) Poussin, M.; Sereno, A.; Wu, X.; Huang, F.; Manro, J.; Cao, S.; Carpenito, C.; Glasebrook, A.; Powell, D. J.; Demarest, S. Dichotomous Impact of Affinity on the Function of T Cell Engaging Bispecific Antibodies. *J Immunother Cancer* **2021**, *9* (7). https://doi.org/10.1136/jitc-2021-002444.

(44) Yousefi, S.; Gü Nther, M.; Hö Rner, M.; Chalupsky, J.; Wess, M.; Brandl, S. M.; Smith, R. W.; Fleck, C.; Kunkel, T.; Zurbriggen, M. D.; Hö Fer, T.; Weber, W.; Wa

Schamel, W. Optogenetic Control Shows That Kinetic Proofreading Regulates the Activity of the T Cell Receptor. **2019**. https://doi.org/10.7554/eLife.42475.001.

(45) Yadav, J.; El Hassani, M.; Sodhi, J.; Lauschke, V. M.; Hartman, J. H.; Russell, L. E. Recent Developments in in Vitro and in Vivo Models for Improved Translation of Preclinical Pharmacokinetics and Pharmacodynamics Data. *Drug Metabolism Reviews*. Taylor and Francis Ltd. 2021, pp 207–233. https://doi.org/10.1080/03602532.2021.1922435.

(46) Bach, T.; Jiang, Y.; Zhang, X.; An, G. General Pharmacokinetic Features of Small-Molecule Compounds Exhibiting Target-Mediated Drug Disposition (TMDD): A Simulation-Based Study. *J Clin Pharmacol* **2019**, *59* (3), 394–405. https://doi.org/10.1002/jcph.1335.

(47) Imai, K.; Takaoka, A. Comparing Antibody and Small-Molecule Therapies for Cancer. *Nature Reviews Cancer*. September 2006, pp 714–727. https://doi.org/10.1038/nrc1913.

(48) Caianiello, D. F.; Zhang, M.; Ray, J. D.; Howell, R. A.; Swartzel, J. C.; Branham, E. M. J.; Chirkin, E.; Sabbasani, V. R.; Gong, A. Z.; McDonald, D. M.; Muthusamy, V.; Spiegel, D. A. Bifunctional Small Molecules That Mediate the Degradation of Extracellular Proteins. *Nat Chem Biol* **2021**, *17* (9), 947–953. https://doi.org/10.1038/s41589-021-00851-1.

(49) Lei, J.; Zhou, Y.; Xie, D.; Zhang, Y. Mechanistic Insights into a Classic Wonder Drug-Aspirin. *J Am Chem Soc* **2015**, *137* (1), 70–73. https://doi.org/10.1021/ja5112964.

(50) Li, D.; Ambrogio, L.; Shimamura, T.; Kubo, S.; Takahashi, M.; Chirieac, L. R.; Padera, R. F.; Shapiro, G. I.; Baum, A.; Himmelsbach, F.; Rettig, W. J.; Meyerson, M.; Solca, F.; Greulich, H.; Wong, K. K. BIBW2992, an Irreversible EGFR/HER2 Inhibitor Highly Effective in Preclinical Lung Cancer Models. *Oncogene* **2008**, *27* (34), 4702–4711. https://doi.org/10.1038/onc.2008.109.

(51) Honigberg, L. A.; Smith, A. M.; Sirisawad, M.; Verner, E.; Loury, D.; Chang, B.; Li, S.; Pan, Z.; Thamm, D. H.; Miller, R. A.; Buggy, J. J. The Bruton Tyrosine Kinase Inhibitor PCI-32765 Blocks B-Cell Activation and Is Efficacious in Models of Autoimmune Disease and B-Cell Malignancy. *Proc Natl Acad Sci U S A* **2010**, *107* (29), 13075–13080. https://doi.org/10.1073/pnas.1004594107.

(52) Zhao, Q.; Ouyang, X.; Wan, X.; Gajiwala, K. S.; Kath, J. C.; Jones, L. H.; Burlingame, A. L.; Taunton, J. Broad-Spectrum Kinase Profiling in Live Cells with Lysine-Targeted Sulfonyl Fluoride Probes. *J Am Chem Soc* **2017**, *139* (2), 680–685. https://doi.org/10.1021/jacs.6b08536.

(53) Mukherjee, H.; Debreczeni, J.; Breed, J.; Tentarelli, S.; Aquila, B.; Dowling, J. E.; Whitty, A.; Grimster, N. P. A Study of the Reactivity of S(VI)-F Containing Warheads with Nucleophilic Amino-Acid Side Chains under Physiological Conditions. *Org Biomol Chem* **2017**, *15* (45), 9685–9695. https://doi.org/10.1039/c7ob02028g.

(54) Darabedian, N.; Ji, W.; Fan, M.; Lin, S.; Seo, H. S.; Vinogradova, E. V.; Yaron, T. M.; Mills, E. L.; Xiao, H.; Senkane, K.; Huntsman, E. M.; Johnson, J. L.; Che, J.; Cantley, L. C.; Cravatt, B. F.; Dhe-Paganon, S.; Stegmaier, K.; Zhang, T.; Gray, N. S.; Chouchani, E. T. Depletion of Creatine Phosphagen Energetics with a Covalent Creatine Kinase Inhibitor. *Nat Chem Biol* **2023**. https://doi.org/10.1038/s41589-023-01273-x.

(55) Mortenson, D. E.; Brighty, G. J.; Plate, L.; Bare, G.; Chen, W.; Li, S.; Wang, H.; Cravatt, B. F.; Forli, S.; Powers, E. T.; Sharpless, K. B.; Wilson, I. A.; Kelly, J. W. "inverse Drug Discovery" Strategy to Identify Proteins That Are Targeted by Latent Electrophiles As Exemplified by Aryl Fluorosulfates. *J Am Chem Soc* **2018**, *140* (1), 200–210. https://doi.org/10.1021/jacs.7b08366.

(56) Ji, Z.; Kozuch, J.; Mathews, I. I.; Diercks, C. S.; Shamsudin, Y.; Schulz, M. A.; Boxer, S. G. Protein Electric Fields Enable Faster and Longer-Lasting Covalent Inhibition of β-Lactamases. *J Am Chem Soc* **2022**, *144* (45), 20947–20954. https://doi.org/10.1021/jacs.2c09876.

(57) Alexander, J. P.; Cravatt, B. F. Mechanism of Carbamate Inactivation of FAAH: Implications for the Design of Covalent Inhibitors and in Vivo Functional Probes for Enzymes. *Chem Biol* **2005**, *12* (11), 1179–1187. https://doi.org/10.1016/j.chembiol.2005.08.011.

(58) Hahn, W. C.; Bader, J. S.; Braun, T. P.; Califano, A.; Clemons, P. A.; Druker, B. J.; Ewald, A. J.; Fu, H.; Jagu, S.; Kemp, C. J.; Kim, W.; Kuo, C. J.; McManus, M.; B. Mills, G.; Mo, X.; Sahni, N.; Schreiber, S. L.; Talamas, J. A.; Tamayo, P.; Tyner, J. W.; Wagner, B. K.; Weiss, W. A.; Gerhard, D. S.; Dancik, V.; Gill, S.; Hua, B.; Sharifnia, T.; Viswanathan, V.; Zou, Y.; Dela Cruz, F.; Kung, A.; Stockwell, B.; Boehm, J.; Dempster, J.; Manguso, R.; Vazquez, F.; Cooper, L. A. D.; Du, Y.; Ivanov, A.; Lonial, S.; Moreno, C. S.; Niu, Q.; Owonikoko, T.; Ramalingam, S.; Reyna, M.; Zhou, W.; Grandori, C.; Shmulevich, I.; Swisher, E.; Cai, J.; Chan, I. S.; Dunworth, M.; Ge, Y.; Georgess, D.; Grasset, E. M.; Henriet, E.; Knútsdóttir, H.; Lerner, M. G.; Padmanaban, V.; Perrone, M. C.; Suhail, Y.; Tsehay, Y.; Warrier, M.; Morrow, Q.; Nechiporuk, T.; Long, N.; Saultz, J.; Kaempf, A.; Minnier, J.; Tognon, C. E.; Kurtz, S. E.; Agarwal, A.; Brown, J.; Watanabe-Smith, K.; Vu, T. Q.; Jacob, T.; Yan, Y.; Robinson, B.; Lind, E. F.; Kosaka, Y.; Demir, E.; Estabrook, J.; Grzadkowski, M.; Nikolova, O.; Chen, K.; Deneen, B.; Liang, H.; Bassik, M. C.; Bhattacharya, A.; Brennan, K.; Curtis, C.; Gevaert, O.; Ji, H. P.; Karlsson, K. A. J.; Karagyozova, K.; Lo, Y. H.; Liu, K.; Nakano, M.; Sathe, A.; Smith, A. R.; Spees, K.; Wong, W. H.; Yuki, K.; Hangauer, M.; Kaufman, D. S.; Balmain, A.; Bollam, S. R.; Chen, W. C.; Fan, Q. W.; Kersten, K.; Krummel, M.; Li, Y. R.; Menard, M.; Nasholm, N.; Schmidt, C.; Serwas, N. K.; Yoda, H. An Expanded Universe of Cancer Targets. *Cell*. Elsevier B.V. March 4, 2021, pp 1142–1155. https://doi.org/10.1016/j.cell.2021.02.020.

(59) Hassin, O.; Oren, M. Drugging P53 in Cancer: One Protein, Many Targets. *Nature Reviews Drug Discovery*. Nature Research February 1, 2023, pp 127–144. https://doi.org/10.1038/s41573-022-00571-8.

(60) Otto, T.; Sicinski, P. Cell Cycle Proteins as Promising Targets in Cancer Therapy. *Nature Reviews Cancer*. Nature Publishing Group January 27, 2017, pp 93–115. https://doi.org/10.1038/nrc.2016.138.

(61) Huang, F.; Han, X.; Xiao, X.; Zhou, J. Covalent Warheads Targeting Cysteine Residue: The Promising Approach in Drug Development. *Molecules*. MDPI November 1, 2022. https://doi.org/10.3390/molecules27227728.

(62) Fan, M.; Lu, W.; Che, J.; Kwiatkowski, N. P.; Gao, Y.; Seo, H.-S.; Ficarro, S. B.; Gokhale, P. C.; Liu, Y.; Geffken, E. A.; Lakhani, J.; Song, K.; Kuljanin, M.; Ji, W.; Jiang, J.; He, Z.; Tse, J.; Boghossian, A. S.; Rees, M. G.; Ronan, M. M.; Roth, J.

A.; Mancias, J. D.; Marto, J. A.; Dhe-Paganon, S.; Zhang, T.; Gray, N. S. Covalent Disruptor of YAP-TEAD Association Suppresses Defective Hippo Signaling. *Elife* **2022**, *11*. https://doi.org/10.7554/eLife.78810.

(63) Deng, W.; Chen, X.; Jiang, K.; Song, X.; Huang, M.; Tu, Z. C.; Zhang, Z.; Lin, X.; Ortega, R.; Patterson, A. V.; Smaill, J. B.; Ding, K.; Chen, S.; Chen, Y.; Lu, X. Investigation of Covalent Warheads in the Design of 2-Aminopyrimidine-Based FGFR4 Inhibitors. *ACS Med Chem Lett* **2021**, *12* (4), 647–652. https://doi.org/10.1021/acsmedchemlett.1c00052.

(64) Reddi, R. N.; Resnick, E.; Rogel, A.; Rao, B. V.; Gabizon, R.; Goldenberg, K.; Gurwicz, N.; Zaidman, D.; Plotnikov, A.; Barr, H.; Shulman, Z.; London, N. Tunable Methacrylamides for Covalent Ligand Directed Release Chemistry. *J Am Chem Soc* **2021**, *143* (13), 4979–4992. https://doi.org/10.1021/jacs.0c10644.

(65) Serafimova, I. M.; Pufall, M. A.; Krishnan, S.; Duda, K.; Cohen, M. S.; Maglathlin, R. L.; McFarland, J. M.; Miller, R. M.; Frödin, M.; Taunton, J. Reversible Targeting of Noncatalytic Cysteines with Chemically Tuned Electrophiles. *Nat Chem Biol* **2012**, *8* (5), 471–476. https://doi.org/10.1038/nchembio.925.

(66) Wang, C.; Zhang, J.; Yin, J.; Gan, Y.; Xu, S.; Gu, Y.; Huang, W. Alternative Approaches to Target Myc for Cancer Treatment. *Signal Transduction and Targeted Therapy*. Springer Nature December 1, 2021. https://doi.org/10.1038/s41392-021-00500-y.

(67) Huang, L.; Guo, Z.; Wang, F.; Fu, L. KRAS Mutation: From Undruggable to Druggable in Cancer. *Signal Transduction and Targeted Therapy*. Springer Nature December 1, 2021. https://doi.org/10.1038/s41392-021-00780-4.

(68) Boike, L.; Cioffi, A. G.; Majewski, F. C.; Co, J.; Henning, N. J.; Jones, M. D.; Liu, G.; McKenna, J. M.; Tallarico, J. A.; Schirle, M.; Nomura, D. K. Discovery of a Functional Covalent Ligand Targeting an Intrinsically Disordered Cysteine within MYC. *Cell Chem Biol* **2021**, *28* (1), 4-13.e17. https://doi.org/10.1016/j.chembiol.2020.09.001.

(69) Lanman, B. A.; Allen, J. R.; Allen, J. G.; Amegadzie, A. K.; Ashton, K. S.; Booker, S. K.; Chen, J. J.; Chen, N.; Frohn, M. J.; Goodman, G.; Kopecky, D. J.; Liu, L.; Lopez, P.; Low, J. D.; Ma, V.; Minatti, A. E.; Nguyen, T. T.; Nishimura, N.; Pickrell, A. J.; Reed, A. B.; Shin, Y.; Siegmund, A. C.; Tamayo, N. A.; Tegley, C. M.; Walton, M. C.; Wang, H. L.; Wurz, R. P.; Xue, M.; Yang, K. C.; Achanta, P.; Bartberger, M. D.; Canon, J.; Hollis, L. S.; McCarter, J. D.; Mohr, C.; Rex, K.; Saiki, A. Y.; San Miguel, T.; Volak, L. P.; Wang, K. H.; Whittington, D. A.; Zech, S. G.; Lipford, J. R.; Cee, V. J. Discovery of a Covalent Inhibitor of KRASG12C (AMG 510) for the Treatment of Solid Tumors. *J Med Chem* **2020**, *63* (1), 52–65. https://doi.org/10.1021/acs.jmedchem.9b01180.

(70) Yang, T.; Cuesta, A.; Wan, X.; Craven, G. B.; Hirakawa, B.; Khamphavong, P.; May, J. R.; Kath, J. C.; Lapek, J. D.; Niessen, S.; Burlingame, A. L.; Carelli, J. D.; Taunton, J. Reversible Lysine-Targeted Probes Reveal Residence Time-Based Kinase Selectivity. *Nat Chem Biol* **2022**, *18* (9), 934–941. https://doi.org/10.1038/s41589-022-01019-1.

(71) Cal, P. M. S. D.; Vicente, J. B.; Pires, E.; Coelho, A. V.; Veiros, L. F.; Cordeiro, C.; Gois, P. M. P. Iminoboronates: A New Strategy for Reversible Protein Modification. *J Am Chem Soc* **2012**, *134* (24), 10299–10305. https://doi.org/10.1021/ja303436y.

(72) Akçay, G.; Belmonte, M. A.; Aquila, B.; Chuaqui, C.; Hird, A. W.; Lamb, M. L.; Rawlins, P. B.; Su, N.; Tentarelli, S.; Grimster, N. P.; Su, Q. Inhibition of Mcl-1 through Covalent Modification of a Noncatalytic Lysine Side Chain. *Nat Chem Biol* **2016**, *12* (11), 931–936. https://doi.org/10.1038/nchembio.2174.

(73) Quach, D.; Uanghui Tang, G.; Othi Anantharajan, J.; Baburajendran, N.; Poulsen, A.; Wee, J. L. K.; Retna, P.; Li, R.; Liu, B.; Tee, D. H. Y.; Kwek, P. Z.; Joy, J. K.; Yang, W.-Q.; Zhang, C.-J.; Foo, K.; Keller, T. H.; Yao, S. Q. Strategic Design of Catalytic Lysine-Targeting Reversible Covalent BCR-ABL Inhibitors**. *Angew. Chem. Int. Ed.* **2021**, *60*, 17131–17137. https://doi.org/10.26434/chemrxiv.13710097.v1.

(74) Chen, P.; Tang, G.; Zhu, C.; Sun, J.; Wang, X.; Xiang, M.; Huang, H.; Wang, W.; Li, L.; Zhang, Z. M.; Gao, L.; Yao, S. Q. 2-Ethynylbenzaldehyde-Based, Lysine-Targeting Irreversible Covalent Inhibitors for Protein Kinases and Nonkinases. *J Am Chem Soc* **2022**. https://doi.org/10.1021/jacs.2c11595.

(75) Yang, T.; Cuesta, A.; Wan, X.; Craven, G. B.; Hirakawa, B.; Khamphavong, P.; May, J. R.; Kath, J. C.; Lapek, J. D.; Niessen, S.; Burlingame, A. L.; Carelli, J. D.; Taunton, J. Reversible Lysine-Targeted Probes Reveal Residence Time-Based Kinase Selectivity. *Nat Chem Biol* **2022**, *18* (9), 934–941. https://doi.org/10.1038/s41589-022-01019-1.

(76) Dubiella, C.; Pinch, B. J.; Koikawa, K.; Zaidman, D.; Poon, E.; Manz, T. D.; Nabet, B.; He, S.; Resnick, E.; Rogel, A.; Langer, E. M.; Daniel, C. J.; Seo, H. S.; Chen, Y.; Adelmant, G.; Sharifzadeh, S.; Ficarro, S. B.; Jamin, Y.; Martins da Costa, B.; Zimmerman, M. W.; Lian, X.; Kibe, S.; Kozono, S.; Doctor, Z. M.; Browne, C. M.; Yang, A.; Stoler-Barak, L.; Shah, R. B.; Vangos, N. E.; Geffken, E. A.; Oren, R.; Koide, E.; Sidi, S.; Shulman, Z.; Wang, C.; Marto, J. A.; Dhe-Paganon, S.; Look, T.; Zhou, X. Z.; Lu, K. P.; Sears, R. C.; Chesler, L.; Gray, N. S.; London, N. Sulfopin Is a Covalent Inhibitor of Pin1 That Blocks Myc-Driven Tumors in Vivo. *Nat Chem Biol* **2021**, *17* (9), 954–963. https://doi.org/10.1038/s41589-021-00786-7.

(77) Pinch, B. J.; Doctor, Z. M.; Nabet, B.; Browne, C. M.; Seo, H. S.; Mohardt, M. L.; Kozono, S.; Lian, X.; Manz, T. D.; Chun, Y.; Kibe, S.; Zaidman, D.; Daitchman, D.; Yeoh, Z. C.; Vangos, N. E.; Geffken, E. A.; Tan, L.; Ficarro, S. B.; London, N.; Marto, J. A.; Buratowski, S.; Dhe-Paganon, S.; Zhou, X. Z.; Lu, K. P.; Gray, N. S. Identification of a Potent and Selective Covalent Pin1 Inhibitor. *Nat Chem Biol* **2020**, *16* (9), 979–987. https://doi.org/10.1038/s41589-020-0550-9.

(78) Li, T.; Maltais, R.; Poirier, D.; Lin, S. X. Combined Biophysical Chemistry Reveals a New Covalent Inhibitor with a Low-Reactivity Alkyl Halide. *Journal of Physical Chemistry Letters* **2018**, *9* (18), 5275–5280. https://doi.org/10.1021/acs.jpclett.8b02225.

(79) Tamura, T.; Ueda, T.; Goto, T.; Tsukidate, T.; Shapira, Y.; Nishikawa, Y.; Fujisawa, A.; Hamachi, I. Rapid Labelling and Covalent Inhibition of Intracellular Native Proteins Using Ligand-Directed N-Acyl-N-Alkyl Sulfonamide. *Nat Commun* **2018**, *9* (1), 1870. https://doi.org/10.1038/s41467-018-04343-0.

(80) Ueda, T.; Tamura, T.; Kawano, M.; Shiono, K.; Hobor, F.; Wilson, A. J.; Hamachi, I. Enhanced Suppression of a Protein-Protein Interaction in Cells Using Small-Molecule Covalent Inhibitors Based on an N-Acyl- N-Alkyl Sulfonamide Warhead. *J Am Chem Soc* **2021**, *143* (12), 4766–4774. https://doi.org/10.1021/jacs.1c00703.

(81) Zheng, Q.; Woehl, J. L.; Kitamura, S.; Santos-Martins, D.; Smedley, C. J.; Li, G.; Forli, S.; Moses, J. E.; Wolan, D. W.; Sharpless, K. B. SuFEx-Enabled, Agnostic Discovery of Covalent Inhibitors of Human Neutrophil Elastase. *Proceedings of the National Academy of Sciences* **2019**, *116* (38), 18808–18814. https://doi.org/10.1073/pnas.1909972116.

(82) Zhao, Q.; Ouyang, X.; Wan, X.; Gajiwala, K. S.; Kath, J. C.; Jones, L. H.; Burlingame, A. L.; Taunton, J. Broad-Spectrum Kinase Profiling in Live Cells with Lysine-Targeted Sulfonyl Fluoride Probes. *J Am Chem Soc* **2017**, *139* (2), 680–685. https://doi.org/10.1021/jacs.6b08536.

(83) Fadeyi, O. O.; Hoth, L. R.; Choi, C.; Feng, X.; Gopalsamy, A.; Hett, E. C.; Kyne, R. E.; Robinson, R. P.; Jones, L. H. Covalent Enzyme Inhibition through Fluorosulfate Modification of a Noncatalytic Serine Residue. *ACS Chem Biol* **2017**, *12* (8), 2015–2020. https://doi.org/10.1021/acschembio.7b00403.

(84) Hahm, H. S.; Toroitich, E. K.; Borne, A. L.; Brulet, J. W.; Libby, A. H.; Yuan, K.; Ware, T. B.; McCloud, R. L.; Ciancone, A. M.; Hsu, K.-L. Global Targeting of Functional Tyrosines Using Sulfur-Triazole Exchange Chemistry. *Nat Chem Biol* **2020**, *16* (2), 150–159. https://doi.org/10.1038/s41589-019-0404-5.

(85) Borne, A. L.; Brulet, J. W.; Yuan, K.; Hsu, K. L. Development and Biological Applications of Sulfur-Triazole Exchange (SuTEx) Chemistry. *RSC Chemical Biology*. Royal Society of Chemistry April 1, 2021, pp 322–337. https://doi.org/10.1039/d0cb00180e.

(86) Mukherjee, H.; Debreczeni, J.; Breed, J.; Tentarelli, S.; Aquila, B.; Dowling, J. E.; Whitty, A.; Grimster, N. P. A Study of the Reactivity of S(VI)-F Containing Warheads with Nucleophilic Amino-Acid Side Chains under Physiological Conditions. *Org Biomol Chem* **2017**, *15* (45), 9685–9695. https://doi.org/10.1039/c7ob02028g.

(87) Chen, X. H.; Xiang, Z.; Hu, Y. S.; Lacey, V. K.; Cang, H.; Wang, L. Genetically Encoding an Electrophilic Amino Acid for Protein Stapling and Covalent Binding to Native Receptors. *ACS Chem Biol* **2014**, *9* (9), 1956–1961. https://doi.org/10.1021/cb500453a.

(88) Liu, J.; Cao, L.; Klauser, P. C.; Cheng, R.; Berdan, V. Y.; Sun, W.; Wang, N.; Ghelichkhani, F.; Yu, B.; Rozovsky, S.; Wang, L. A Genetically Encoded Fluorosulfonyloxybenzoyl- l -Lysine for Expansive Covalent Bonding of Proteins via SuFEx Chemistry. *J Am Chem Soc* **2021**, *143* (27), 10341–10351. https://doi.org/10.1021/jacs.1c04259.

(89) Klauser, P. C.; Berdan, V. Y.; Cao, L.; Wang, L. Encoding Latent SuFEx Reactive Meta-Fluorosulfate Tyrosine to Expand Covalent Bonding of Proteins. *Chemical Communications* **2022**, *58* (48), 6861–6864. https://doi.org/10.1039/d2cc01902g.

(90) Nanxi, W.; Bing, Y.; Caiyun, F.; He, Z.; Feng, Z.; Tomonori, K.; Jun, L.; Shanshan, L.; Cheng, M.; Peng G., W.; Qian, W.; Lei, W. Genetically Encoding Fluorosulfate-L-tyrosine To React with Lysine, Histidine, and Tyrosine via SuFEx in Proteins in Vivo. *J Am Chem Soc* **2018**, *140* (15), 4995–4999.

(91) Li, Q.; Chen, Q.; Klauser, P. C.; Li, M.; Zheng, F.; Wang, N.; Li, X.; Zhang, Q.; Fu, X.; Wang, Q.; Xu, Y.; Wang, L. Developing Covalent Protein Drugs via Proximity-Enabled Reactive Therapeutics. *Cell* **2020**, *182* (1), 85-97.e16. https://doi.org/10.1016/j.cell.2020.05.028.

(92) Zhang, H.; Han, Y.; Yang, Y.; Lin, F.; Li, K.; Kong, L.; Liu, H.; Dang, Y.; Lin, J.; Chen, P. R. Covalently Engineered Nanobody Chimeras for Targeted Membrane Protein Degradation. *J Am Chem Soc* **2021**, *143* (40), 16377–16382. https://doi.org/10.1021/jacs.1c08521.
(93) Cigler, M.; Müller, T. G.; Horn-Ghetko, D.; von Wrisberg, M.-K.; Fottner, M.; Goody, R. S.; Itzen, A.; Müller, M. P.; Lang, K. Proximitäts-Vermittelte Kovalente Stabilisierung Niedrig-Affiner Proteinkomplexe in Vitro Und in Vivo. *Angewandte Chemie* **2017**, *129* (49), 15943–15947. https://doi.org/10.1002/ange.201706927.
(94) Li, S.; Wang, N.; Yu, B.; Sun, W.; Wang, L. Genetically Encoded Chemical Crosslinking of Carbohydrate. *Nat Chem* **2022**. https://doi.org/10.1038/s41557-022-01059-z.
(95) Sun, W.; Wang, N.; Liu, H.; Yu, B.; Jin, L.; Ren, X.; Shen, Y.; Wang, L. Genetically Encoded Chemical Crosslinking of RNA in Vivo. *Nat Chem* **2022**. https://doi.org/10.1038/s41557-022-01038-4.
(96) Hoppmann, C.; Wang, L. Proximity-Enabled Bioreactivity to Generate Covalent Peptide Inhibitors of P53-Mdm4. *Chemical Communications* **2016**, *52* (29), 5140–5143. https://doi.org/10.1039/c6cc01226d.
(97) Gambini, L.; Udompholkul, P.; Baggio, C.; Muralidharan, A.; Kenjić, N.; Assar, Z.; Perry, J. J. P.; Pellecchia, M. Design, Synthesis, and Structural Characterization of Lysine Covalent BH3 Peptides Targeting Mcl-1. *J Med Chem* **2021**, *64* (8), 4903–4912. https://doi.org/10.1021/acs.jmedchem.1c00005.
(98) Chaudhry, C. Mathematical Model for Covalent Proteolysis Targeting Chimeras: Thermodynamics and Kinetics Underlying Catalytic Efficiency. *J Med Chem* **2023**. https://doi.org/10.1021/acs.jmedchem.2c02076.
(99) Buckley, D. L.; Raina, K.; Darricarrere, N.; Hines, J.; Gustafson, J. L.; Smith, I. E.; Miah, A. H.; Harling, J. D.; Crews, C. M. HaloPROTACS: Use of Small Molecule PROTACs to Induce Degradation of HaloTag Fusion Proteins. *ACS Chem Biol* **2015**, *10* (8), 1831–1837. https://doi.org/10.1021/acschembio.5b00442.
(100) Tinworth, C. P.; Lithgow, H.; Dittus, L.; Bassi, Z. I.; Hughes, S. E.; Muelbaier, M.; Dai, H.; Smith, I. E. D.; Kerr, W. J.; Burley, G. A.; Bantscheff, M.; Harling, J. D. PROTAC-Mediated Degradation of Bruton's Tyrosine Kinase Is Inhibited by Covalent Binding. *ACS Chem Biol* **2019**, *14* (3), 342–347. https://doi.org/10.1021/acschembio.8b01094.
(101) Xue, G.; Chen, J.; Liu, L.; Zhou, D.; Zuo, Y.; Fu, T.; Pan, Z. Protein Degradation through Covalent Inhibitor-Based PROTACs. *Chemical Communications* **2020**, *56* (10), 1521–1524. https://doi.org/10.1039/c9cc08238g.
(102) Zeng, M.; Xiong, Y.; Safaee, N.; Nowak, R. P.; Donovan, K. A.; Yuan, C. J.; Nabet, B.; Gero, T. W.; Feru, F.; Li, L.; Gondi, S.; Ombelets, L. J.; Quan, C.; Jänne, P. A.; Kostic, M.; Scott, D. A.; Westover, K. D.; Fischer, E. S.; Gray, N. S. Exploring Targeted Degradation Strategy for Oncogenic KRASG12C. *Cell Chem Biol* **2020**, *27* (1), 19-31.e6. https://doi.org/10.1016/j.chembiol.2019.12.006.
(103) Henning, N. J.; Manford, A. G.; Spradlin, J. N.; Brittain, S. M.; Zhang, E.; McKenna, J. M.; Tallarico, J. A.; Schirle, M.; Rape, M.; Nomura, D. K. Discovery of a Covalent FEM1B Recruiter for Targeted Protein Degradation Applications. *J Am Chem Soc* **2022**, *144* (2), 701–708. https://doi.org/10.1021/jacs.1c03980.

(104) Tao, Y.; Remillard, D.; Vinogradova, E. V.; Yokoyama, M.; Banchenko, S.; Schwefel, D.; Melillo, B.; Schreiber, S. L.; Zhang, X.; Cravatt, B. F. Targeted Protein Degradation by Electrophilic PROTACs That Stereoselectively and Site-Specifically Engage DCAF1. *J Am Chem Soc* **2022**. https://doi.org/10.1021/jacs.2c08964.
(105) Henning, N. J.; Manford, A. G.; Spradlin, J. N.; Brittain, S. M.; Zhang, E.; McKenna, J. M.; Tallarico, J. A.; Schirle, M.; Rape, M.; Nomura, D. K. Discovery of a Covalent FEM1B Recruiter for Targeted Protein Degradation Applications. *J Am Chem Soc* **2022**, *144* (2), 701–708. https://doi.org/10.1021/jacs.1c03980.
(106) Bond, M. J.; Chu, L.; Nalawansha, D. A.; Li, K.; Crews, C. M. Targeted Degradation of Oncogenic KRASG12Cby VHL-Recruiting PROTACs. *ACS Cent Sci* **2020**, *6* (8), 1367–1375. https://doi.org/10.1021/acscentsci.0c00411.
(107) Pei, J.; Xiao, Y.; Liu, X.; Hu, W.; Sobh, A.; Yuan, Y.; Zhou, S.; Hua, N.; Mackintosh, S. G.; Zhang, X.; Basso, K. B.; Kamat, M.; Yang, Q.; Licht, J. D.; Zheng, G.; Zhou, D.; Lv, D. Piperlongumine Conjugates Induce Targeted Protein Degradation. *Cell Chem Biol* **2023**, *30* (2), 203-213.e17. https://doi.org/10.1016/j.chembiol.2023.01.004.
(108) Gabizon, R.; Shraga, A.; Gehrtz, P.; Livnah, E.; Shorer, Y.; Gurwicz, N.; Avram, L.; Unger, T.; Aharoni, H.; Albeck, S.; Brandis, A.; Shulman, Z.; Katz, B. Z.; Herishanu, Y.; London, N. Efficient Targeted Degradation via Reversible and Irreversible Covalent PROTACs. *J Am Chem Soc* **2020**, *142* (27), 11734–11742. https://doi.org/10.1021/jacs.9b13907.
(109) Guo, W. H.; Qi, X.; Yu, X.; Liu, Y.; Chung, C. I.; Bai, F.; Lin, X.; Lu, D.; Wang, L.; Chen, J.; Su, L. H.; Nomie, K. J.; Li, F.; Wang, M. C.; Shu, X.; Onuchic, J. N.; Woyach, J. A.; Wang, M. L.; Wang, J. Enhancing Intracellular Accumulation and Target Engagement of PROTACs with Reversible Covalent Chemistry. *Nat Commun* **2020**, *11* (1). https://doi.org/10.1038/s41467-020-17997-6.
(110) Tong, B.; Luo, M.; Xie, Y.; Spradlin, J. N.; Tallarico, J. A.; McKenna, J. M.; Schirle, M.; Maimone, T. J.; Nomura, D. K. Bardoxolone Conjugation Enables Targeted Protein Degradation of BRD4. *Sci Rep* **2020**, *10* (1). https://doi.org/10.1038/s41598-020-72491-9.
(111) Henning, N. J.; Boike, L.; Spradlin, J. N.; Ward, C. C.; Liu, G.; Zhang, E.; Belcher, B. P.; Brittain, S. M.; Hesse, M. J.; Dovala, D.; McGregor, L. M.; Valdez Misiolek, R.; Plasschaert, L. W.; Rowlands, D. J.; Wang, F.; Frank, A. O.; Fuller, D.; Estes, A. R.; Randal, K. L.; Panidapu, A.; McKenna, J. M.; Tallarico, J. A.; Schirle, M.; Nomura, D. K. Deubiquitinase-Targeting Chimeras for Targeted Protein Stabilization. *Nat Chem Biol* **2022**, *18* (4), 412–421. https://doi.org/10.1038/s41589-022-00971-2.
(112) Chan, W. C.; Liu, X.; Magin, R. S.; Girardi, N. M.; Ficarro, S. B.; Hu, W.; Tarazona Guzman, M. I.; Starnbach, C. A.; Felix, A.; Adelmant, G.; Varca, A. C.; Hu, B.; Bratt, A. S.; DaSilva, E.; Schauer, N. J.; Jaen Maisonet, I.; Dolen, E. K.; Ayala, A. X.; Marto, J. A.; Buhrlage, S. J. Accelerating Inhibitor Discovery for Deubiquitinating Enzymes. *Nat Commun* **2023**, *14* (1). https://doi.org/10.1038/s41467-023-36246-0.
(113) Pergu, R.; Shoba, V. M.; Chaudhary, S. K.; Godage, D. N. P. M.; Deb, A.; Singha, S.; Dhawa, U.; Anokhina, V.; Singh, S.; Siriwardena, S. U.; Choudhary, A. Development and Applications of Chimera Platforms for Tyrosine Phosphorylation. https://doi.org/10.1101/2023.03.05.531183.

(114) Reddi, R. N.; Rogel, A.; Gabizon, R.; Rawale, D. G.; Harish, B.; Marom, S.; Tivon, B.; Arbel, Y. S.; Gurwicz, N.; Oren, R.; David, K.; Liu, J.; Duberstein, S.; Itkin, M.; Malitsky, S.; Barr, H.; Katz, B. Z.; Herishanu, Y.; Shachar, I.; Shulman, Z.; London, N. Sulfamate Acetamides as Self-Immolative Electrophiles for Covalent Ligand-Directed Release Chemistry. *J Am Chem Soc* **2023**, *145* (6), 3346–3360. https://doi.org/10.1021/jacs.2c08853.

(115) Reddi, R. N.; Rogel, A.; Resnick, E.; Gabizon, R.; Prasad, P. K.; Gurwicz, N.; Barr, H.; Shulman, Z.; London, N. Site-Specific Labeling of Endogenous Proteins Using CoLDR Chemistry. *J Am Chem Soc* **2021**, *143* (48), 20095–20108. https://doi.org/10.1021/jacs.1c06167.

(116) Parker, C. G.; Domaoal, R. A.; Anderson, K. S.; Spiegel, D. A. An Antibody-Recruiting Small Molecule That Targets HIV Gp120. *J Am Chem Soc* **2009**, *131* (45), 16392–16394. https://doi.org/10.1021/ja9057647.

(117) Lake, B.; Serniuck, N.; Kapcan, E.; Wang, A.; Rullo, A. F. Covalent Immune Recruiters: Tools to Gain Chemical Control over Immune Recognition. *ACS Chem Biol* **2020**, *15* (4), 1089–1095. https://doi.org/10.1021/acschembio.0c00112.

(118) M. McCann, H.; P.M. Lake, B.; S. Hoffman, K.; E. Davola, M.; L. Mossman, K.; F. Rullo, A. Covalent Immune Proximity-Induction Strategy Using SuFEx-Engineered Bifunctional Viral Peptides. *ACS Chem Biol* **2022**, *17* (5), 1269–1281. https://doi.org/10.1021/acschembio.2c00233.

(119) Jakab, A.; Schlosser, G.; Feijlbrief, M.; Welling-Wester, S.; Manea, M.; Vila-Perello, M.; Andreu, D.; Hudecz, F.; Mező, G. Synthesis and Antibody Recognition of Cyclic Epitope Peptides, Together with Their Dimer and Conjugated Derivatives Based on Residues 9-22 of Herpes Simplex Virus Type 1 Glycoprotein D. *Bioconjug Chem* **2009**, *20* (4), 683–692. https://doi.org/10.1021/bc800324g.

(120) Daëron, M. *FC RECEPTOR BIOLOGY*; 1997; Vol. 15. www.annualreviews.org.

(121) Martín-Gago, P.; Olsen, C. A. Medicinal Chemistry Arylfluorosulfate-Based Electrophiles for Covalent Protein Labeling: A New Addition to the Arsenal. Angewandte Chemie. **2019**, *58*, 57–966. https://doi.org/10.1002/ange.201806037.

(122) Liu, X.; Malins, L. R.; Roche, M.; Sterjovski, J.; Duncan, R.; Garcia, M. L.; Barnes, N. C.; Anderson, D. A.; Stone, M. J.; Gorry, P. R.; Payne, R. J. Site-Selective Solid-Phase Synthesis of a CCR5 Sulfopeptide Library to Interrogate HIV Binding and Entry. *ACS Chem Biol* **2014**, *9* (9), 2074–2081. https://doi.org/10.1021/cb500337r.

(123) Strelow, J. M. A Perspective on the Kinetics of Covalent and Irreversible Inhibition. *Journal of Biomolecular Screening*. SAGE Publications Inc. January 1, 2017, pp 3–20. https://doi.org/10.1177/1087057116671509.

(124) Hulme, E. C.; Trevethick, M. A. Ligand Binding Assays at Equilibrium: Validation and Interpretation. *British Journal of Pharmacology*. November 2010, pp 1219–1237. https://doi.org/10.1111/j.1476-5381.2009.00604.x.

(125) Gilbert, K. E.; Vuorinen, A.; Aatkar, A.; Pogány, P.; Pettinger, J.; Grant, E. K.; Kirkpatrick, J. M.; Rittinger, K.; House, D.; Burley, G. A.; Bush, J. T. Profiling Sulfur(VI) Fluorides as Reactive Functionalities for Chemical Biology Tools and Expansion of the Ligandable Proteome. *ACS Chem Biol* **2023**, *18* (2), 285–295. https://doi.org/10.1021/acschembio.2c00633.

(126) Xu, F.; Schillinger, J. A.; Sternberg, M. R.; Johnson, R. E.; Lee, F. K.; Nahmias, A. J.; Markowitz, L. E. Seroprevalence and Coinfection with Herpes Simplex Virus

Type 1 and Type 2 in the United States, 1988–1994. *J Infect Dis* **2002**, *185* (8), 1019–1024. https://doi.org/10.1086/340041.

(127) Chemaitelly, H.; Nagelkerke, N.; Omori, R.; Abu-Raddad, L. J. Characterizing Herpes Simplex Virus Type 1 and Type 2 Seroprevalence Declines and Epidemiological Association in the United States. *PLoS One* **2019**, *14* (6). https://doi.org/10.1371/journal.pone.0214151.

(128) Hemminki, O.; Dos Santos, J. M.; Hemminki, A. Oncolytic Viruses for Cancer Immunotherapy. *Journal of Hematology and Oncology*. BioMed Central June 29, 2020. https://doi.org/10.1186/s13045-020-00922-1.

(129) Liu, X. Q.; Xin, H. Y.; Lyu, Y. N.; Ma, Z. W.; Peng, X. C.; Xiang, Y.; Wang, Y. Y.; Wu, Z. J.; Cheng, J. T.; Ji, J. F.; Zhong, J. X.; Ren, B. X.; Wang, X. W.; Xin, H. W. Oncolytic Herpes Simplex Virus Tumor Targeting and Neutralization Escape by Engineering Viral Envelope Glycoproteins. *Drug Delivery*. Taylor and Francis Ltd December 4, 2018, pp 1950–1962. https://doi.org/10.1080/10717544.2018.1534895.

10. **Supplemental**

10.1. **Organic Synthesis**

All chemical reagents and solvents were obtained from commercial suppliers (Sigma Aldrich, Broadpharm) and used without further purification. DBCO-NHS was generously provided by A. Adronov (McMaster University, Canada). Tert-butyl-protected glutamate urea lysine (OtBu-GU-lysine) was synthesized as previously described.[117] Milli-Q water was purified using a Milli-Q® EQ 7000 Ultrapure Water Purification System (Millipore, Cat. No. C228480). All column chromatography purification was conducted using a Buchi Pure C-810 Flash purification system using normal phase silica gel (Buchi) or reverse phase C18 columns (Buchi). ^{1}H, ^{13}C, and ^{19}F NMR spectra were all recorded in deuterated dimethyl sulfoxide (DMSO-d_6), deuterated chloroform ($CDCl_3$), deuterated acetonitrile (CD_3CN), or deuterated water (D_2O) on a Bruker 700 MHz spectrometer. LC-MS data was obtained on an LTQ Orbitrap XL system using a 5% to 95% water (0.1% formic acid)/acetonitrile (0.1% formic acid) gradient. LC-HRMS was obtained using a BRUKER MicroTOF II mass spectrometer. Where indicated, a ThermoFisher DIONEX UltiMate 3000 UHPLC+, with a Hypersil GOLD, 150x10mm, 5 µm, C18 column purchased

from Sigma Aldrich (Cat. No. 25005-159070) was used for HPLC purification with a 5% to 95% water (0.1% formic acid)/acetonitrile (0.1% formic acid) gradient.

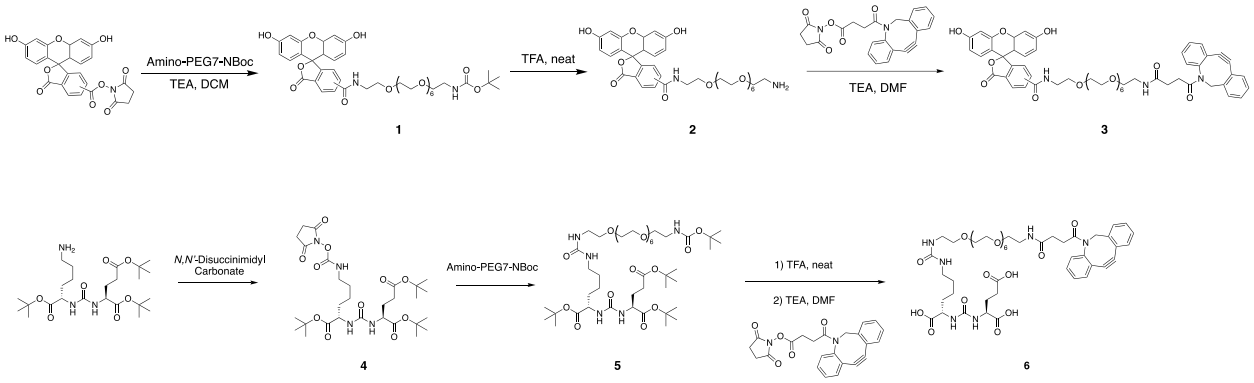

Scheme 1. Synthesis of intermediates **1-8**.

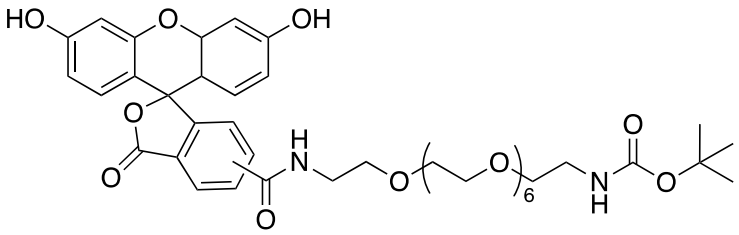

Intermediate 1. Amino-PEG7-NBoc (119 mg, 0.254 mmol, 1.2 eq), TEA (60 µL, 0.432 mmol, 2 eq), and DMF (4 mL) were added to a vial with a stir bar. (5/6)-carboxy fluorescein NHS ester (100 mg, 0.211 mmol, 1 eq) was added and the reaction was performed away from light for 24 hours. A 12 g C18 column with a 5% to 95% water/acetonitrile gradient was used to isolate the final product in 28.13% yield (49.3 mg, 0.0595 mmol). ^{1}H NMR (700 MHz, $CDCl_3$) δ 8.43 (s, 0.5H), 8.15 (m, J = 3.4 Hz, 1H), 8.04 (d, J = 8.1 Hz, 0.5H), 7.58 (s, 0.5H), 7.54 (s, 0.5H), 7.37 (s, 0.5H), 7.20 (d, J = 7.9 Hz, 0.5H), 6.73 (d, J = 2.0 Hz, 1H), 6.70 (d, J = 2.3 Hz, 1H), 6.59 (s, 1H), 6.49 (m, 4H), 5.22 (m, 1H), 3.59 (m, 32H), 1.42 (s, 9H).

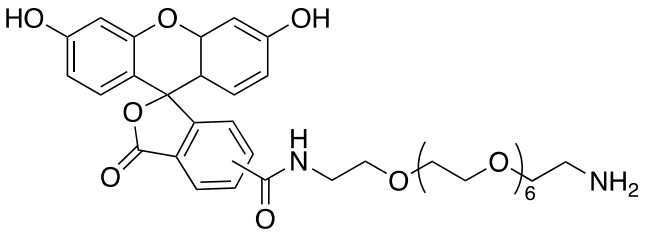

Intermediate 2. TFA (excess, 1 mL) was added to a vial with a stir bar and intermediate **1** (49.3 mg, 0.0595 mmol). After 3 hours of stirring, the TFA was removed by evaporation using continuous airflow. DCM was transferred to the product and co-evaporated three times to aid in TFA removal. The product was obtained in quantitative yield and carried over to the next reaction step. ^{1}H NMR (700 MHz, D_2O) δ 8.62 (s, 0.5H), 8.35 (d, J = 8.5 Hz, 0.5H), 8.19 (d, J = 7.7 Hz, 0.5H), 8.15 (d, J = 8.7 Hz, 0.5H), 7.65 (s, 0.5H), 7.44 (d, J = 7.5 Hz, 0.5H), 7.27 (d, J = 9.0 Hz, 1H), 7.24 (d, J = 9.1 Hz, 1H), 7.12 (s, 1H), 7.09 (s, 1H), 6.98 (d, J = 9.4 Hz, 1H), 6.95 (q, J = 3.4 Hz, 1H), 3.64 (m, 34H), 3.19 (t, J = 4.8 Hz, 1H).

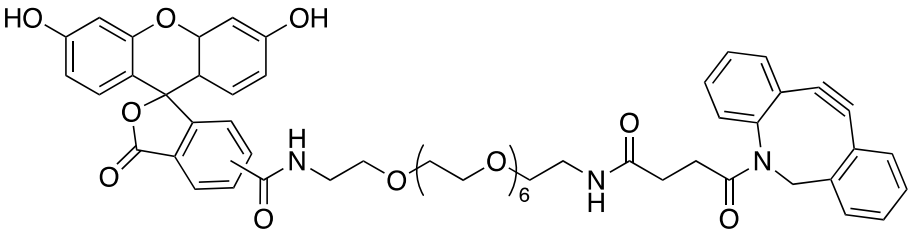

Intermediate 3. Intermediate **2** (17.5 mg, 0.0241 mmol, 1 eq), TEA (3.36 µL, 0.0241 mmol, 1 eq), and DCM (1 mL) were added to a vial with a stir bar. DBCO-NHS (11.6 mg, 0.0289 mmol, 1.2 eq) was added while stirring. After 3 hours, the reaction was washed twice with water and once with brine. The crude product was purified by normal phase flash chromatography to isolate the final product in 18% yield (4.4 mg, 0.00434 mmol).

^{1}H NMR (700 MHz, $CDCl_3$) δ 8.47 (s, 0.5H), 8.17 (d, J = 8.0 Hz, 0.5H), 8.14 (d, J = 8.0 Hz, 0.5H), 8.05 (d, J = 8.1 Hz, 0.5H), 7.64 (t, J = 6.4 Hz, 1H), 7.57 (s, 1H) 7.56 (s, 0.5H), 7.50 (m, 1H), 7.36 (m, 3H), 7.30 (m, 2H), 7.17 (m, 0.5H), 6.71 (s, 1H), 6.69 (s, 1H) 6.60 (m, 2H), 6.49 (m, 2H), 6.39 (m, 2H), 5.13 (dd, J = 6.6, 14.1 Hz, 1H), 3.65 (m, 7H), 3.52 (m, 24H), 3.40 (m, 2H), 3.29 (m, 2H), 2.80 (m, 1H), 2.43 (m, 1H), 2.20 (m, 1H), 1.97 (m, 1H). LC-HRMS $[M+H]^+$ m/z calc for $[C_{56}H_{61}N_3O_{15}]$ 1015.41027, found 1014.4351.

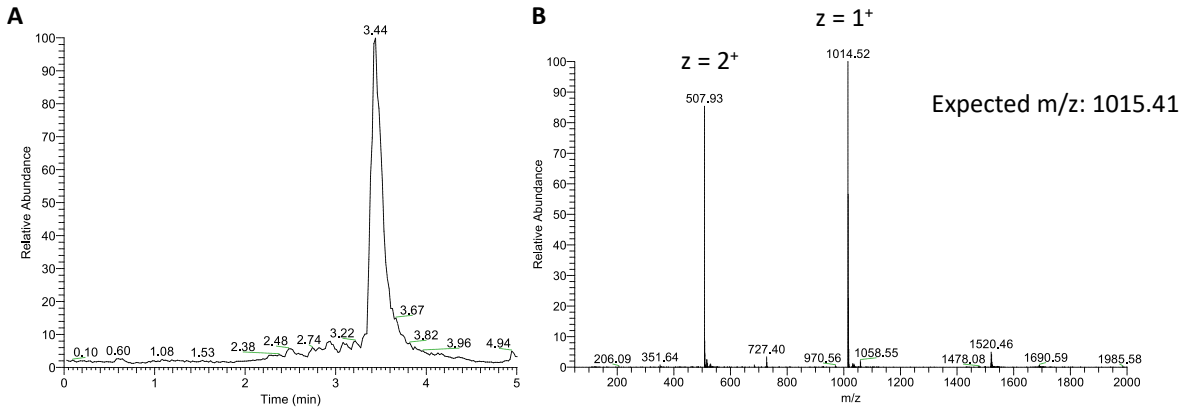

Figure 26. LC-MS characterization of 3. **A)** Total ion chromatogram and **B)** ions detected at 3.44 minutes.

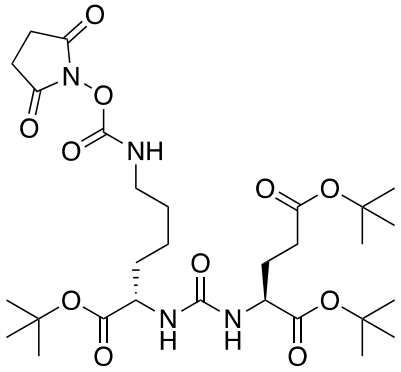

Intermediate 4. OtBu-GU-lysine (154.6 mg, 0.317 mmol, 1 eq) was dissolved in toluene (2 mL) and evaporated under vacuum to remove residual water. All steps were then performed under anhydrous conditions and inert nitrogen atmosphere. DMF (14.3 mL), *N*,*N*'-disuccinimidyl carbonate (89.4 mg, 0.349 mmol, 1.1 eq), and TEA (44.2 µL, 0.317

mmol, 1 eq) were added. The solution was left to stir overnight. The reaction solution was then diluted with EtOAc (50 mL) and washed with 10% citric acid three times, followed by three brine washes. The organic layer was dried over anhydrous Mg_2SO_4 and concentrated under vacuum. The crude product was purified via flash silica gel column chromatography (3:1 EtOAc/Hexanes) to yield intermediate I-**7** in 26.7% yield (53.2 mg, 0.0846 mmol), as a clear oil. ^{1}H NMR (700 MHz, $CDCl_3$) δ 6.62 (s, 1H), 5.55 (d, J = 8.0 Hz, 2H), 5.46 (d, J = 8.3 Hz, 2H), 4.31 (m, J = 4.1 Hz, 2H), 3.24 (m, J = 7.6 Hz, 2H), 2.83 (s, 4H), 2.28 (m, J = 5.4 Hz, 2H), 2.02 (s, 1H), 1.80 (m, J = 4.6 Hz, 1H), 1.74 (m, J = 4.8 Hz, 1H), 1.60 (m, J = 4.6 Hz, 1H), 1.54 (m, J = 7.0 Hz, 1H), 1.43 (s, 9H), 1.43 (s, 9H), 1.41 (s, 9H), 1.35 (m, J = 6.1 Hz, 1H).

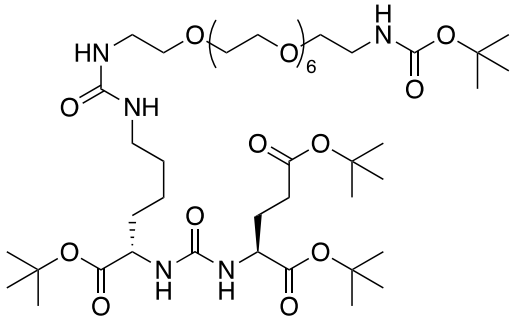

Intermediate 5. Amino-PEG7-NBoc (208.53 mg, 0.445 mmol, 1.5 eq) and TEA (50.9 µL, 0.365 mmol, 1.2 eq) were dissolved in DCM (2 mL). Intermediate **4** (186.73 mg, 0.297 mmol, 1 eq) was added to the vial while stirring. The reaction was left for 24 hours, before purification by normal phase flash chromatography using a 5% to 20% DCM/MeOH gradient. The final product was isolated in 43.99% yield (125.72 mg, 0.128 mmol). ^{1}H NMR (700 MHz, CD_3CN) δ 5.66 (d, *J* = 7.8 Hz, 1H), 5.45 (d, *J* = 8.1 Hz, 1H), 5.40 (s, 1H), 5.17 (t, *J* = 5.7 Hz, 1H), 5.13 (t, *J* = 5.3 Hz, 1H), 4.13 (m, 1H), 4.03 (m, 1H), 3.56 (m 25H), 3.45 (m, 4H), 3.23 (q, *J* = 5.4 Hz, 2H), 3.18 (q, *J* = 5.6 Hz, 2H), 3.06 (q, *J* = 6.5 Hz, 2H),

2.25 (m, 2H), 1.96 (s, 1H), 1.74 (m, 1H), 1.69 (m, *J* = 3.7 Hz, 1H), 1.61 (m, *J* = 6.2 Hz, 1H), 1.42 (q, *J* = 7.3 Hz, 40H).

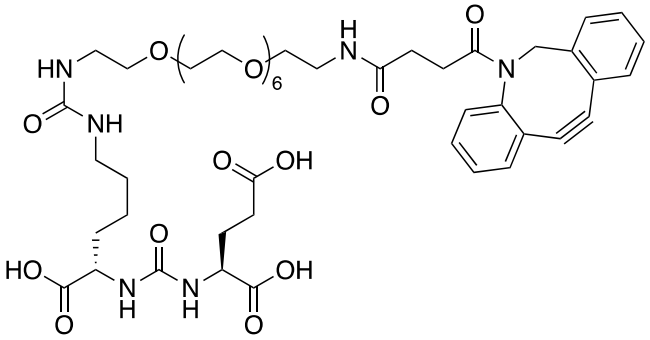

Intermediate 6. Intermediate **5** (30.45 mg, 0.031 mmol, 1 eq) was added to TFA (2 mL, neat) while stirring vigorously. After 24 hours, the TFA was evaporated, and the deprotected product dissolved in 1X PBS (pH 7.2, 0.75 mL). DBCO-NHS (24.14 mg, 0.060 mmol, 4 eq) was dissolved in acetonitrile (0.5 mL) and added to 0.25 mL of GU-PEG7-NH_2 (13.23 mg, 0.015 mmol, 1 eq), while stirring vigorously. After 3 hours, the product was purified by HPLC for a final yield of 16.65% (5.2 mg, 0.0052 mmol) in sufficient analytical quantities to continue. LC-HRMS $[M+H]^+$ m/z calc for $C_{48}H_{68}N_6O_{17}$ 1000.4641, found 1000.4964.

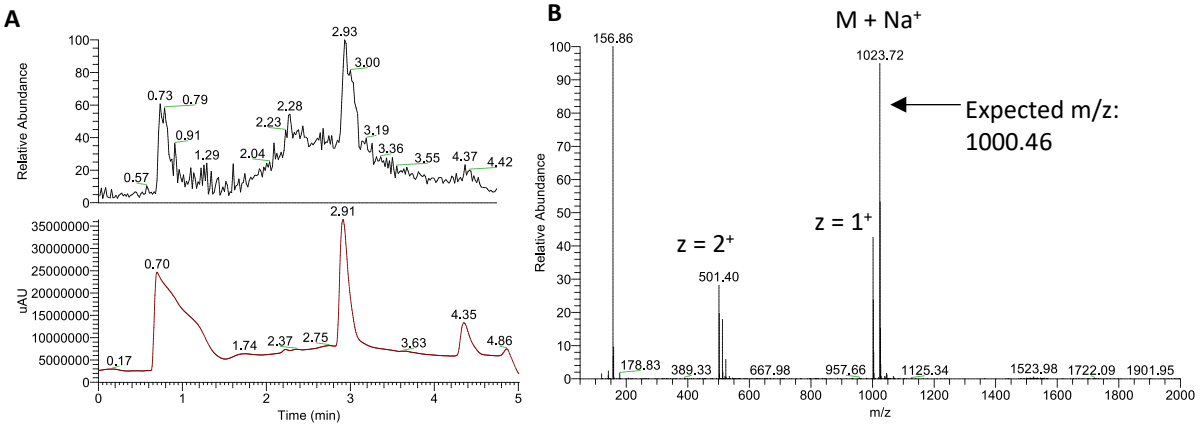

Figure 27. LC-MS characterization of 6. **A)** Total ion chromatogram, **B)** UV trace chromatogram, and **C)** ions detected at 2.93 minutes. A peak appearing at 0.70 minutes corresponds to PBS/acetonitrile.

10.2. **Peptide Synthesis**

General. Each peptide was synthesized by solid phase peptide synthesis (SPPS) on a CEM Liberty Blue peptide synthesizer using Fmoc protecting group chemistry. Rink amide resin was used on a 0.1 mmol scale. Each Fmoc deprotection was performed using 20% piperidine in DMF at 90˚C for 1 minute. Each amino acid coupling was performed using 1 mL of DIC (1.0 M) in DMF, 0.5 mL of OxymaPure (1.0 M) in DMF, and 2.5 mL of each respective amino acid (0.2 M) in DMF. Couplings were performed at 90˚C for 2 minutes. Double couplings were performed for two consecutive non-polar amino acids (amino acids A, P, V, L, I, M, F, W), as well as arginine. Once aspartic acid was added to a peptide, all subsequent couplings/deprotections were performed at 40˚C for 10 minutes. Three washes were performed after each Fmoc deprotection and amino acid coupling.

Capping Protocol. Acetic anhydride was used to cap the N-terminus on bead using a 10% acetic anhydride solution in DMF. This was performed at 40˚C for 10 minutes.

SuFEx Installation. To equip peptides with tyrosine fluorosulfate (FSY) handles, an O-Allyl-protected tyrosine was installed in the desired sequential location using SPPS. After N-terminal acetylation, the O-Allyl protecting group was removed with $Pd(PPh_3)_4$ (0.025 mmol, 0.25 eq) and $PhSiH_3$ (0.5 mmol, 5 eq) in DCM (1 mL). This was done for 30 minutes and repeated once. Following this, the resin was washed 5x with DCM. AISF (0.267 mmol, 8 eq) was then added with DBU (0.267 mmol, 8 eq) in DCM (4 mL) for 30 minutes, while agitating. This was washed 5x with DCM and then vacuum dried. Aryl sulfonyl fluoride (ASF) handles were installed onto peptides in place of N-terminal acetylation. This was

done as a standard amino acid coupling, using 1 mL DIC (1.0 M) and 0.5 mL OxymaPure (1.0 M).

Cleavage Protocol. Peptides were cleaved from the Rink amide resin using 5 mL of a cleavage cocktail (92.5% TFA, 2.5% water, 2.5% phenol, and 2.5% TIPS) for 3 hours, with gentle agitation. Peptide cleavage solutions were diluted with an additional 5 mL of cleavage cocktail, where the total volume was split and precipitated in -20˚C diethyl ether (45 mL) in tandem. Precipitated crude peptide was pelleted with an RCF of 1750 g over a 15-minute period and resuspended in 1% acetic acid in water. This was lyophilized to yield the final crude, capped peptides. A modified cleavage cocktail (95% TFA, 2.5% water, 2.5% TIPS) was used to cleave FSY- and ASF-equipped peptides.

Peptide Purification. An optional HPLC-purification step followed peptide cleavage. Peptides were dissolved in MeOH, followed by water, reaching a ratio of 10% MeOH to 90% water, and a final concentration of 20 mg/mL. Sonication was used to promote the solvation of difficult peptides. Undissolved crude material was pelleted by centrifugation prior to HPLC-purification. A 5% to 95% water/acetonitrile gradient was used to isolate pure peptides on a reverse phase HPLC column.

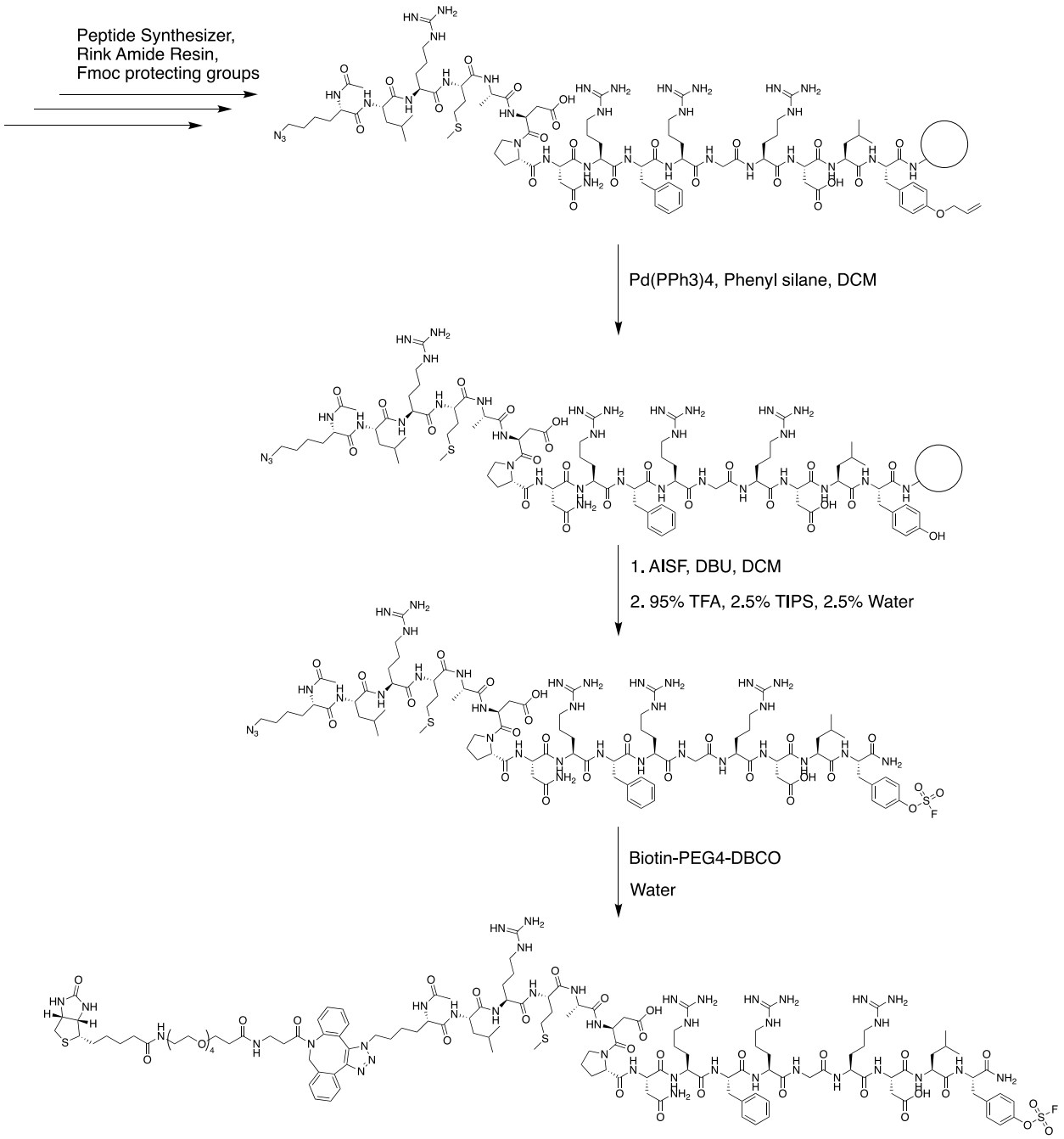

Scheme 2. Chemical synthesis of FSY-modified gD peptides. Provided above is an example for the synthesis of Biotin-gD-FSY.

10.2.1. **Covalent Peptide Synthesis**

Each covalent peptide was synthesized as above using SPPS. Yields were calculated as an estimated yield based on amount of purified peptide after purifying 20 mg of crude peptide. Pure peptides were characterized by LC-MS.

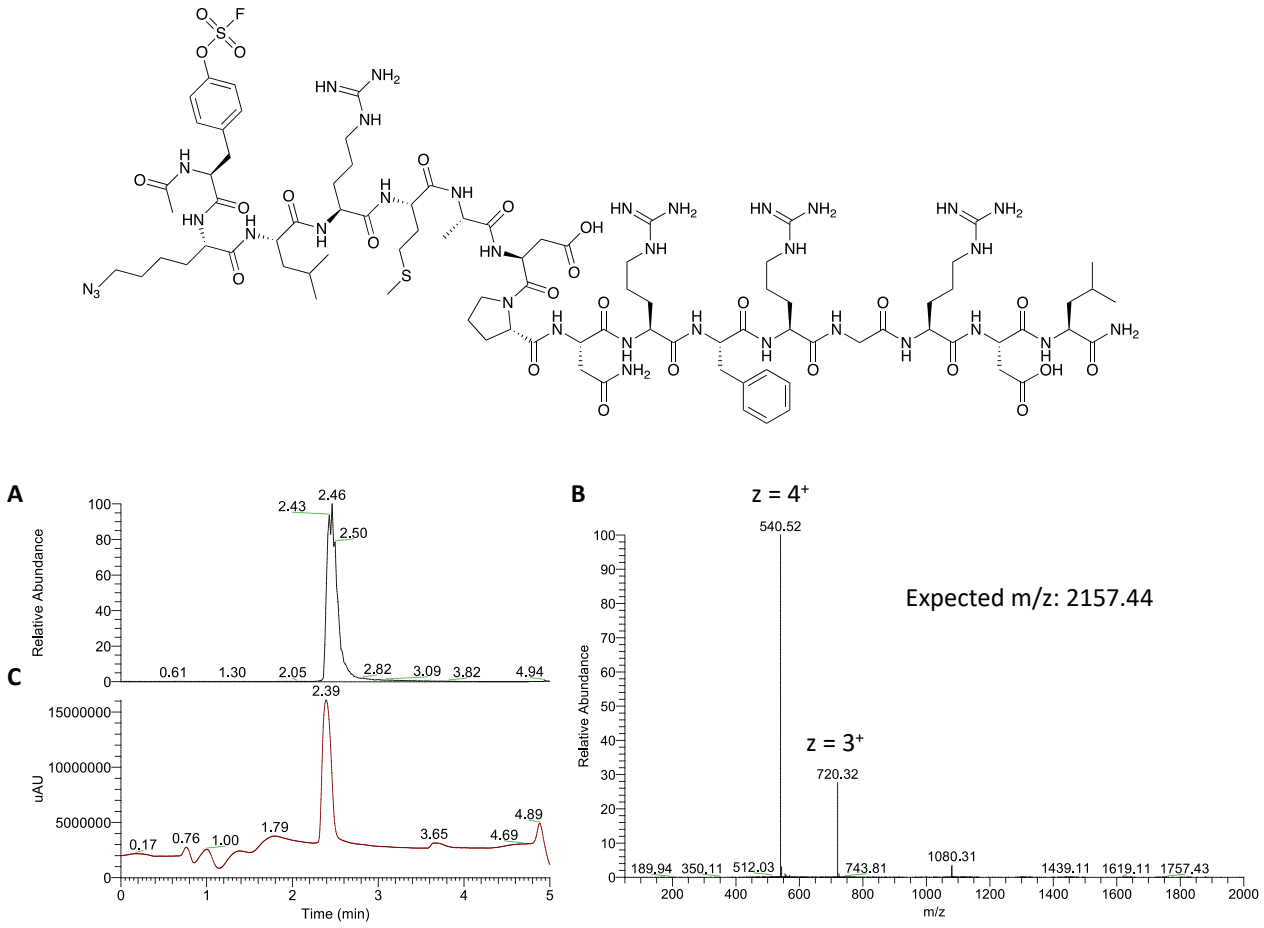

Figure 28. Synthesis of azido-FSY-gD (Peptide sequence: H-Ac-(Y-OSO_2F)-(N_3-K)-LRMADPNRFRGRDL-NH_2). The final peptide was synthesized with an estimated yield of 34%. **A)** Total ion chromatogram, **B)** UV trace chromatogram, and **C)** ions detected at 2.46 minutes.

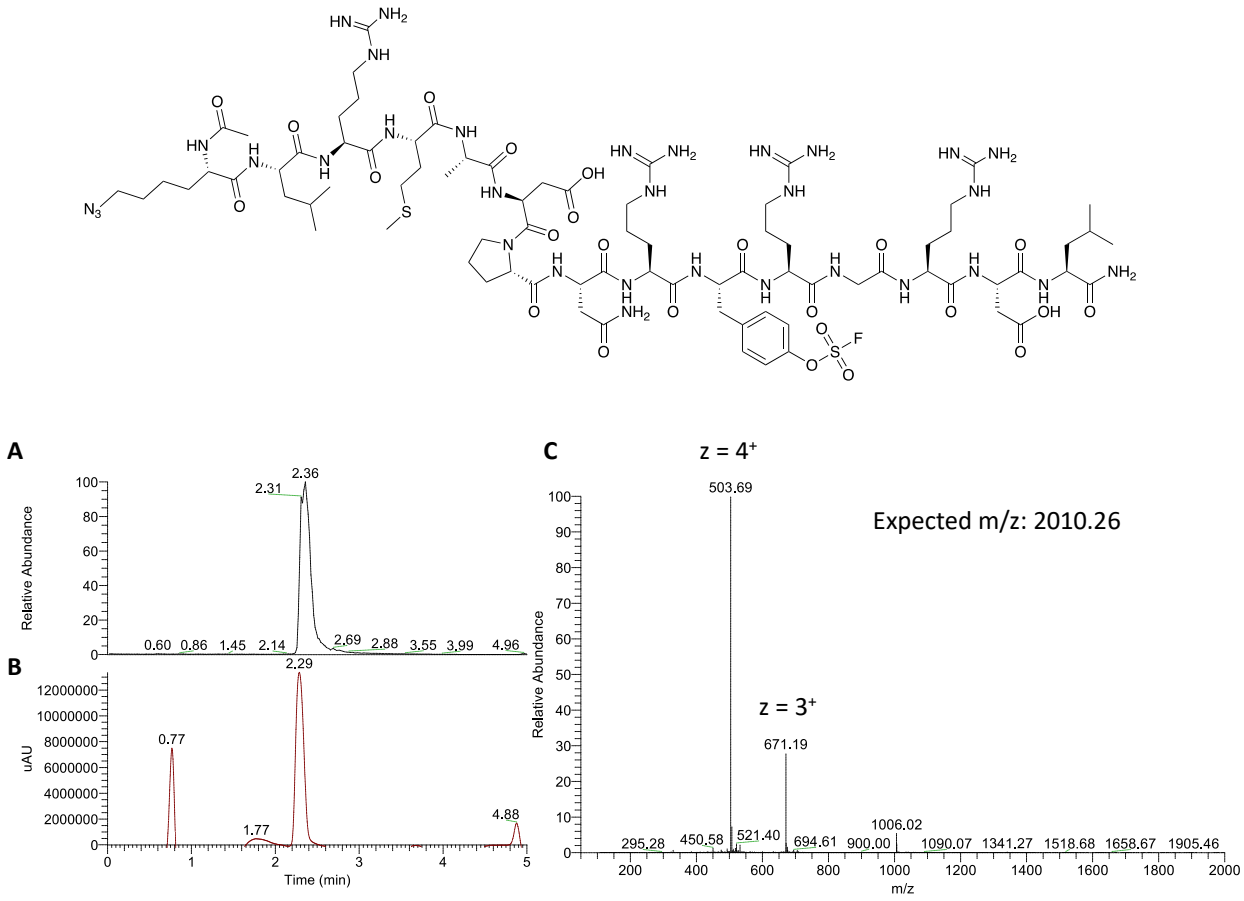

Figure 29. Synthesis of azido-gD(F10FSY) (Peptide sequence: H-Ac-(N_3-K)-LRMADPNR-(Y-OSO_2F)-RGRDL-NH_2). The final peptide was synthesized with an estimated yield of 21%. **A)** Total ion chromatogram, **B)** UV trace chromatogram, and **C)** ions detected at 2.36 minutes. A sharp peak at 0.77 minutes corresponds to acetonitrile.

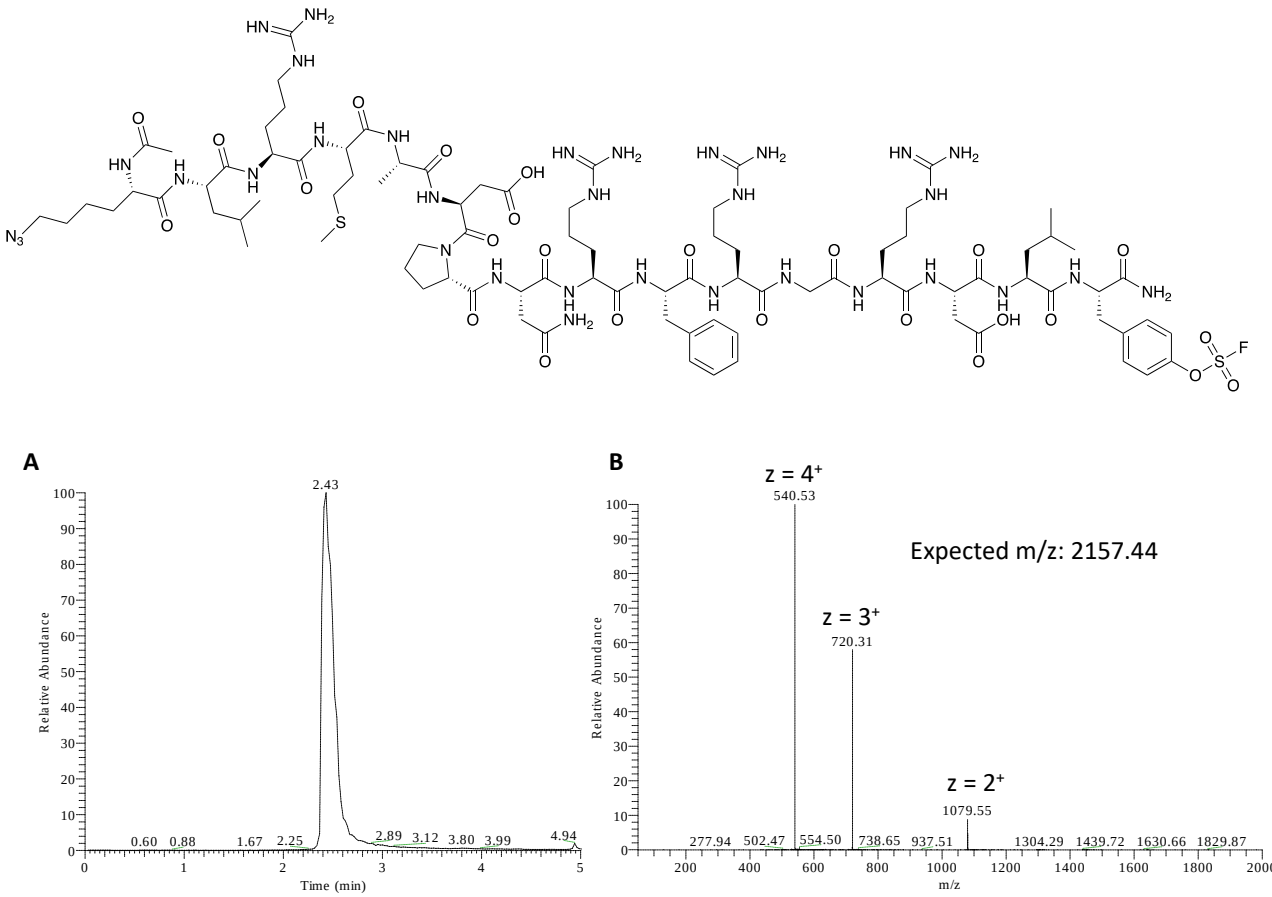

Figure 30. Synthesis of azido-gD-FSY (Peptide sequence: H-Ac-(N_3-K)-LRMADPNRFRGRDL-(Y-OSO_2F)-NH_2). The final peptide was synthesized with an estimated yield of 44%. **A)** Total ion chromatogram and **B)** ions detected at 2.43 minutes.

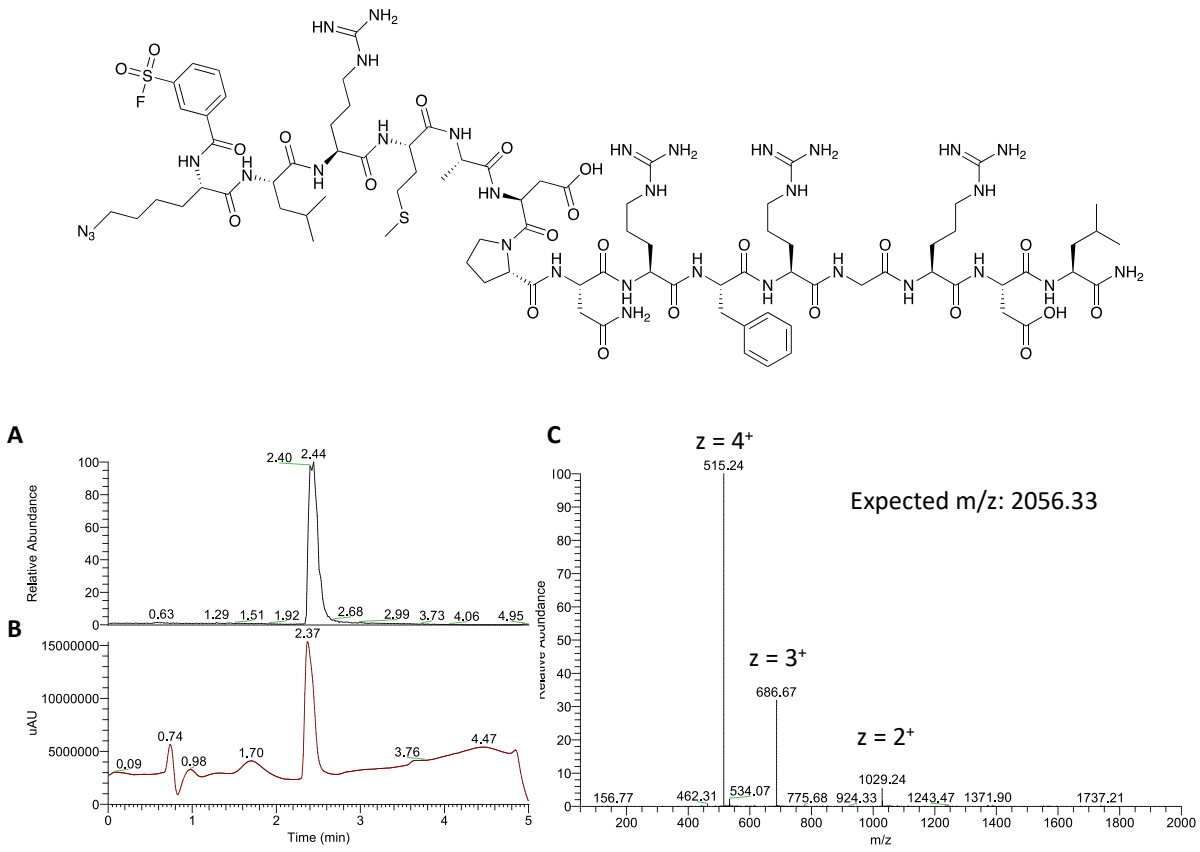

Figure 31. Synthesis of azido-ASF-gD (Peptide Sequence: H-(Aryl-SO_2F)-(N_3-K)-LRMADPNRFRGRDL-NH_2). The final peptide was synthesized with an estimated yield of 13%. **A)** Total ion chromatogram, **B)** UV trace chromatogram, and **C)** ions detected at 2.44 minutes.

10.2.2. **Non-Covalent Binding Peptide Synthesis**

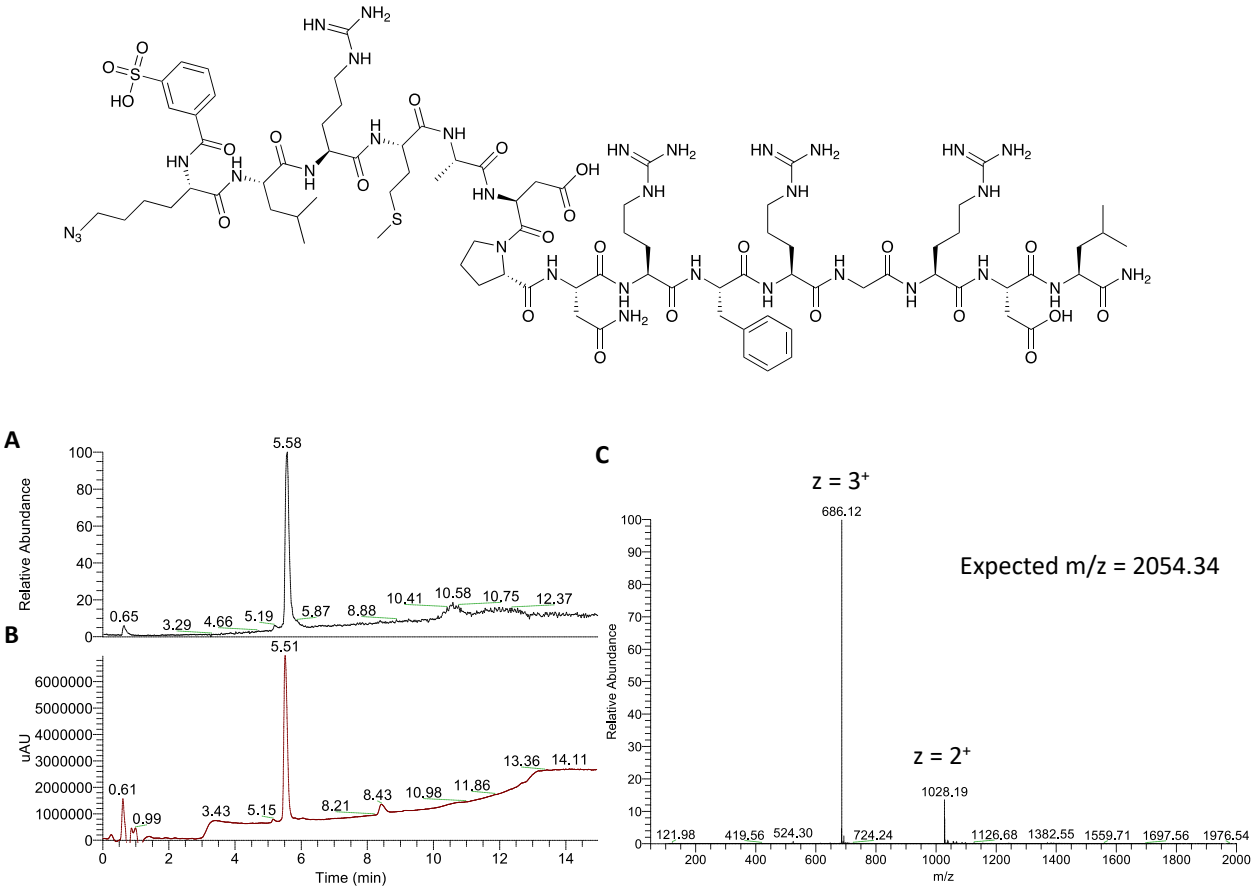

Figure 32. Synthesis of azido-SO_3H-gD (Peptide sequence: H-(Aryl-SO_3H)-(N_3-K)-LRMADPNRFRGRDL-NH_2). The final peptide was synthesized via azido-ASF-gD hydrolysis in 1X PBS over one week. **A)** Total ion chromatogram, **B)** UV trace chromatogram, and **C)** ions detected at 5.58 minutes, using a 15-minute LC-MS method.

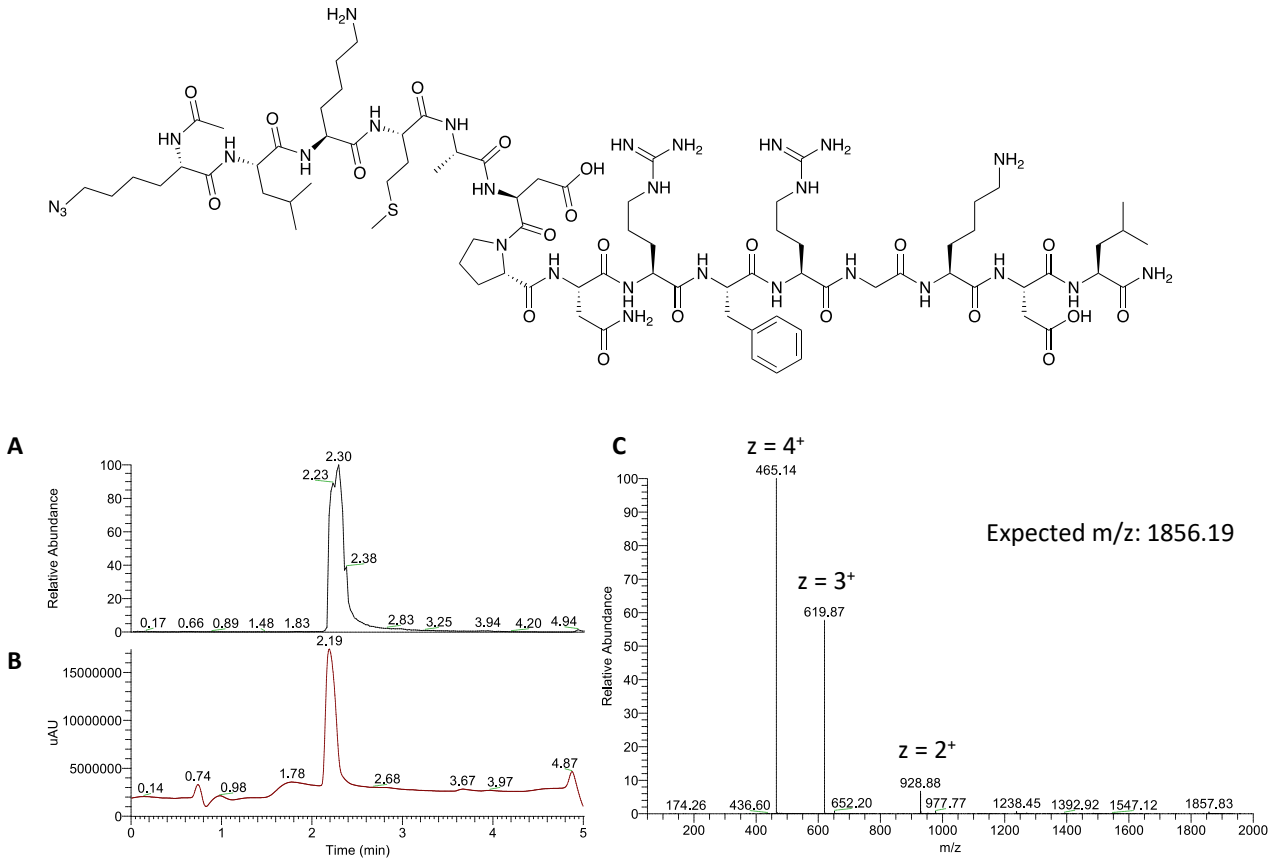

Figure 33. Synthesis of azido-gD (Peptide sequence: H-Ac-(N_3-K)-LKMADPNRFRGKDL-NH_2). The final peptide was synthesized with an estimated yield of 18%. **A)** Total ion chromatogram, **B)** UV trace chromatogram, and **C)** ions detected at 2.30 minutes.

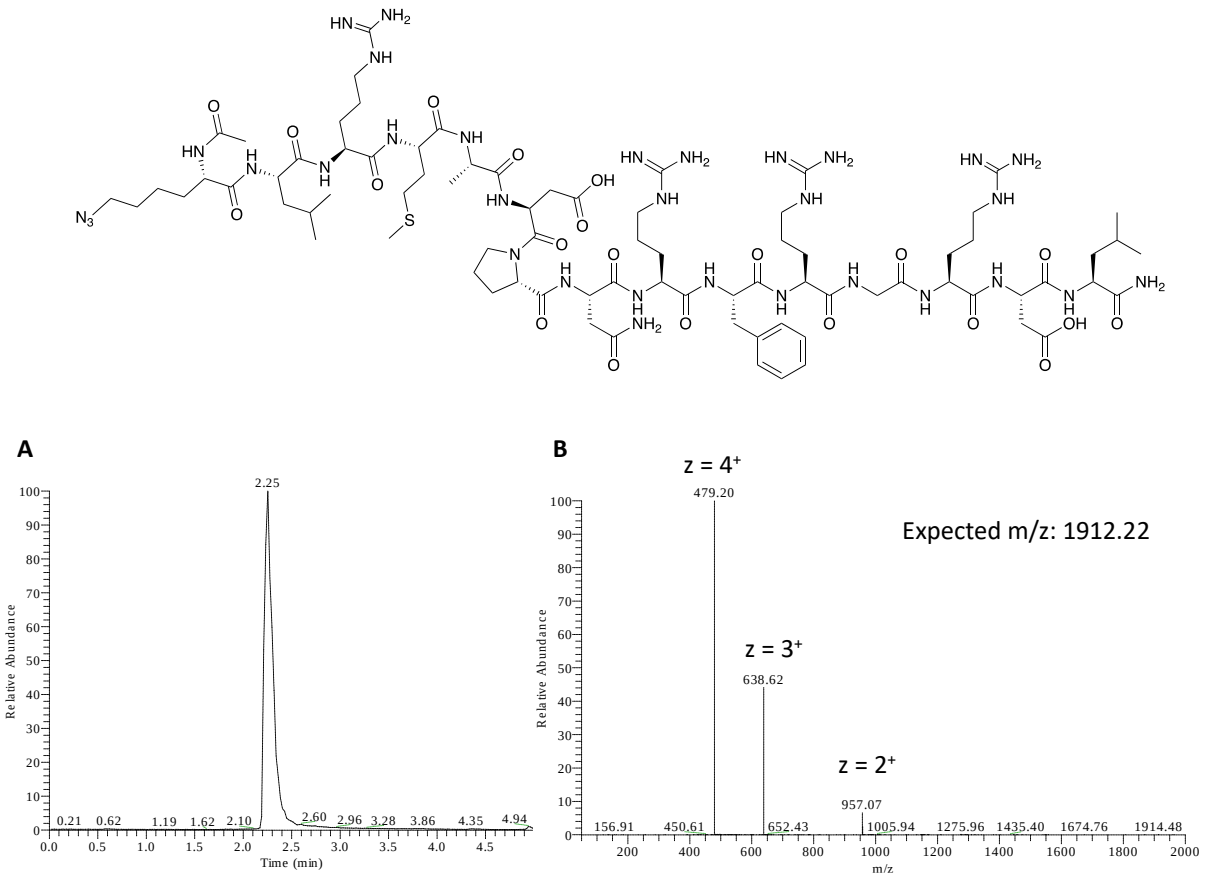

Figure 34. Synthesis of azido-gD-R (Peptide sequence: H-Ac-(N_3-K)-LRMADPNRFRGRDL-NH_2). The final peptide was synthesized with an estimated yield of 28%. **A)** Total ion chromatogram and **B)** ions detected at 2.25 minutes.

10.3. **Synthesis of Covalent Bifunctional Peptides**

Covalent bifunctional peptides were constructed via SPAAC to modularly attach biotin, fluorescein, or GU motifs. Reactions were carried out for three hours, or until complete product conversion was observed. Final bifunctional cARMs were characterized by LC-HRMS.

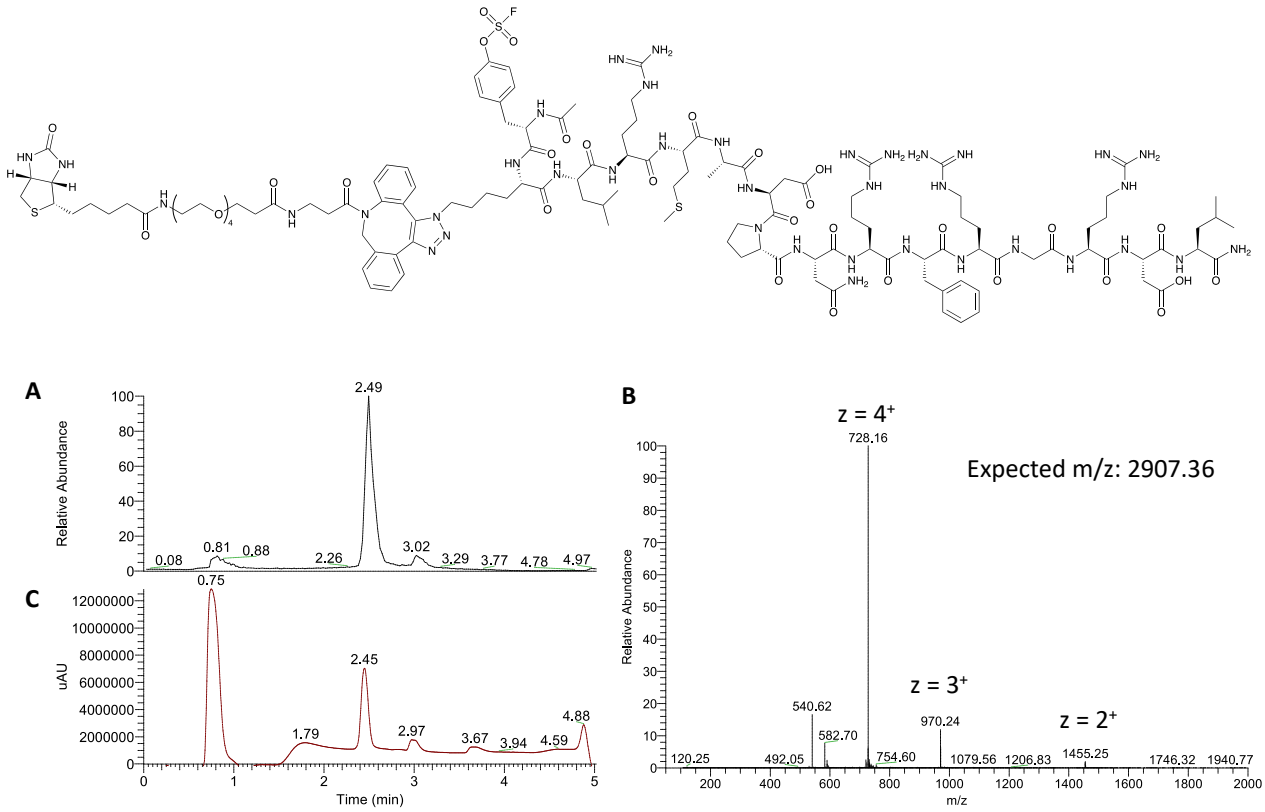

Figure 35. Biotin-FSY-gD was synthesized from azido-FSY-gD and biotin-PEG4-DBCO. LC-HRMS $[M+4H]^{4+}$ m/z calc for $[C_{128}H_{193}FN_{38}O_{33}S_3]$ 727.3535, found 727.6269. **A)** Total ion chromatogram, **B)** UV trace chromatogram, and **C)** ions detected at 2.49 minutes. A sharp peak at 0.75 minutes corresponds to DMSO used to dissolve Biotin-PEG4-DBCO.

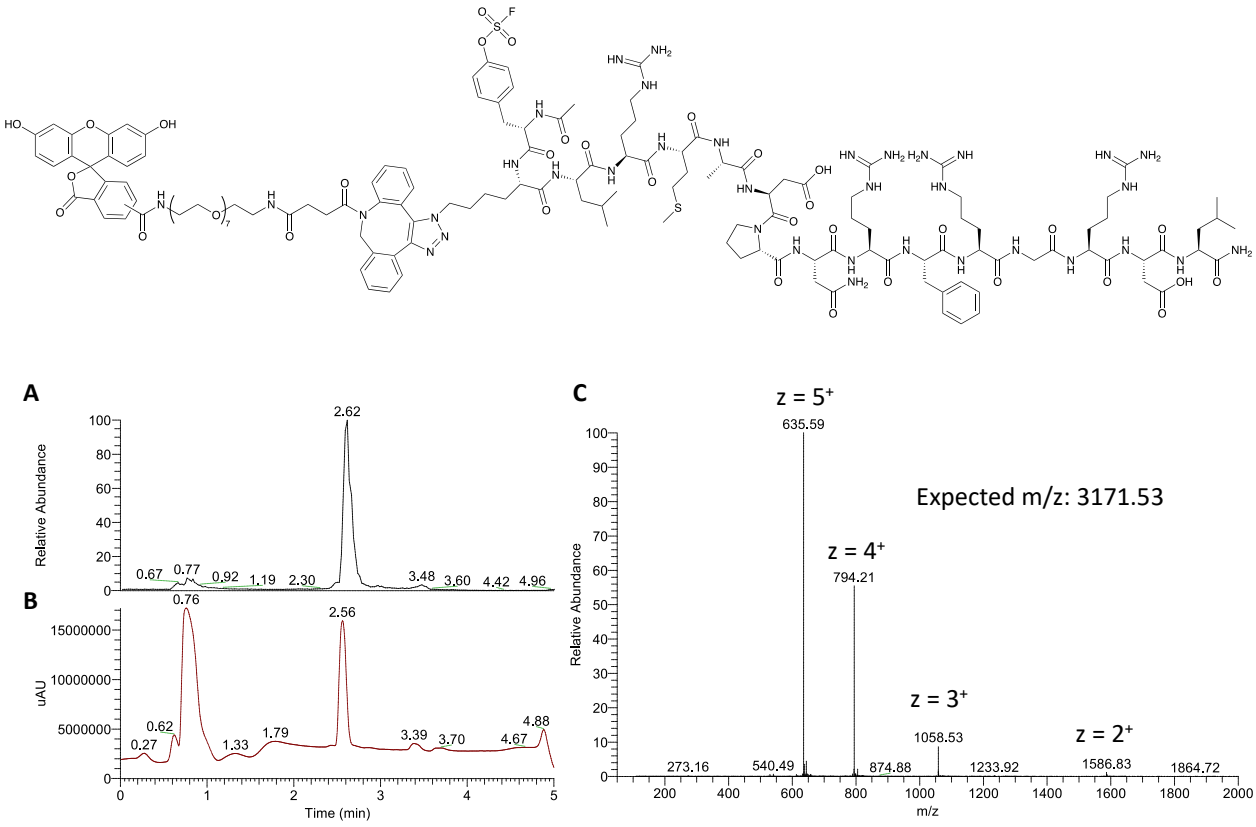

Figure 36. Fluor-FSY-gD was synthesized from azido-FSY-gD and intermediate **3**. LC-HRMS $[M+5H]^{5+}$ m/z calc for $[C_{145}H_{201}FN_{36}O_{40}S_2]$ 634.8845, found 635.3055. **A)** Total ion chromatogram, **B)** UV trace chromatogram, and **C)** ions detected at 2.62 minutes. A sharp UV peak at 0.76 minutes is from DMSO used to dissolve intermediate **3**.

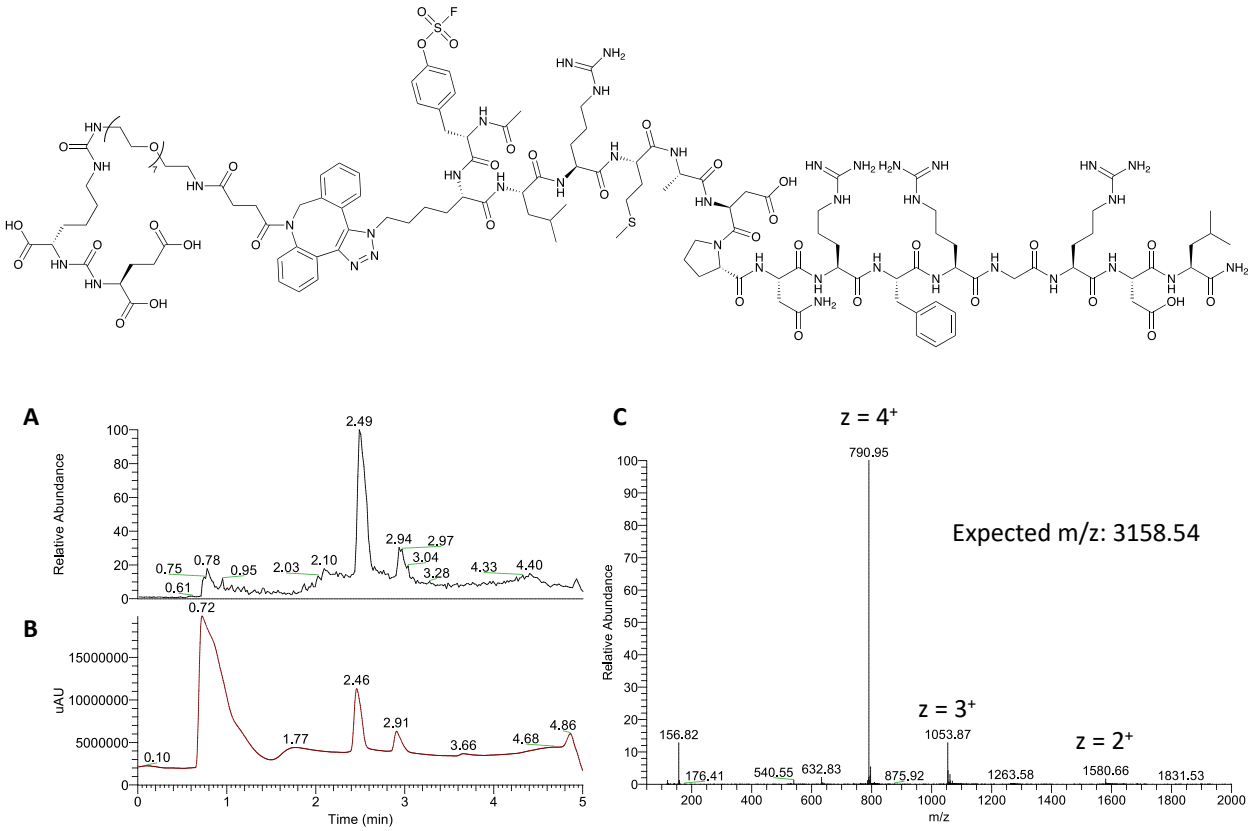

Figure 37. GU-FSY-gD was synthesized from azido-FSY-gD and intermediate **6**. LC-HRMS $[M+4H]^{4+}$ m/z calc for $[C_{137}H_{210}FN_{39}O_{42}S_2]$ 790.1230, found 790.4005. **A)** Total ion chromatogram, **B)** UV trace chromatogram, and **C)** ions detected at 2.49 minutes. A UV peak at 0.72 minutes is from DMSO used to dissolve intermediate **6**.

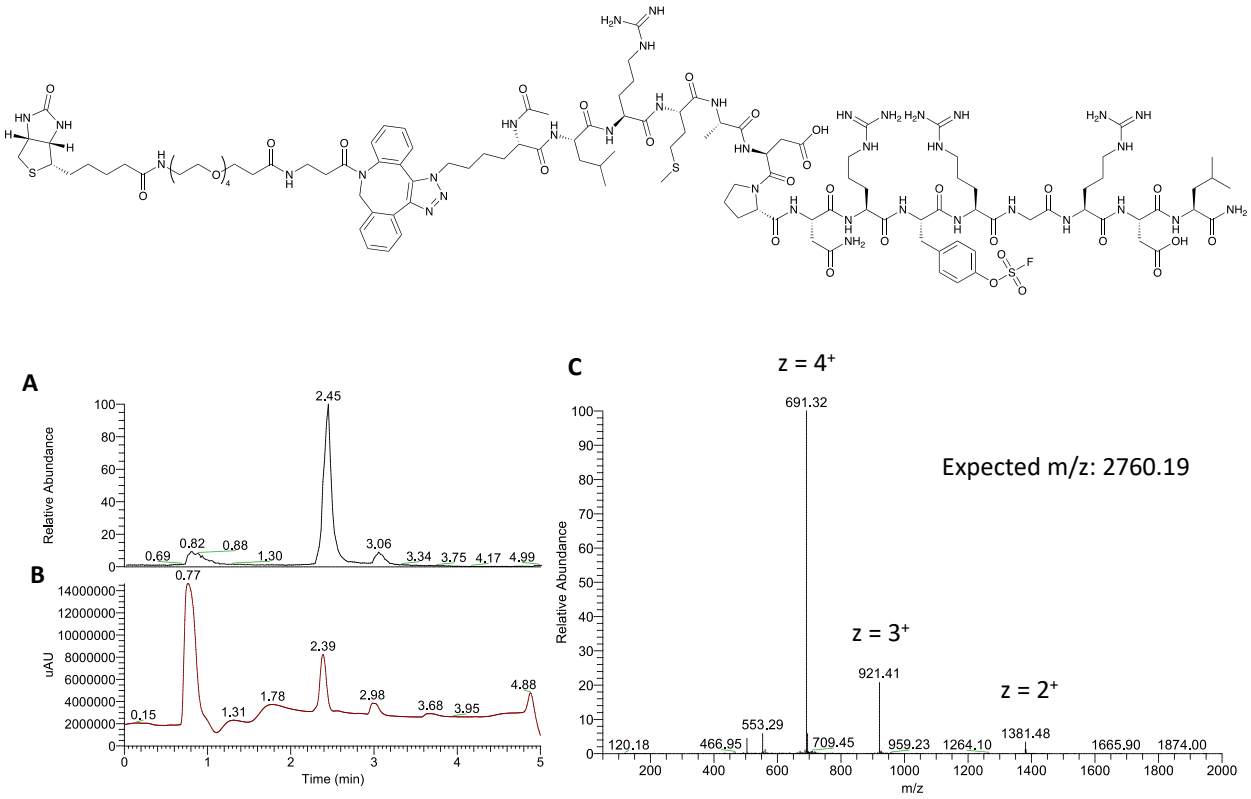

Figure 38. Biotin-gD(F10FSY) was synthesized using azido-gD-(F10FSY) and biotin-PEG4-DBCO. LC-HRMS $[M+4H]^{4+}$ m/z calc for $[C_{119}H_{184}FN_{37}O_{32}S_3]$ 690.5764, found 690.8548. **A)** Total ion chromatogram, **B)** UV trace chromatogram, and **C)** ions detected at 2.45 minutes. A sharp peak at 0.76 minutes corresponds to DMSO used to dissolve Biotin-PEG4-DBCO.

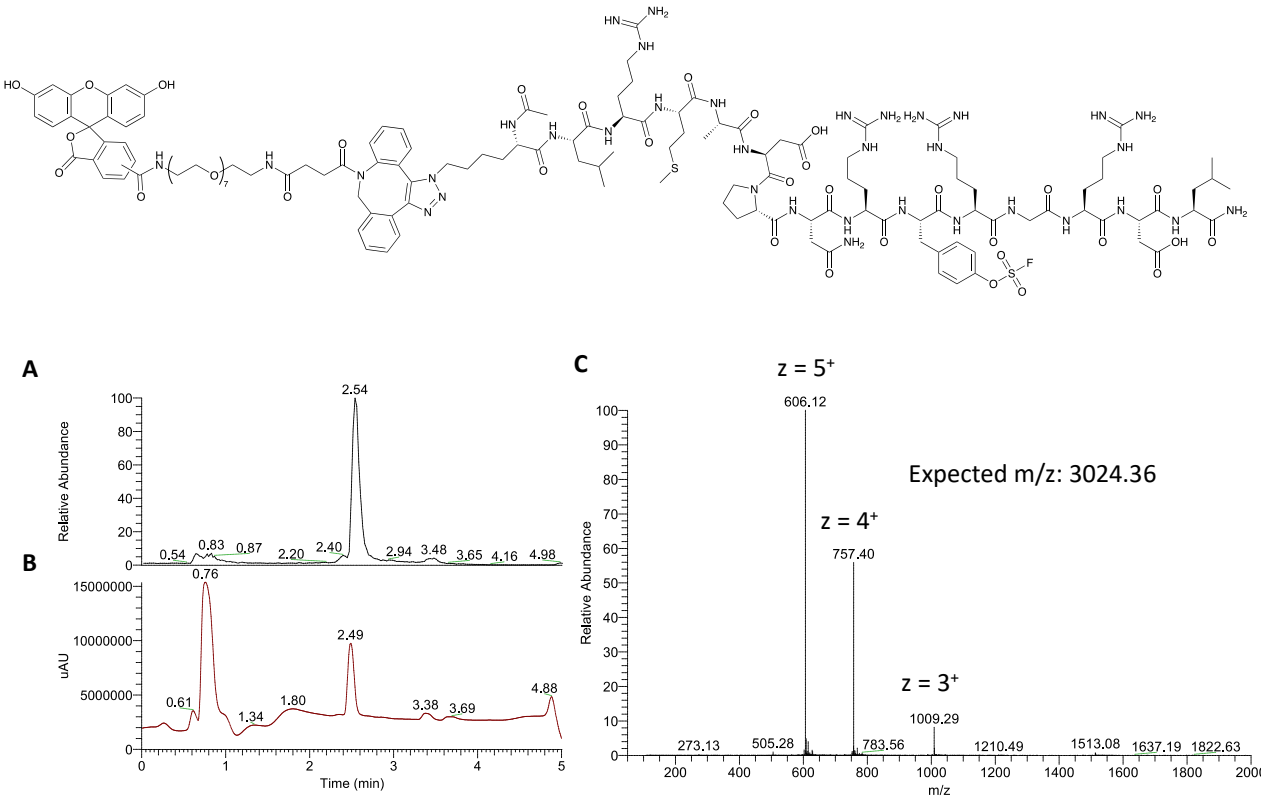

Figure 39. Fluor-gD(F10FSY) was synthesized using azido-gD(F10FSY) and intermediate **3**. LC-HRMS $[M+5H]^{5+}$ m/z calc for $[C_{136}H_{192}FN_{35}O_{39}S_2]$ 605.4708, found 605.6925. **A)** Total ion chromatogram, **B)** UV trace chromatogram, and **C)** ions detected at 2.54 minutes. A sharp peak at 0.76 minutes corresponds to DMSO used to dissolve intermediate **3**.

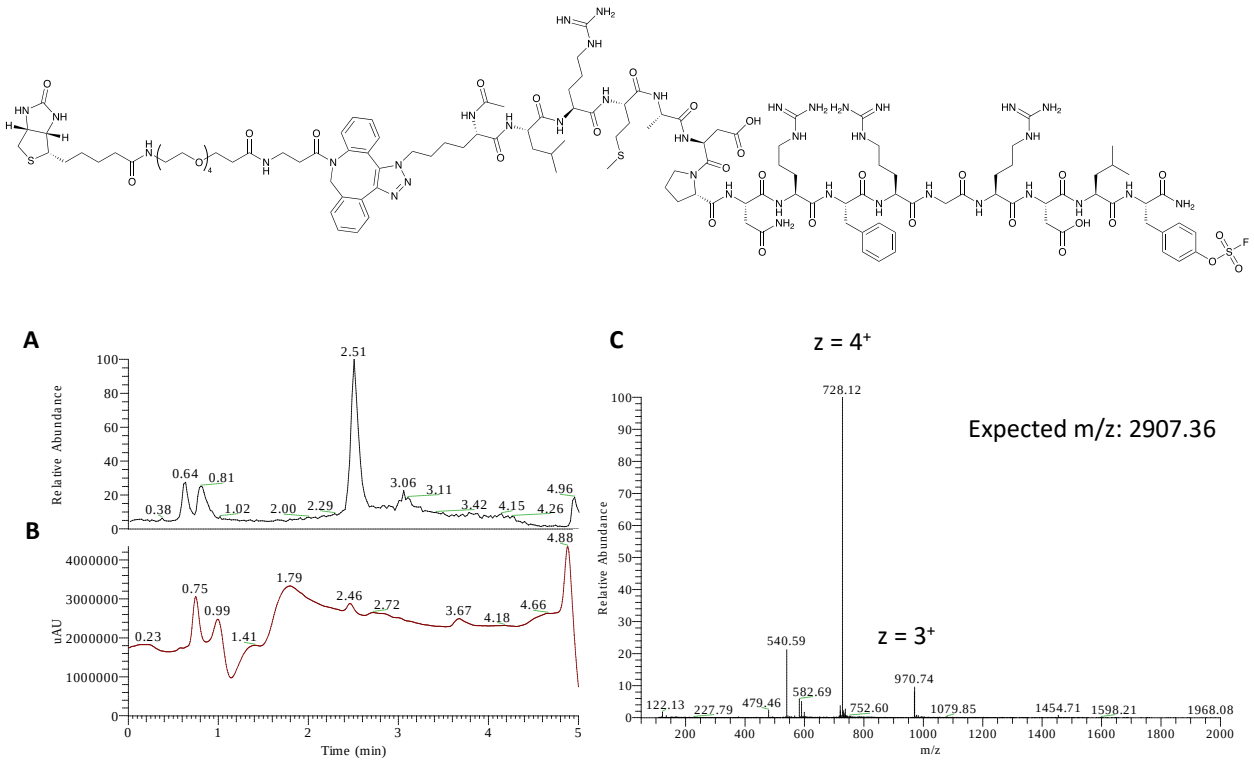

Figure 40. Biotin-gD-FSY was synthesized using azido-gD-FSY and biotin-PEG4-DBCO. LC-HRMS $[M+4H]^{4+}$ m/z calc for $[C_{128}H_{193}FN_{38}O_{33}S_3]$ 727.3435, found 707.1320. **A)** Total ion chromatogram, **B)** UV trace chromatogram, and **C)** ions detected at 2.51 minutes. Peaks appearing at 0.75 & 0.99 minutes correspond to DMSO & MeOH, used to help dissolve Biotin-PEG4-DBCO & azido-gD-FSY, respectively.

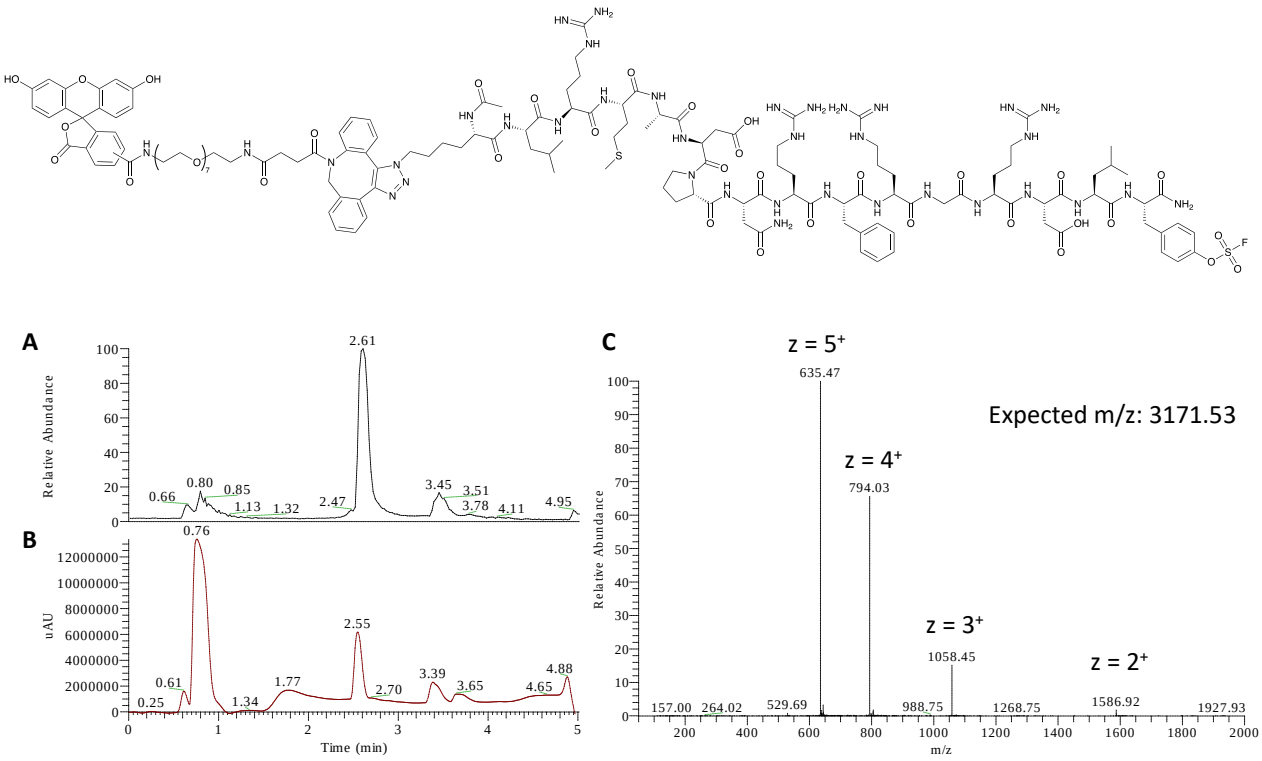

Figure 41. Fluor-gD-FSY was synthesized using azido-gD-FSY and intermediate **3**. LC-HRMS $[M+5H]^{5+}$ m/z calc for $[C_{145}H_{201}FN_{36}O_{40}S_2]$ 634.8845, found 635.1087. **A)** Total ion chromatogram, **B)** UV trace chromatogram, and **C)** ions detected at 2.61 minutes. A sharp peak at 0.76 minutes corresponds to DMSO used to dissolve intermediate **3.**

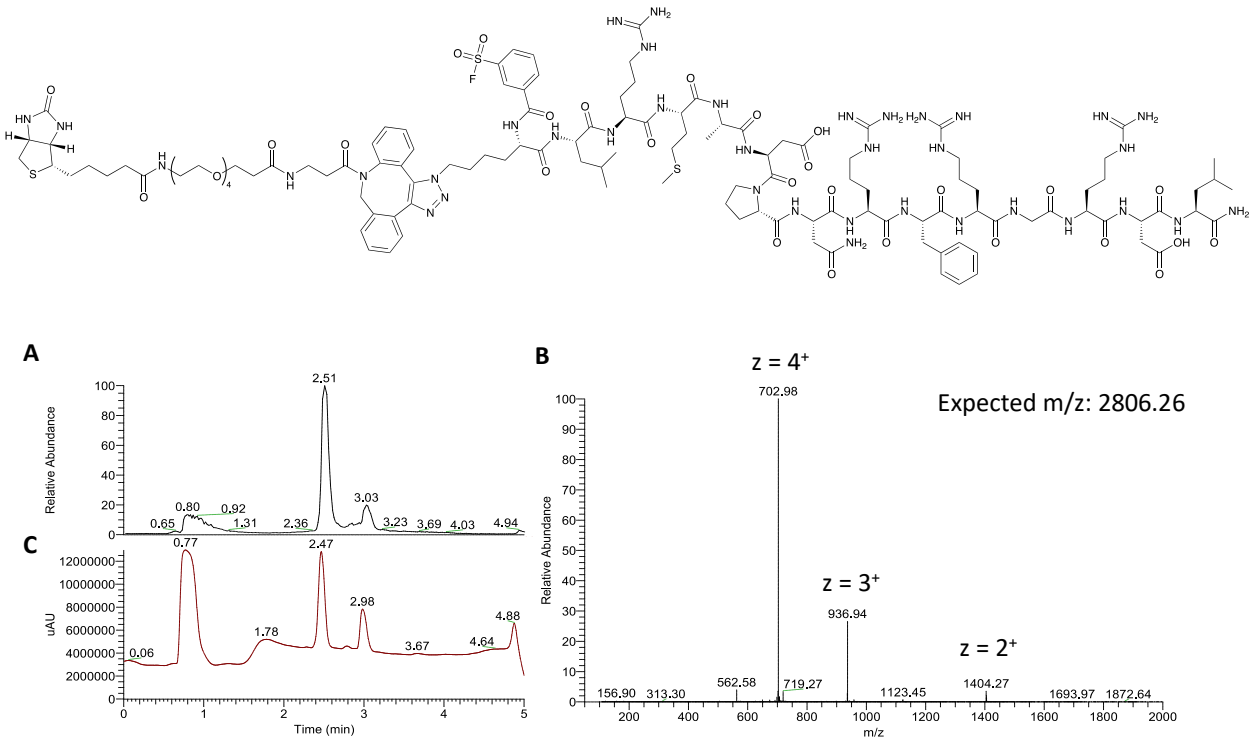

Figure 42. Biotin-ASF-gD was synthesized using azido-ASF-gD and biotin-PEG4-DBCO. LC-HRMS $[M+4H]^{4+}$ m/z calc for $[C_{124}H_{186}FN_{37}O_{31}S_3]$ 702.0816, found 702.3633. **A)** Total ion chromatogram, **B)** UV trace chromatogram, and **C)** ions detected at 2.51 minutes. A sharp peak at 0.77 minutes corresponds to DMSO used to dissolve biotin-PEG4-DBCO. A UV peak at 2.98 minutes corresponds to unreacted Biotin-PEG4-DBCO.

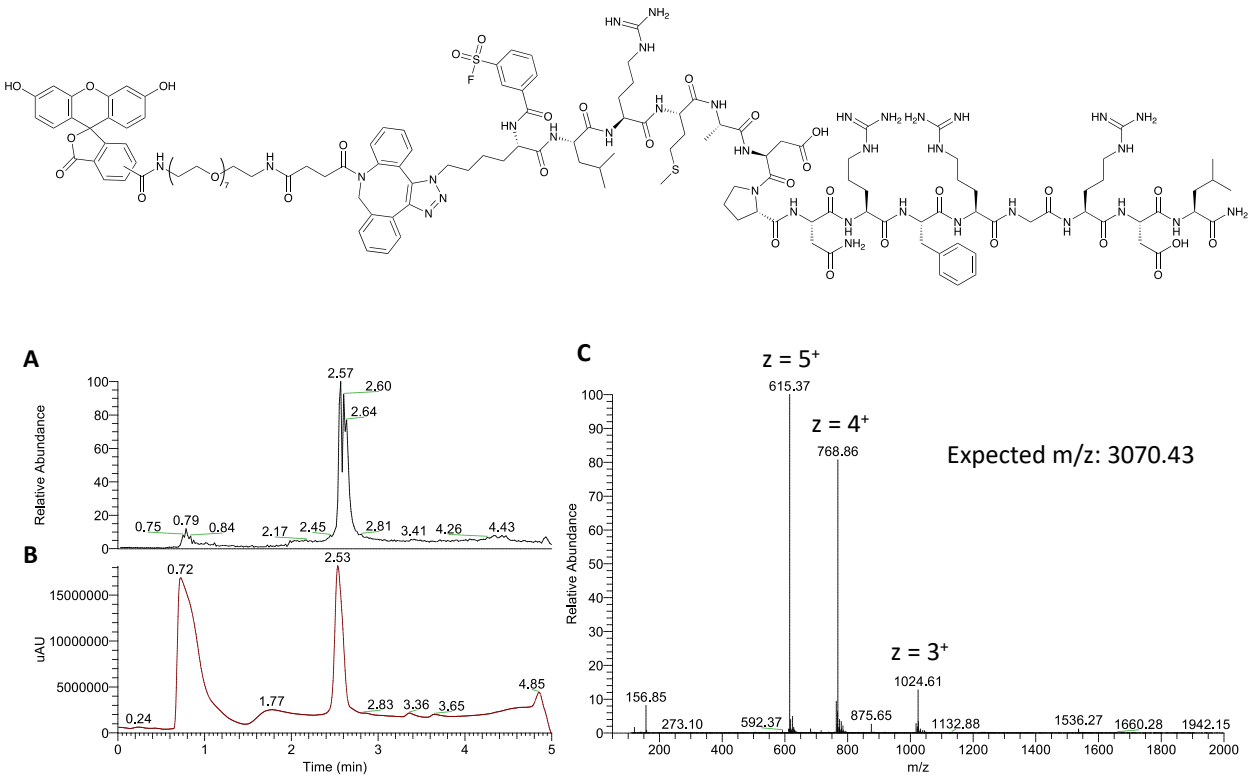

Figure 43. Fluor-ASF-gD was synthesized using azido-ASF-gD and intermediate **3**. LC-HRMS $[M+5H]^{5+}$ m/z calc for $[C_{141}H_{194}FN_{35}O_{38}S_2]$ 614.6750, found 614.9042. **A)** Total ion chromatogram, **B)** UV trace chromatogram, and **C)** ions detected at 2.57 minutes. A sharp peak at 0.72 minutes corresponds to DMSO used to dissolve intermediate **3**.

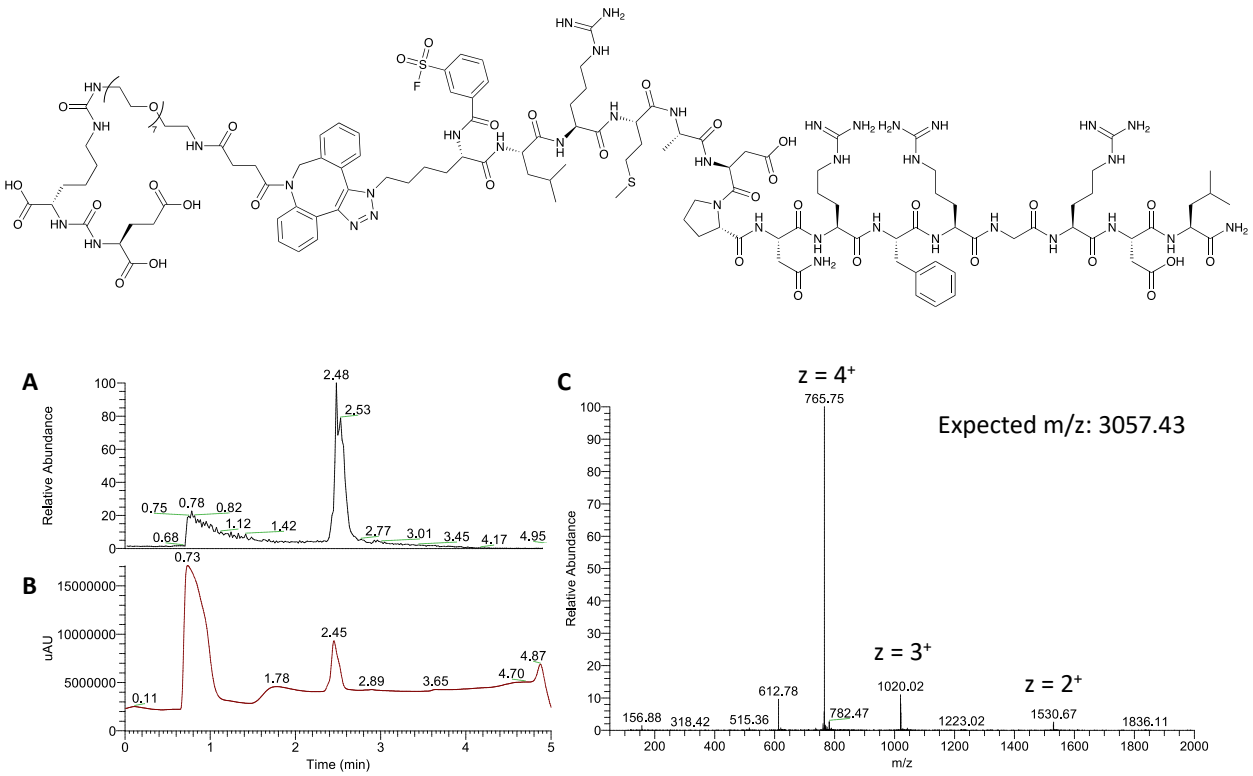

Figure 44. GU-ASF-gD was synthesized using azido-ASF-gD and intermediate **6**. LC-HRMS $[M+4H]^{4+}$ m/z calc for $[C_{133}H_{203}FN_{38}O_{40}S_2]$ 764.8611, found 765.1390. **A)** Total ion chromatogram, **B)** UV trace chromatogram, and **C)** ions detected at 2.48 minutes. A sharp peak at 0.76 minutes corresponds to DMSO used to dissolve intermediate **6**.

10.4. **Synthesis of Non-Covalent Bifunctional Peptides**

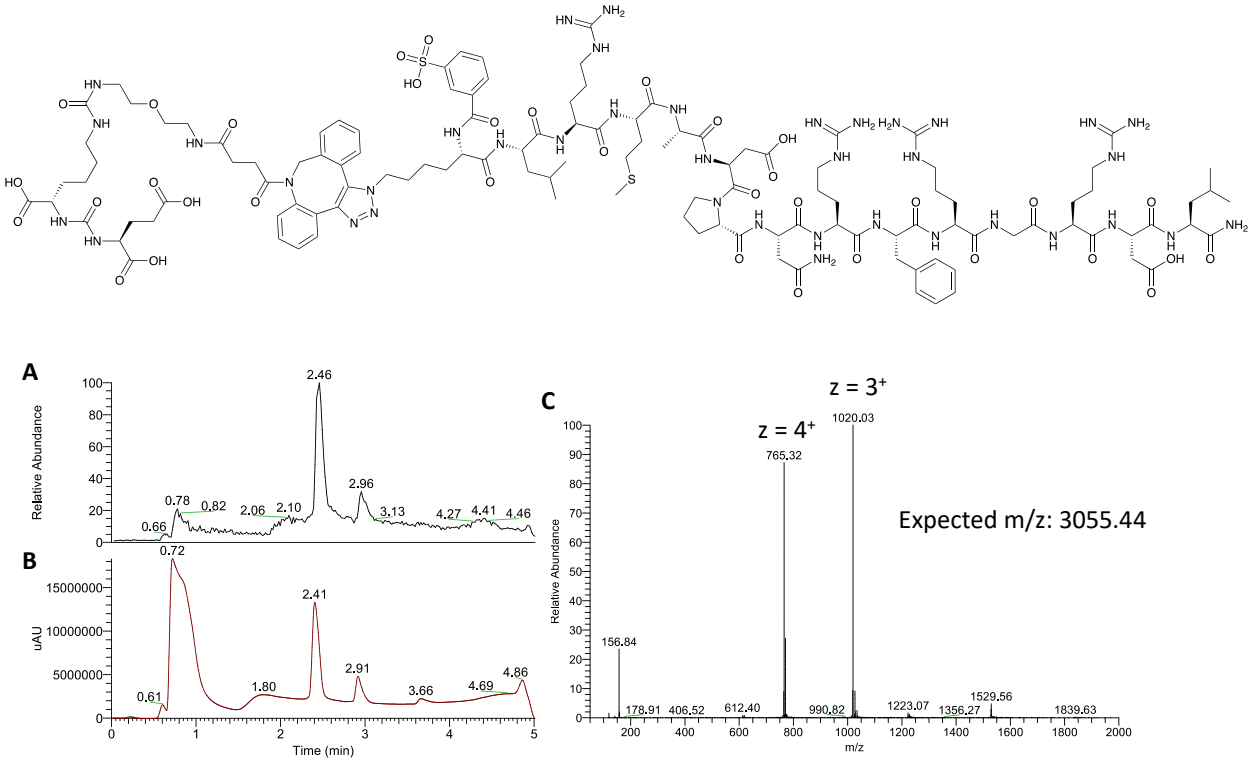

Figure 45. GU-SO_3H-gD was synthesized from azido-SO_3H-gD and intermediate **6**. LC-MS characterization of GU-SO_3H-gD. **A)** Total ion chromatogram, **B)** UV trace chromatogram, and **C)** ions detected at 2.46 minutes. A sharp peak at 0.72 minutes corresponds to DMSO used to dissolve intermediate **6**.

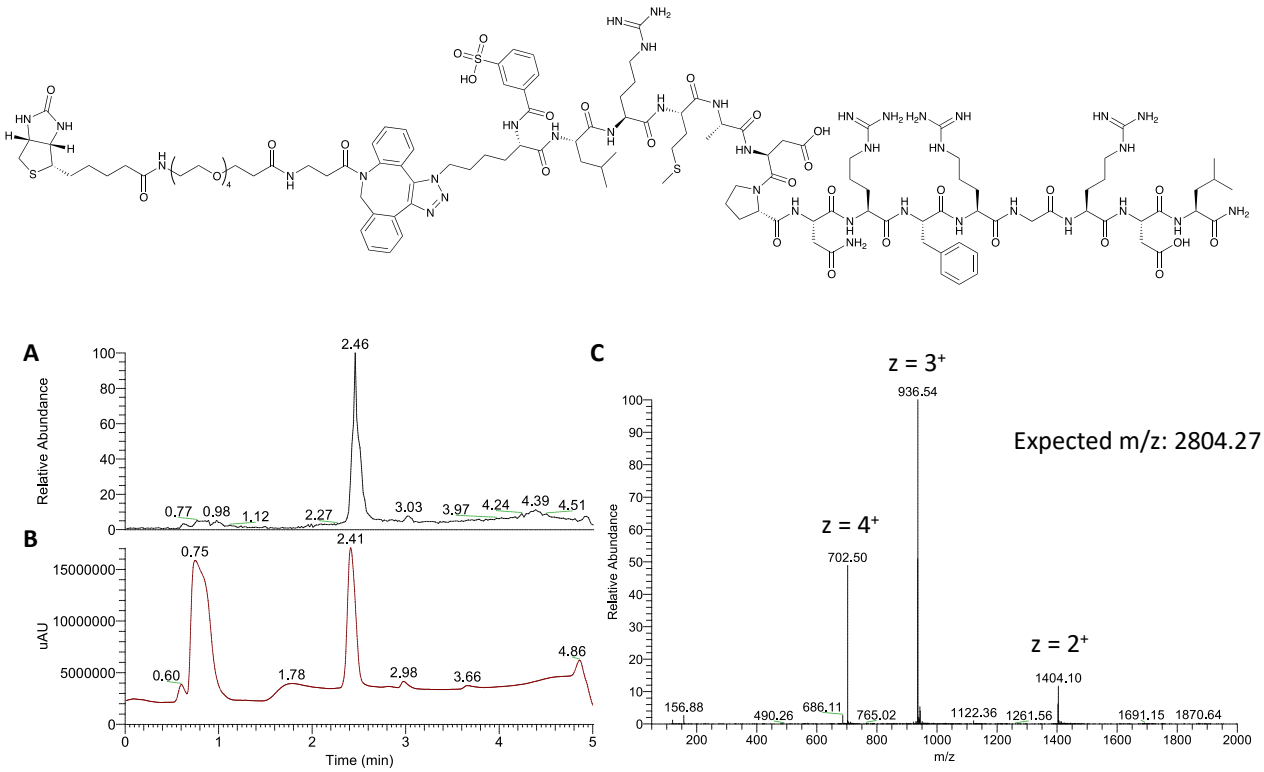

Figure 46. Biotin-SO_3H-gD was synthesized from azido-SO_3H-gD and biotin-PEG4-DBCO. **A)** Total ion chromatogram, **B)** UV trace chromatogram, and **C)** ions detected at 2.46 minutes. A large UV peak at 0.75 minutes corresponds to DMSO used to dissolve biotin-PEG4-DBCO.

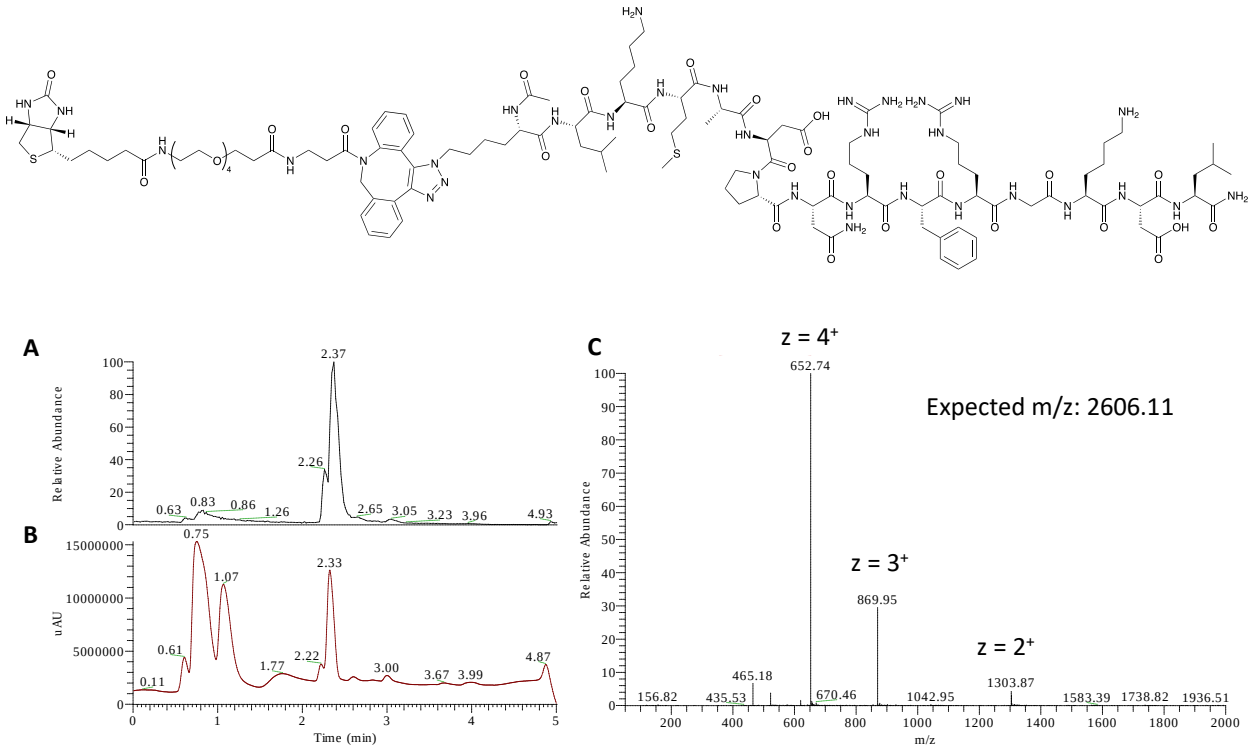

Figure 47. Biotin-gD was synthesized from biotin-PEG4-DBCO and azido-gD. **A)** Total ion chromatogram, **B)** UV trace chromatogram, and **C)** ions detected at 2.37 minutes. Large UV peaks at 0.75 and 1.07 minutes correspond to solvent fronts (DMSO and MeOH).

10.5. **LC-HRMS Stability Study Protocol**

General. LC-HRMS data was obtained on a BRUKER MicroTOF II mass spectrometer. Samples were dissolved in 1X PBS at 500 µM concentrations and were monitored for stability at room temperature over the indicated periods of time. The presence of larger masses indicative of intermolecular crosslinking was investigated. Additionally, the presence of specific m/z -20 amu (loss of H^+ & F^-) and m/z -2 amu (F/OH exchange) masses were monitored to probe off-pathway cyclization and hydrolysis reactions, respectively.

10.6. **SDS-PAGE Protocol**

General. SDS-PAGE was performed to visualize covalent antibody labeling through the appearance of fluorescent protein bands under reducing/ denaturing conditions. Samples were worked up prior to SDSPAGE by diluting with 2× Laemmli sample buffer and heating at 95 °C for 5 min. 14−20 μL of the reduced, denatured protein sample was separated using a 14% acrylamide gel and 1× tris glycine running buffer (24.76 mM tris, 1.73 mM SDS, 95.91 mM glycine, and Milli-Q water). Bands were stacked by applying 90 V for 15 min, followed by a 50 min separation at 120 V. Fluorescent bands were imaged using a Typhoon laser-scanner platform with a Cy2 laser and the auto-PMT setting. Mean fluorescence intensity was quantified using ImageJ. Stained gels were imaged using a 700 nM laser on an Odyssey CLx imager. Incubations were carried out in the dark at room temperature, with 1 μM antibody and 2 μM covalent peptide for 24 h in 1x PBS.

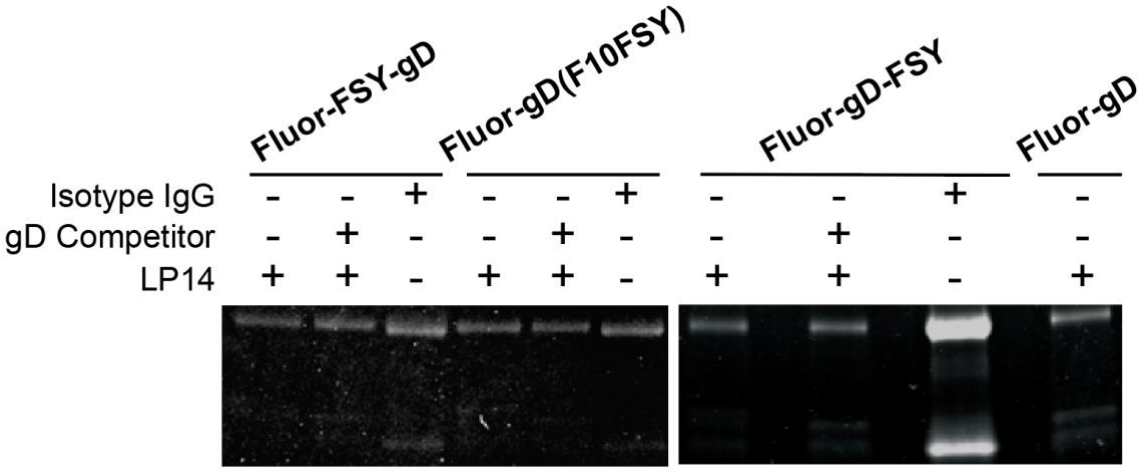

Figure 48. Coomassie stained image for Figure 14A.

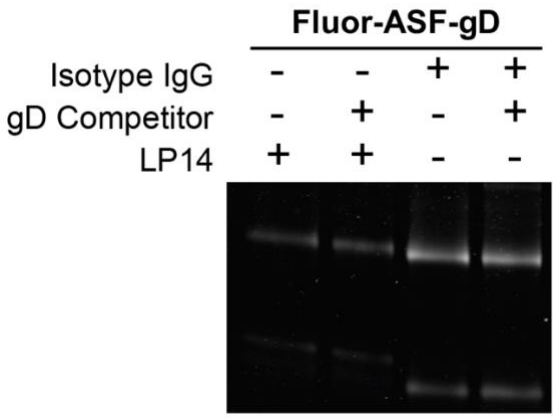

Figure 49. Coomassie stained image for Figure 14B.

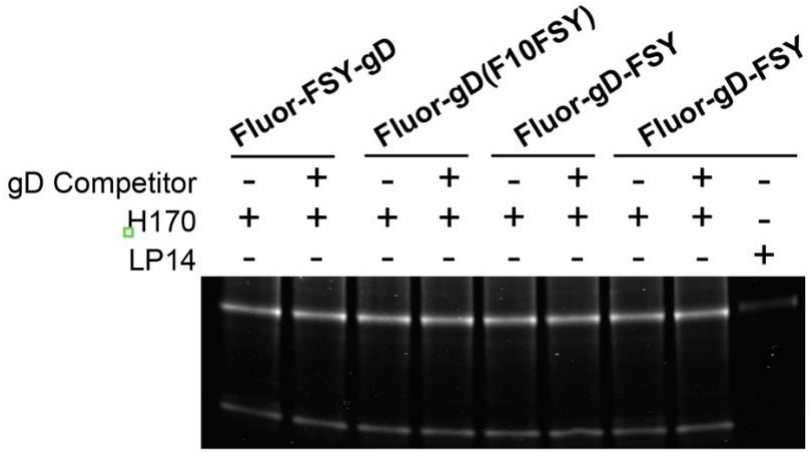

Figure 50. Coomassie stained image for 14C.

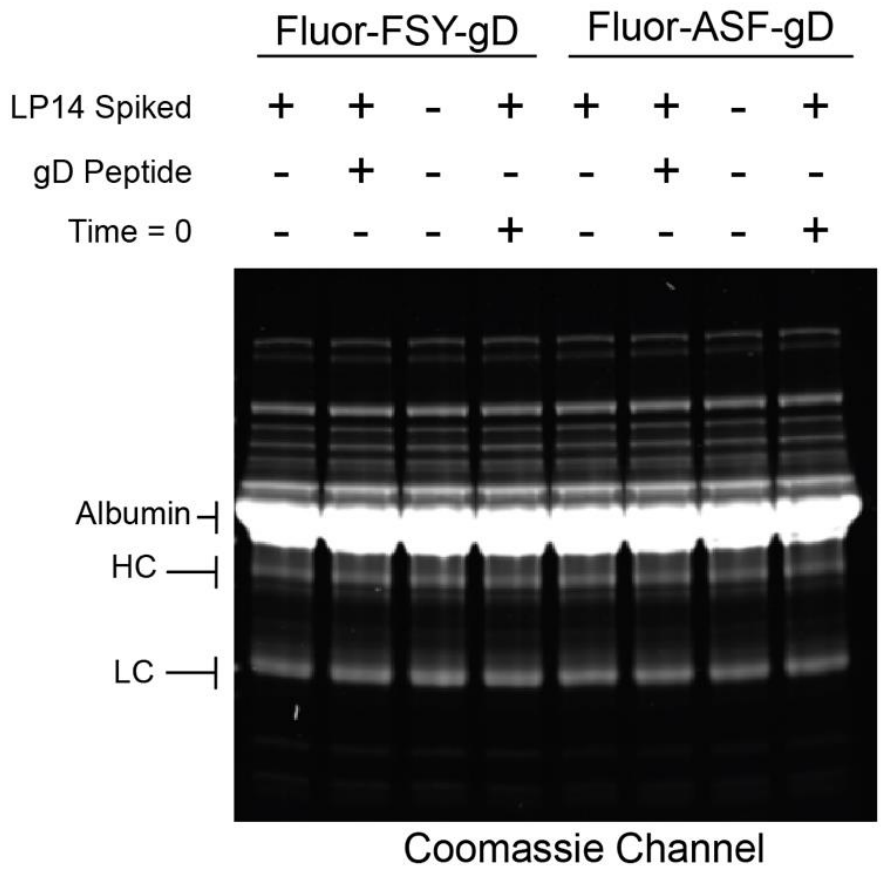

Figure 51. Coomassie stained image for 14D.

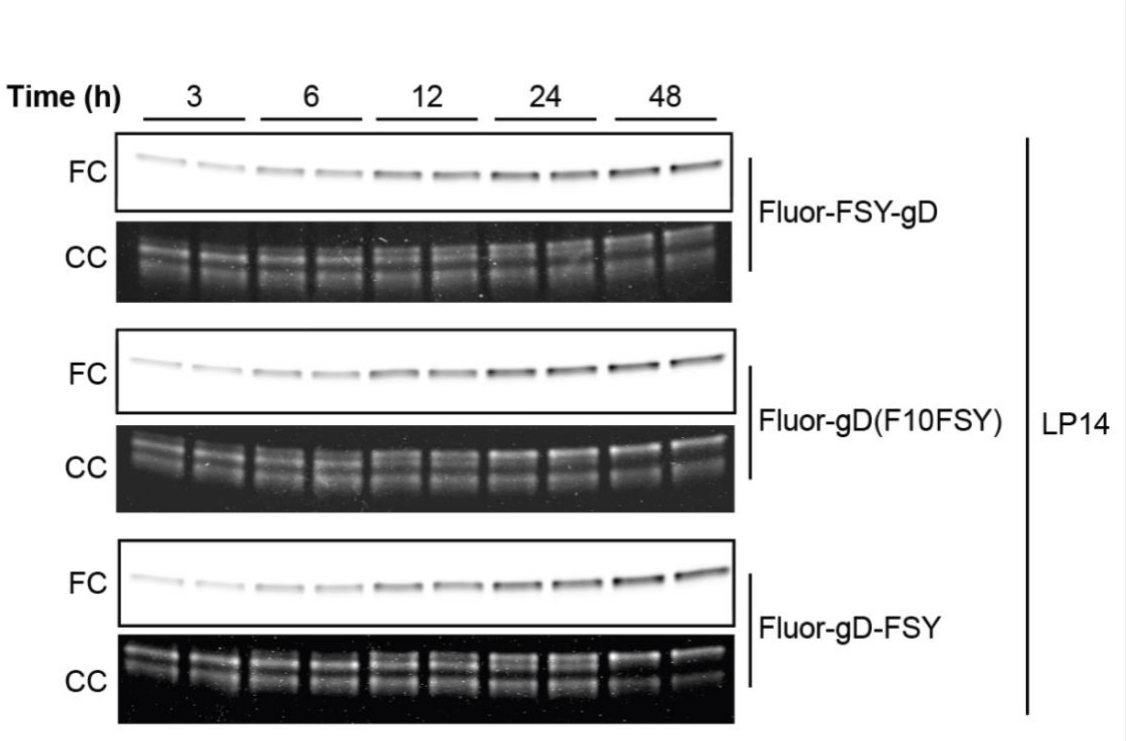

Figure 52. Fluorescent SDS-PAGE time course study for the reaction between FSY-peptides and anti-gD LP14 antibody. **A)** FSY-Peptides (20 µM) were incubated with LP14 (1 µM) for 0, 3, 6, 12, 24, and 48 hours before SDS-PAGE and fluorescent detection. A second unknown low MW band appearing under the light chain was consistent between LP14 samples, likely an impurity from commercial antibody purification. Data was quantified from two replicate measurements and summarized as the mean and standard error of the mean. **B)** Examples of DynaFit analysis for reaction kinetics between (from left to right): Fluor-FSY-gD, Fluor-gD(F10FSY), and Fluor-gD-FSY with LP14.

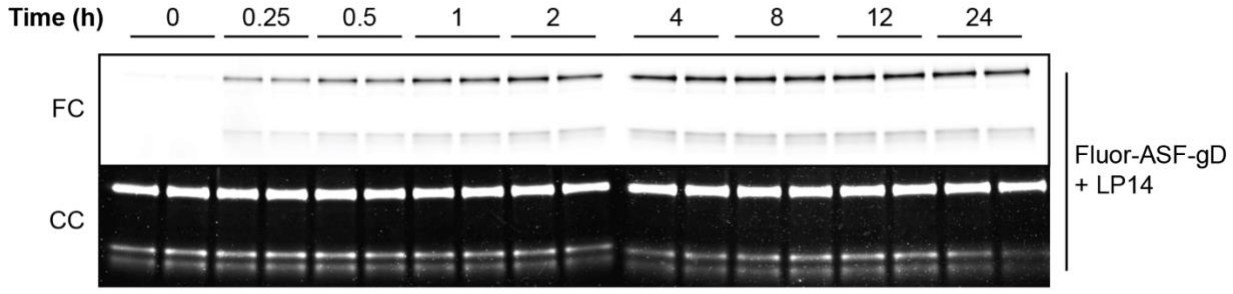

Figure 53. Fluorescent SDS-PAGE time course study of labeling kinetics between Fluor-ASF-gD (20 µM) and anti-gD LP14 antibody (1 µM). Data was quantified from two replicate measurements and summarized as the mean and standard error of the mean.

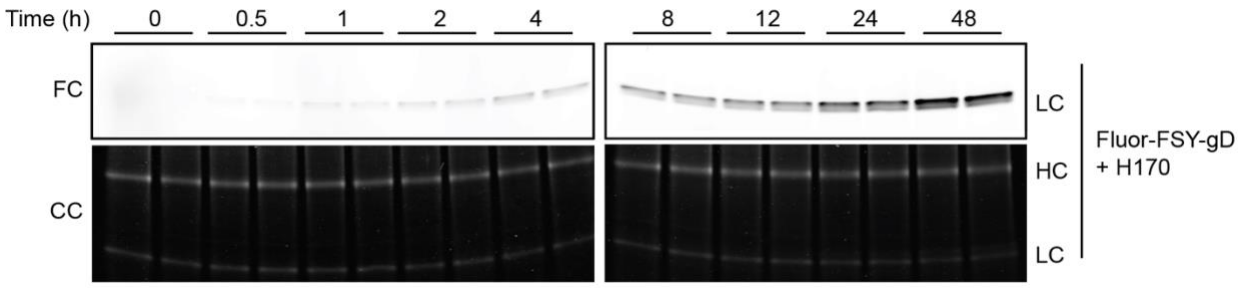

Figure 54. Fluorescent SDS-PAGE time course study of labeling kinetics between Fluor-FSY-gD (10 µM) and anti-gD H170 antibody (0.5 µM). Data was quantified from two replicate measurements and summarized as the mean and standard error of the mean.

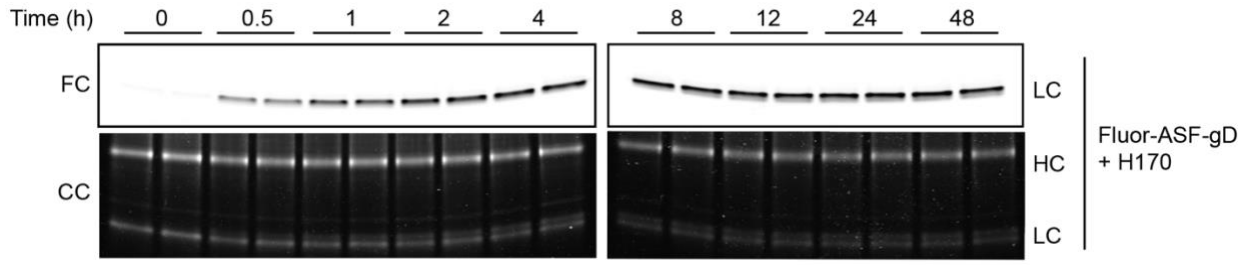

Figure 55. Fluorescent SDS-PAGE time course study of labeling kinetics between Fluor-ASF-gD (10 µM) and anti-gD H170 antibody (0.5 µM). Data was quantified from two replicate measurements and summarized as the mean and standard error of the mean.

10.7. **ELISA Protocol**

All absorbance measurements were done on a TECAN SPARK plate reader. Pierce Streptavidin Coated High-Capacity ELISA plates pre-blocked with SuperBlock were purchased from Sigma Aldrich (Cat. No. 15500). The Mouse/Rat HSV-1 IgG ELISA Kit was purchased from Creative Diagnostics (Cat. No. DEIA3555). Goat anti-human IgG (H+L) secondary antibody-HRP conjugate was purchased from Thermo Scientific (Cat. No. A18805). Goat anti-mouse IgG (H+L) secondary antibody-HRP conjugate was purchased from Thermo Scientific (Cat. No. 62-6520). The Pierce™ TMB Substrate Kit

was purchased from Fisher Scientific (Cat. No. 34-021). Sulfuric acid (2M) was purchased from VWR (Cat. No. 470302-860). Wash buffer was prepared with 50 mg/mL BSA and 0.005% Tween 20 (v/v) in 1X PBS.

Serum from mice inoculated with oncolytic HSV-1d810 was probed for antibodies generated against the N-terminal gD peptide. To accomplish this, the serum of five mice "boosted" with HSV OV was pooled and compared against the pooled serum of three control mice. 50 µL of 4 µM gD-Biotin or wash buffer was incubated in the designated wells for 30 minutes. Wells were then washed 3x with 300 µL wash buffer. Diluted serum samples (100 µL) were added to their respective wells and incubated for 1 hour. After this, each well was washed 3x with 300 µL wash buffer. The anti-mouse IgG HRP conjugate (100 µL) was added to each well for 30 minutes. After this, each well was washed 3x with 300 µL wash buffer. For detection, 100 µL TMB substrate was added to each well for 10 minutes, followed by 100 µL 2M sulfuric acid. A readout was performed using absorbance at 450 nm, with a reference filter set to 620 nm.

10.8. **Flow Cytometry Protocol**

All flow cytometry experiments were run on a BD LSRII Flow Cytometer. The human IgG isotype control used was purchased from Jackson ImmunoResearch (Cat. No. 009-000-003). The mouse IgG2a monoclonal anti-HSV antibody was purchased from sigma-aldrich (Cat. No. MABF1975). PSMA expression was confirmed with an anti-PSMA antibody alexa 647 conjugate (Novus Biologicals, Cat. No. FAB4234R). Hek-293T (PSMA+/-) cell lines were generously provided by C. Barinka (Institute of Biotechnology CAS, Czech Republic). LnCAP cells were generously provided by K. Mossman. C4-2

cells were obtained from Cedarlane (Cat. No. CRL-3314). U937 cells were generously provided by J. Valliant (McMaster University, Canada). IFN-γ was purchased from Fischer Scientific (Cat. No. PHC4031). Ultra-low IgG FBS was purchased from Fischer Scientific (Cat. No. A3381901). The anti-mouse IgG (H+L) secondary antibody (PE conjugate) was purchased from Thermo Fisher Scientific (Cat. No. 12-4010-82). RPMI-1640 was purchased as a powder from Fischer Scientific (Cat. No. 31800089) and resuspended. DMEM was purchased as a powder from Fischer Scientific (Cat. No. 12800082) and resuspended. DiD cell dye was purchased from Fischer Scientific (Cat. No. V22887). DiO cell dye was purchased from Fischer Scientific (Cat. No. V22886). TrypLE Express was purchased from Fischer Scientific (Cat. No. 12604013). 96-Well U-bottom plates were purchased from FischerScientific (Cat. No. 08-772-17). Pen/Strep was purchased from Fischer Scientific (Cat. No. 15140-122). FBS was purchased from Fischer Scientific (Cat. No. 12484-028). Zeocin was purchased from Fischer Scientific (Cat. No. R25001). HEK293 (PSMA+) cells were cultured in DMEM media with 2mM L-glut, 1% Pen/Strep, 10% FBS, and 50ug/mL Zeocin. HEK293 cells were cultured in DMEM media with 2mM L-glut, 1% Pen/Strep, and 10% FBS. U937 monocytes, LnCAP, and C4-2 cells were cultured in RPMI media with 2mM L-Glut, 1% Pen/Strep, and 10% FBS.

Antibody labeling studies were performed by incubating GU-FSY-gD (500 nM) or GU-gD (500 nM) with LP14 mAb (250 nM) at room temperature overnight. Where HSV competitor is used, azido-gD was used at a concentration of 100X excess of non-covalent peptide to covalent peptide. Competition conditions had competitor present during incubation, while quench conditions had competitor added after overnight incubation. Before antibody recruitment, conditions were diluted down in a 2X dilution series and 20

µL of each was plated in a 96-well plate in duplicate. HEK293 cells transfected with PSMA (90% confluent in a T-150 flask) were suspended with TrypLE and quenched washed 3X with 4˚C flow buffer (4% FBS, 0.5 mM EDTA/EGTA, 0.1% Sodium Azide) and resuspended to a concentration of 5 x 106 Cells/mL. Following this, 20 µL of cells were added to the 96-well plate (100 000 Cells per sample) and kept on ice. Afterwards 10 µL of appropriate 20X diluted (in flow buffer) secondary antibody was added to each well. PSMA loading/expression was confirmed with an anti-PSMA antibody alexa 647 conjugate, where 0.75 µL was diluted to 10 µL and added in place of secondary antibody. The plate was then allowed to incubate on ice for 20 minutes and run on a flow cytometer. Voltages used were FSC: 390, SSC: 290, Alexa 647: 490, PE: 350

Equation 5. Calculating percent target phagocytosis from flow cytometry data.

$$\%\ Target\ Phagocytosed = \left(\frac{Double\ Positive\ Events}{Target\ Only\ Events + Double\ Positive\ Events}\right) * 100$$

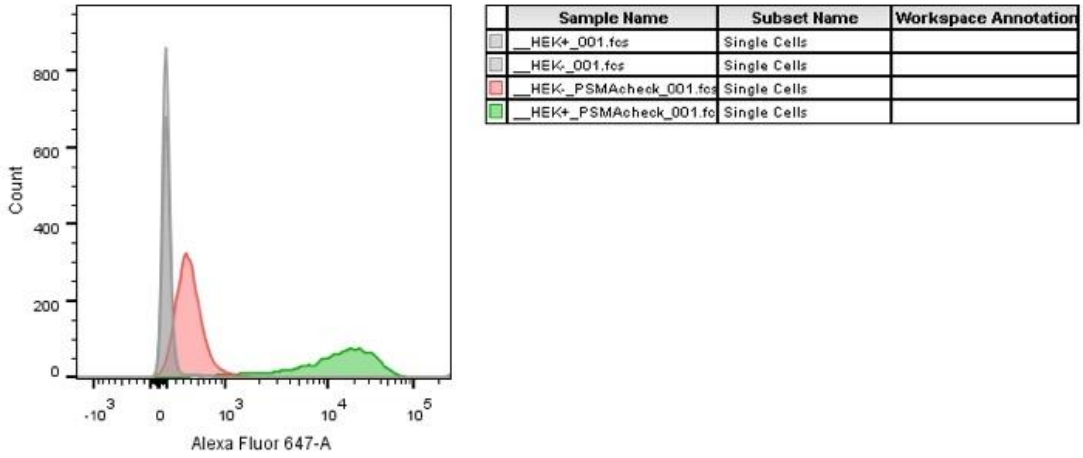

Figure 56. PSMA expression on HEK293 (PSMA+/-) cells was monitored using an anti-PSMA A647 antibody. Only HEK293 (PSMA+) cells (green) were found to express PSMA. HEK293 cells demonstrated very little fluorescence, likely from non-specific binding. Without anti-PSMA A647 antibody, no fluorescence was detected (grey).

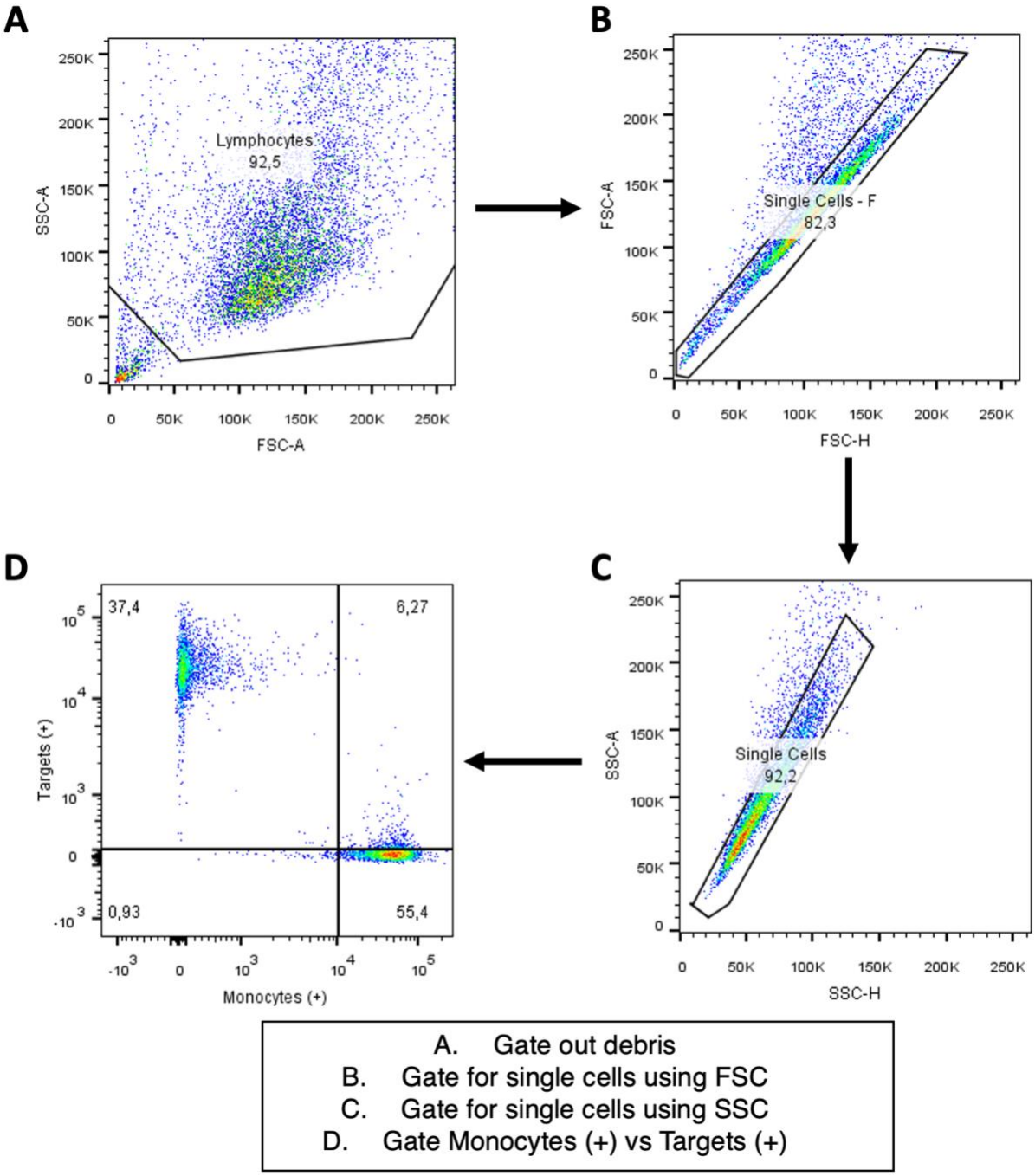

Figure 57. Flow cytometry scatter plots demonstrating gating protocols for selecting single cells when evaluating double positives, reflecting ADCP events.

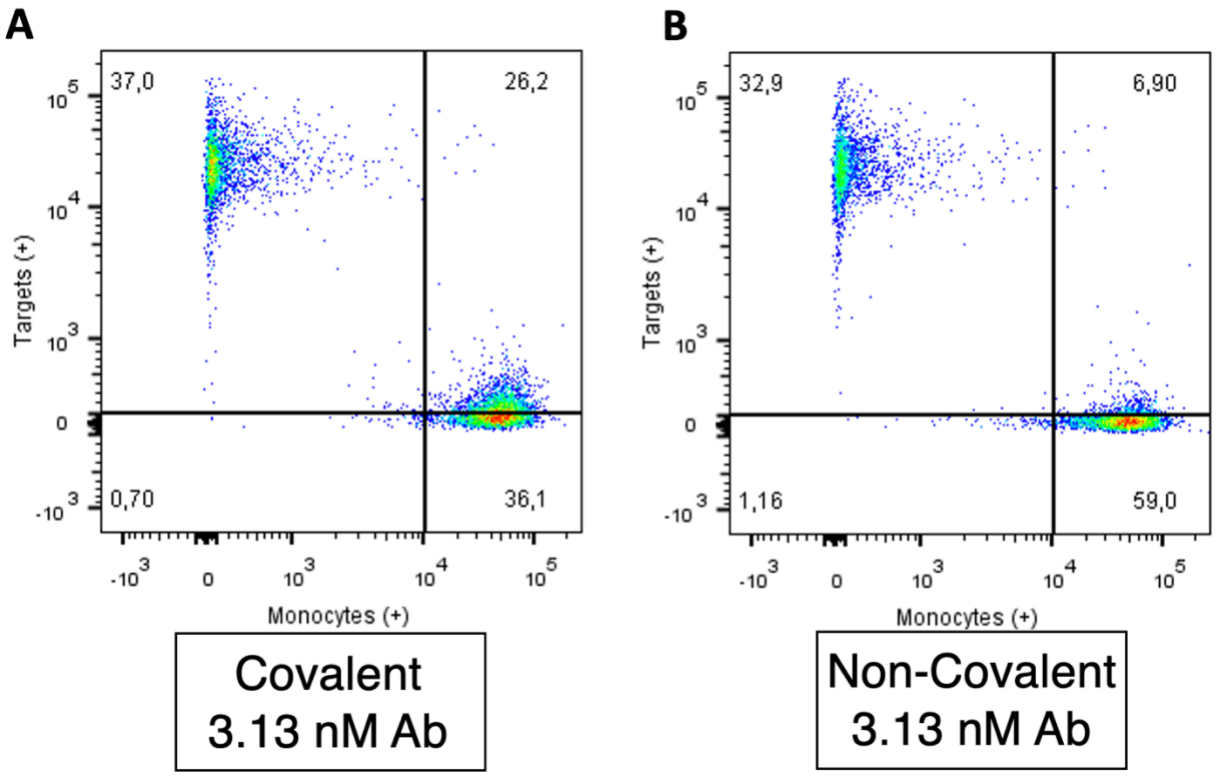

Figure 58. Flow cytometry scatter plots comparing ADCP of HEK293 (PSMA)+ cells by u937 monocytes. This was performed in the presence of 3.13 nM LP14 mAb with **A)** 6.26 nM GU-FSY-gD, or **B)** 6.26 nM GU-gD. Quadrant 1 (top left) indicates target cells, quadrant 2 (top right) indicates phagocytosed cells, quadrant 3 (bottom left) indicates cellular debris, and quadrant 4 (bottom right) indicates monocytes.

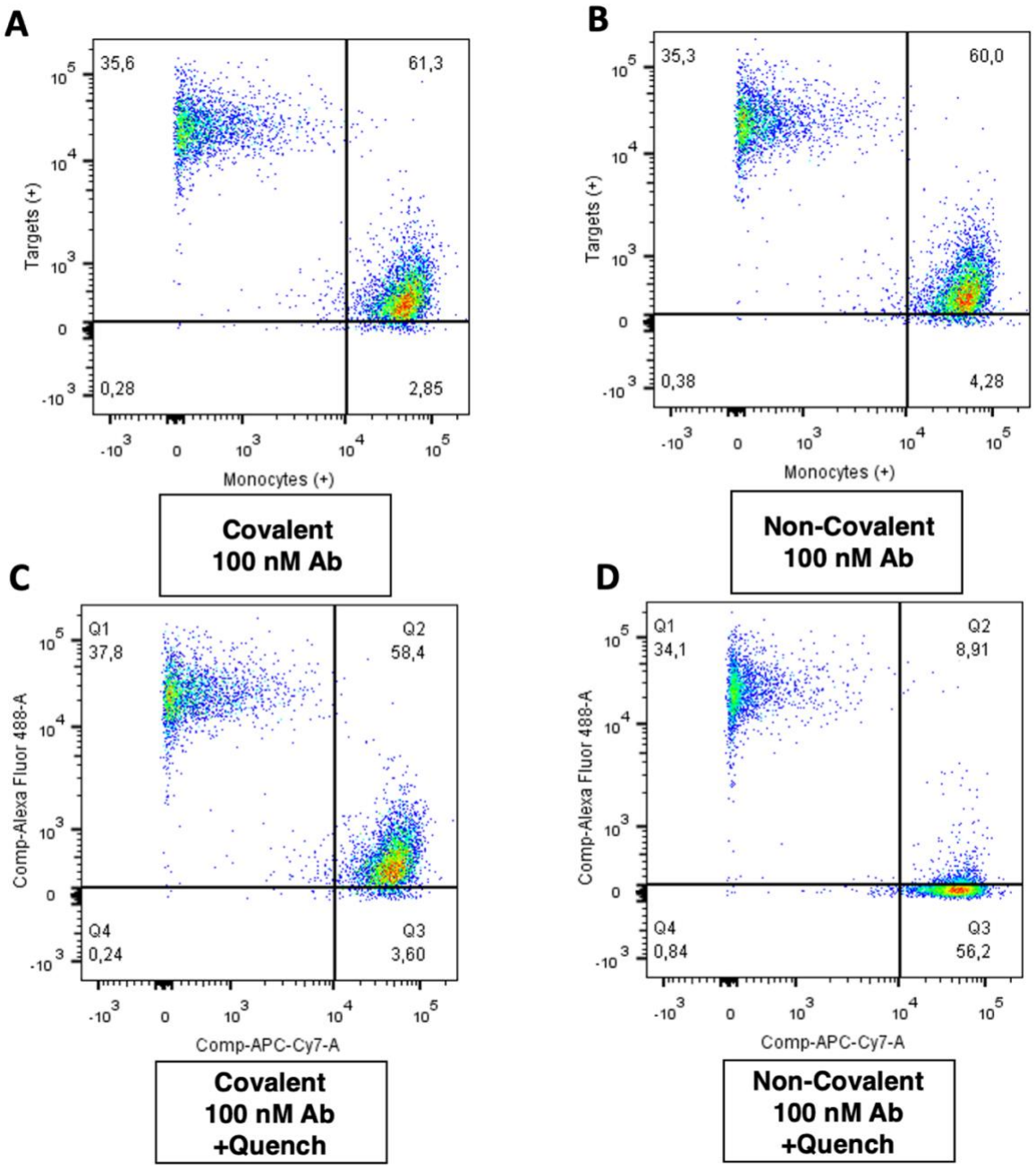

Figure 59. Flow cytometry scatter plots comparing ADCP of HEK293 (PSMA)+ cells using GU-FSY-gD (**A/C**) or GU-gD (**B/D**). At 100 nM antibody and 200 nM peptide, both molecules show maximum ADCP (quadrant 2, top right). A quench was performed by adding 100 µM azido-gD peptide after incubating antibody with GU-FSY-gD or GU-gD overnight to demonstrate a covalent linkage (**C/D**). After quenching, GU-FSY-gD maintained the same level of ADCP, whereas GU-gD lost all function.

10.9. **Spectra and Characterization Data**

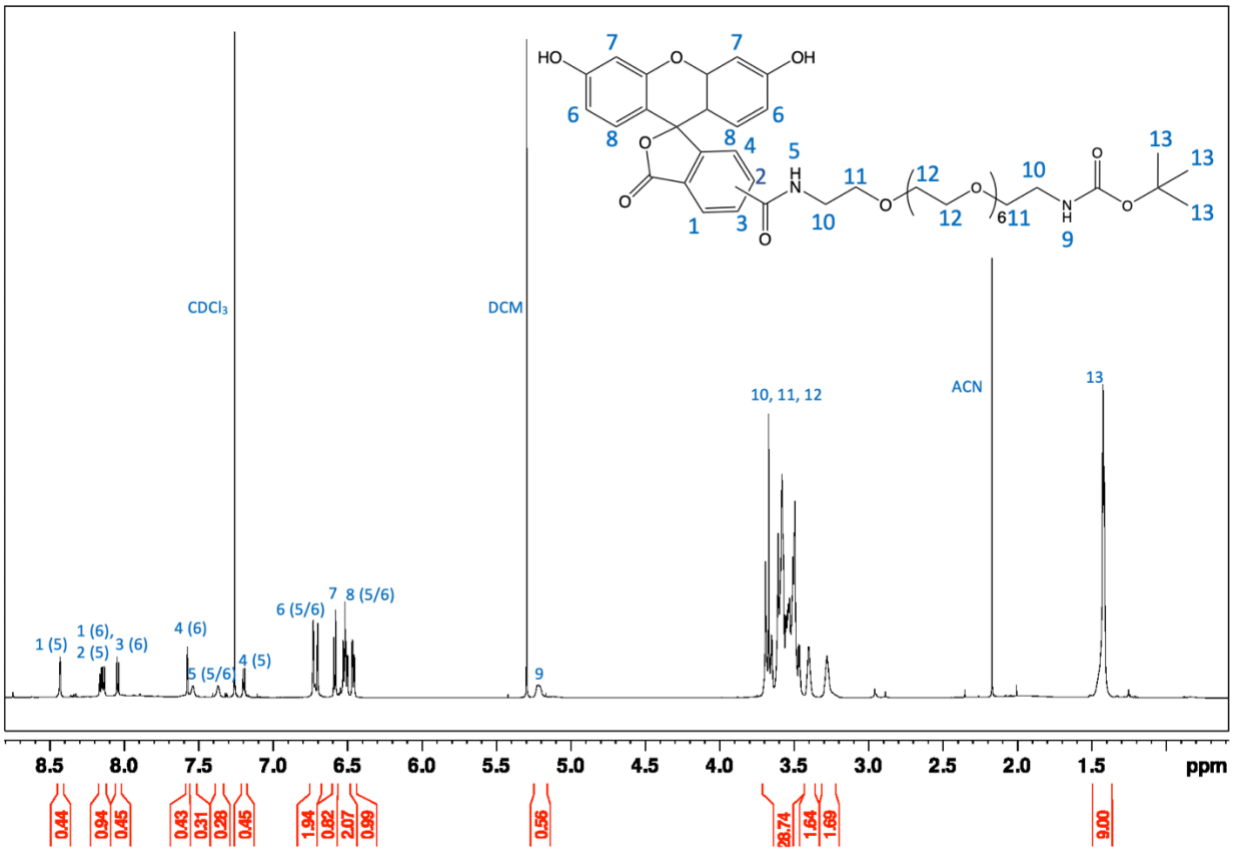

Figure 60. 700 MHz ^{1}H NMR of intermediate I-**4** in $CDCl_3$.

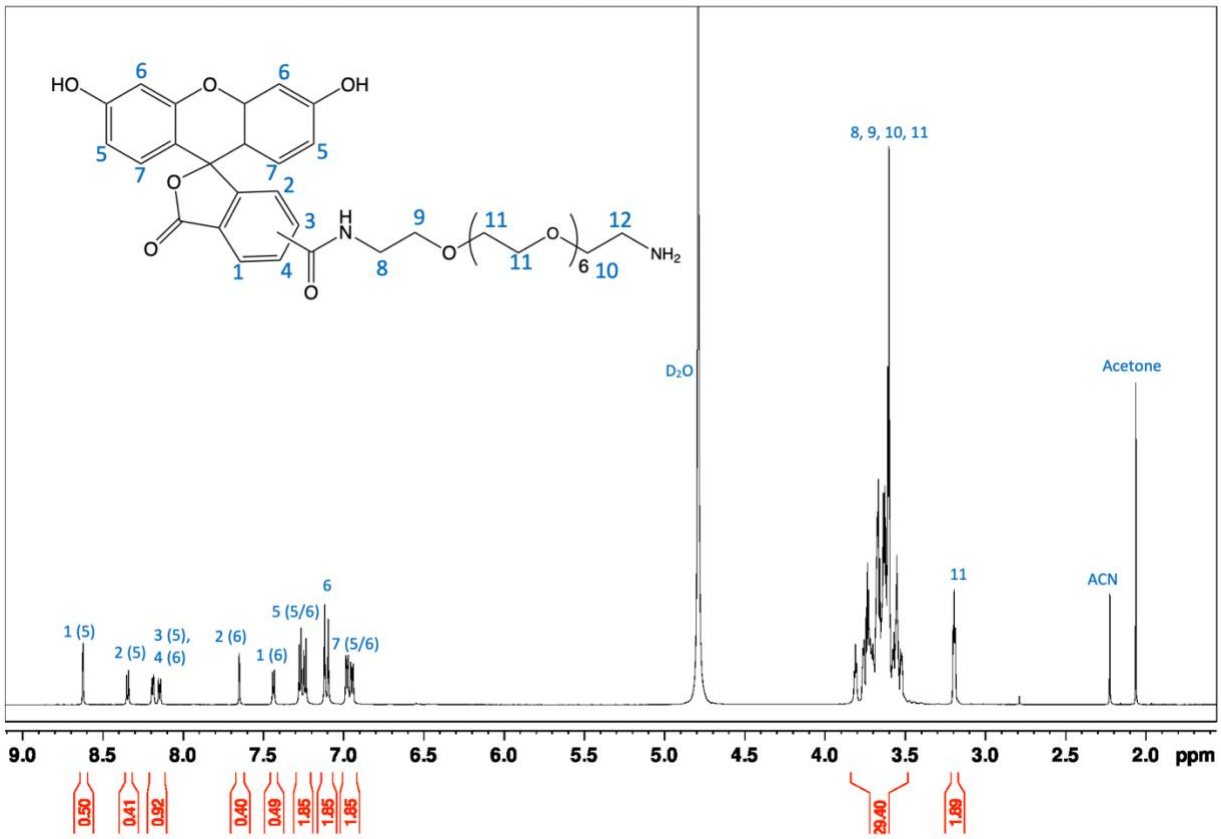

Figure 61. 700 MHz ^{1}H NMR of intermediate I-**5** in D_2O.

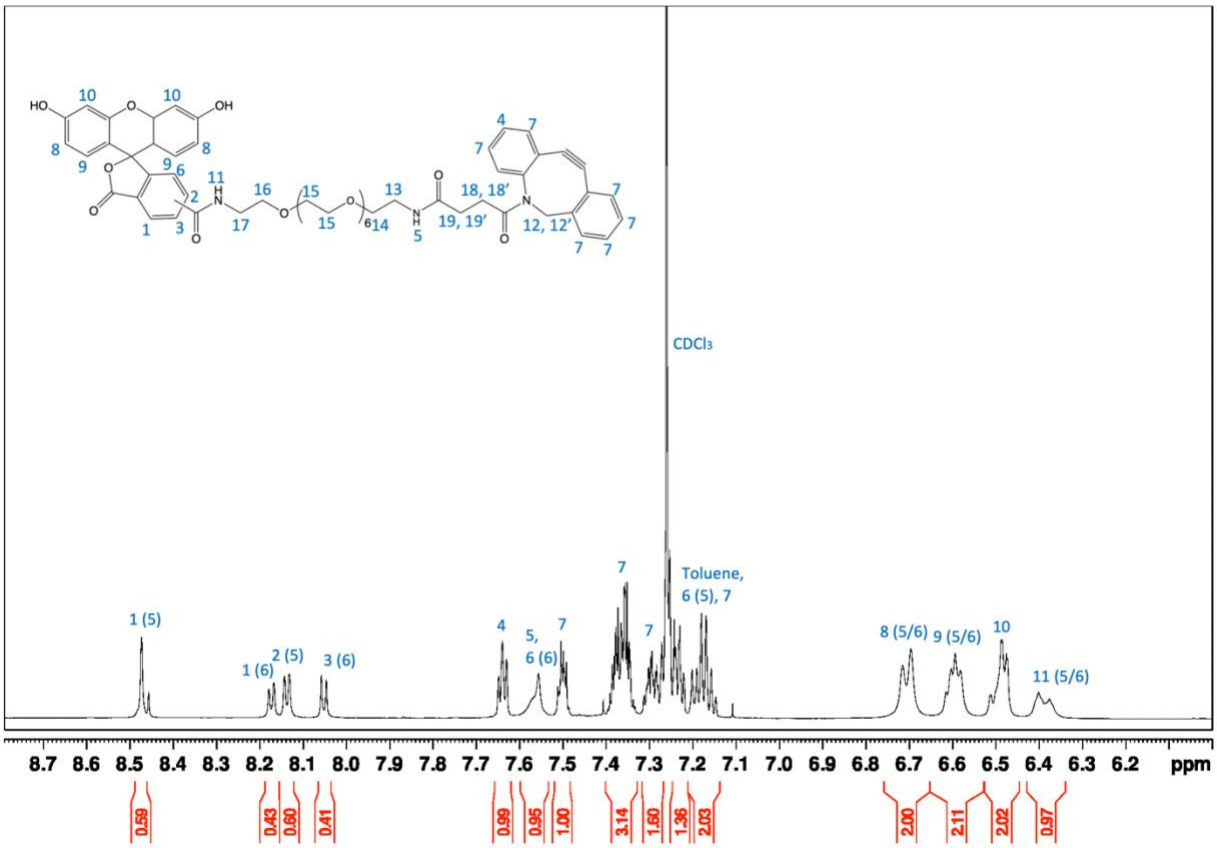

Figure 62. Downfield portion of 700 MHz ^{1}H NMR of intermediate I-**6** in $CDCl_3$.

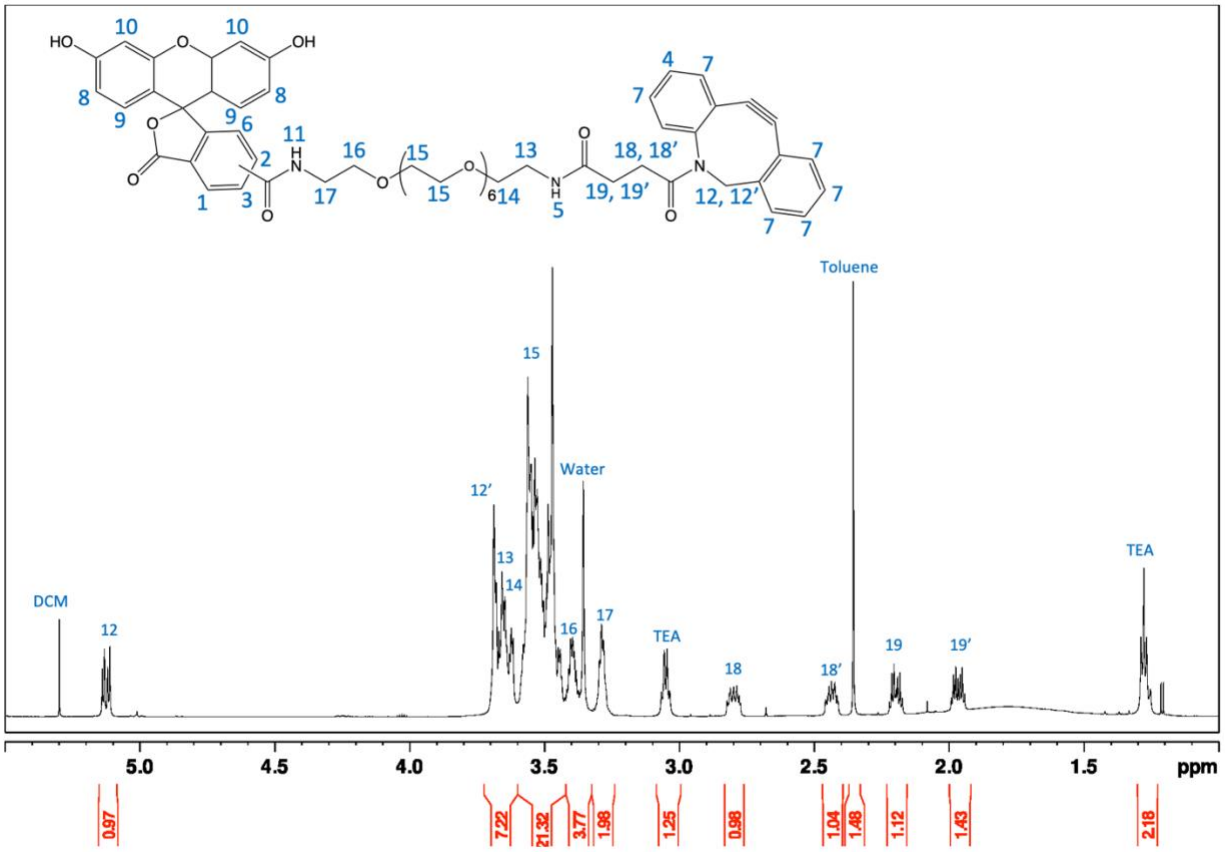

Figure 63. Upfield portion of 700 MHz ^{1}H NMR of intermediate I-**6** in $CDCl_3$.

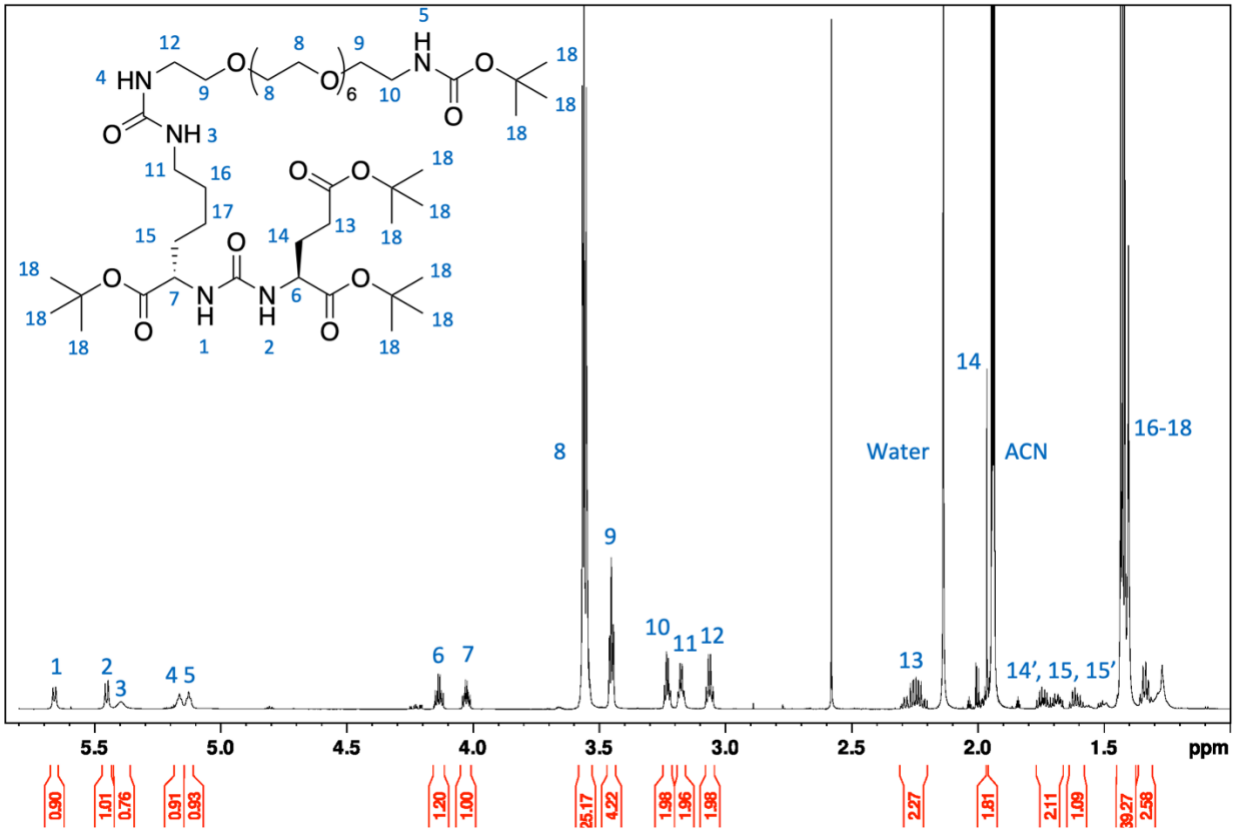

Figure 64. 700 MHz ^{1}H NMR of intermediate I-**9** in CD_3CN.

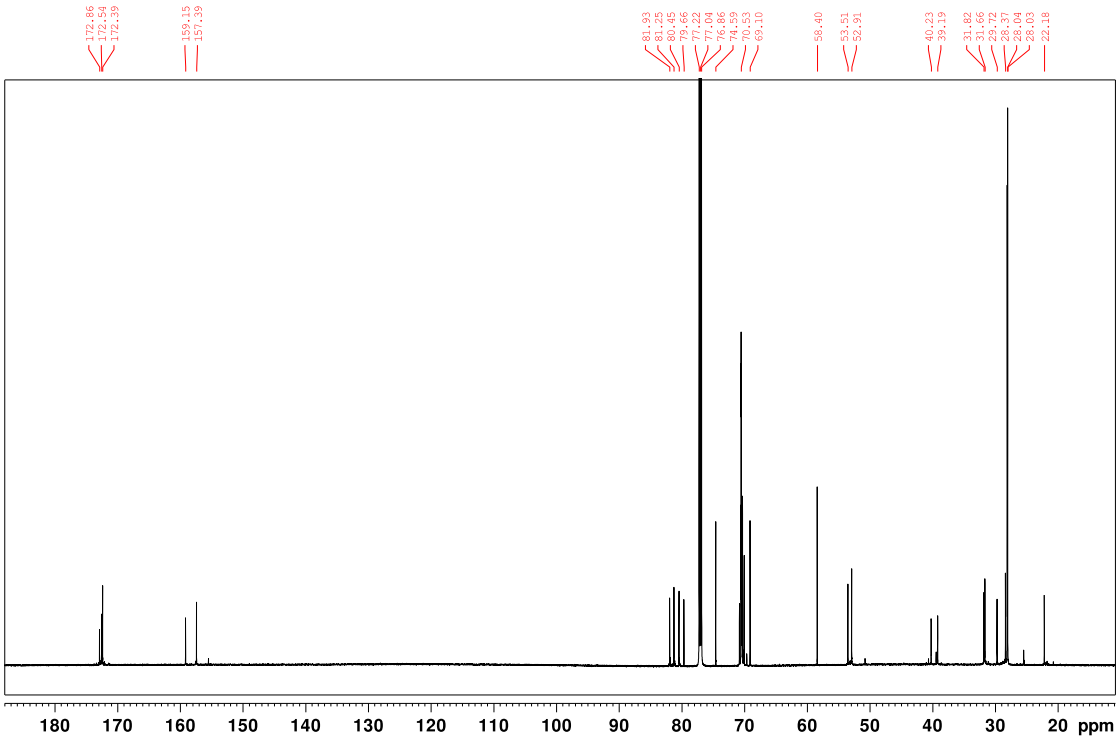

Figure 65. 700 MHz ^{13}C NMR of intermediate I-**8** in $CDCl_3$.

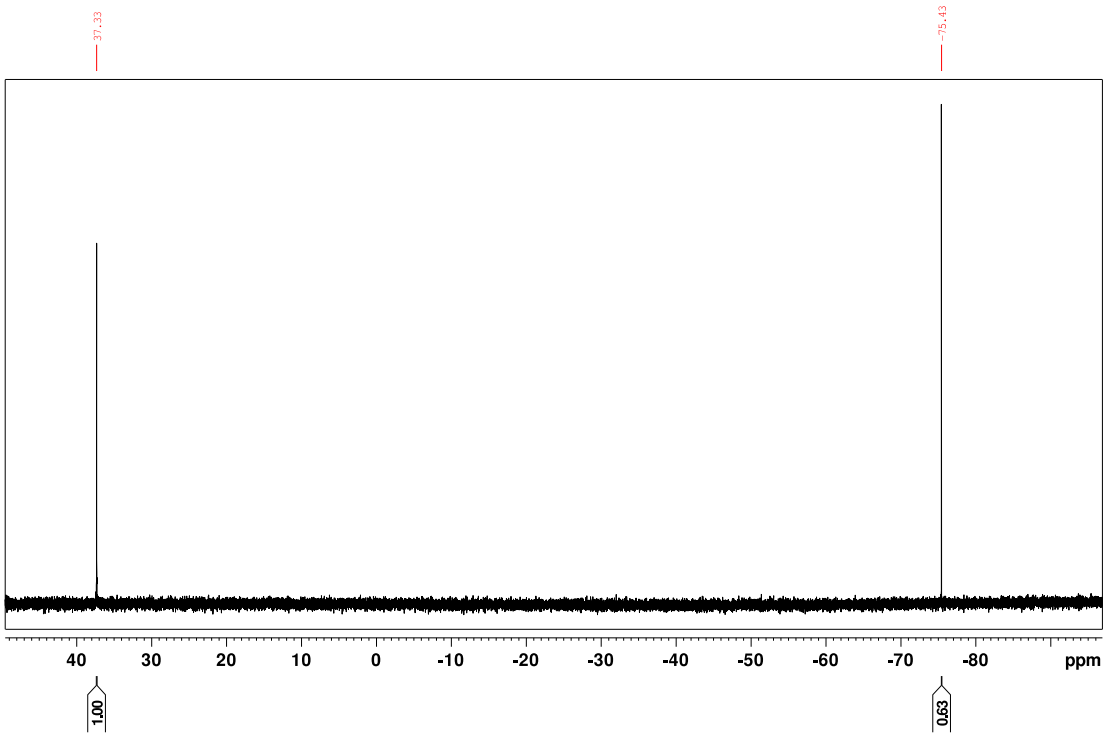

Figure 66. 700 MHz 19F NMR of azido-gD-FSY containing a TFA internal standard and 90% 1X PBS, 10% D2O.

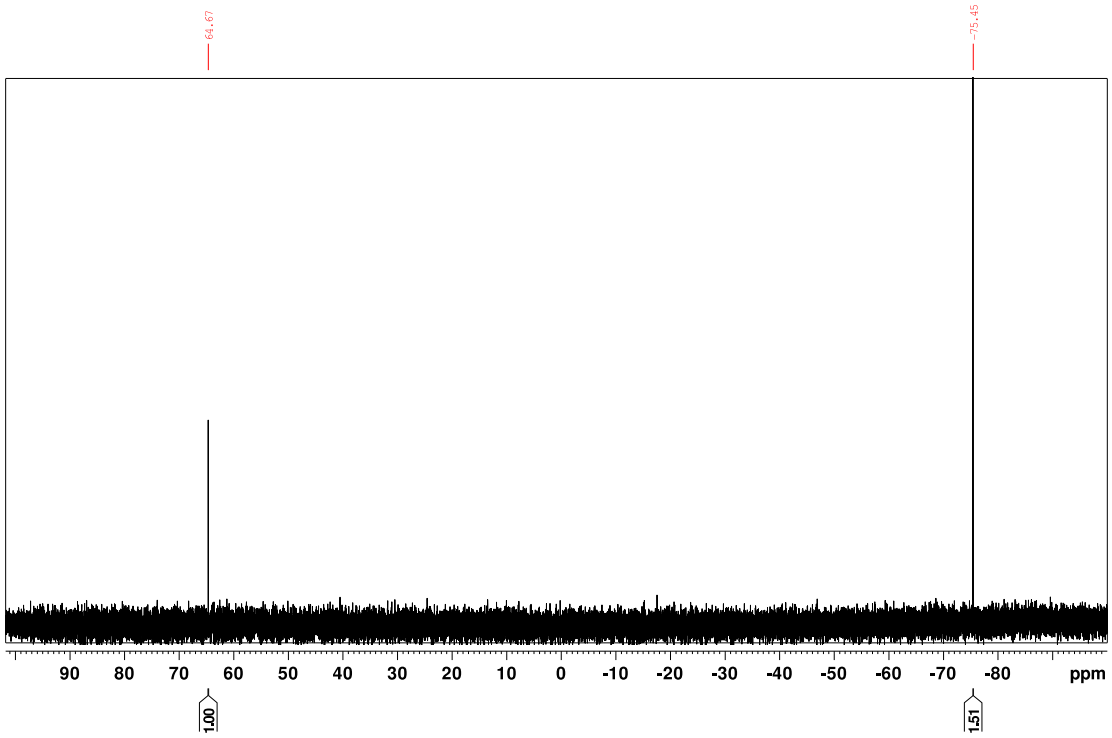

Figure 67. 700 MHz 19F NMR of azido-ASF-gD containing a TFA internal standard and 90% 1X PBS, 10% D2O.